

Corrosion behaviour of welded joints within chloride and chloride/CO[2] environments.

ABDURRAHIM, Ali A.

Available from the Sheffield Hallam University Research Archive (SHURA) at:

<http://shura.shu.ac.uk/19190/>

A Sheffield Hallam University thesis

This thesis is protected by copyright which belongs to the author.

The content must not be changed in any way or sold commercially in any format or medium without the formal permission of the author.

When referring to this work, full bibliographic details including the author, title, awarding institution and date of the thesis must be given.

Please visit <http://shura.shu.ac.uk/19190/> and <http://shura.shu.ac.uk/information.html> for further details about copyright and re-use permissions.

SHEFFIELD HALLAM UNIVERSITY
LEARNING CENTRE
CITY CAMPUS, POND STREET,
SHEFFIELD S1 1WB.



Fines are charged at 50p per hour

05 OCT 2006 9.00pm

REFERENCE

ProQuest Number: 10694070

All rights reserved

INFORMATION TO ALL USERS

The quality of this reproduction is dependent upon the quality of the copy submitted.

In the unlikely event that the author did not send a complete manuscript and there are missing pages, these will be noted. Also, if material had to be removed, a note will indicate the deletion.



ProQuest 10694070

Published by ProQuest LLC (2017). Copyright of the Dissertation is held by the Author.

All rights reserved.

This work is protected against unauthorized copying under Title 17, United States Code
Microform Edition © ProQuest LLC.

ProQuest LLC.
789 East Eisenhower Parkway
P.O. Box 1346
Ann Arbor, MI 48106 – 1346

CORROSION BEHAVIOUR OF WELDED JOINTS WITHIN CHLORIDE AND CHLORIDE/CO₂ ENVIRONMENTS

Ali Abdunnabi Abdurrahim

A thesis submitted in partial fulfilment of the
requirements of Sheffield Hallam University
for the Degree of Master of Philosophy



August, 2004

Table of contents

Table of contents	i
Abstract	iii
Acknowledgements	iv
Nomenclature	v
1. Introduction	1
2. Literature survey	5
2.1 Carbon steel	5
2.1.1 Composition and classification	5
2.1.2 Weldability	6
2.2 Corrosion and localised corrosion	7
2.2.1 Corrosion	7
2.2.2 Localised corrosion	11
2.3 Aqueous corrosion within different electrolytes	14
2.4 Pitting corrosion	16
2.5 Crevice corrosion	18
2.6 Corrosion of weldments	19
2.6.1 Introduction	19
2.7 Metallurgy of welding	22
2.7.1 Transformation and microstructure of carbon steel	22
2.7.2 Microstructure of the WM	26
2.7.3 Microstructure of the HAZ	26
2.8 Effect of microstructure and composition	27
2.9 Corrosion susceptibility of welds	28
2.10 Summary	30
3. Experimental work	31
3.1 Introduction	31
3.2 Materials	31
3.3 Chemical composition	32
3.4. Mechanical properties	32
3.5 Sample preparation	33
3.6 Microstructural characterisation	35
3.7 Electrochemical tests	35
3.7.1 Introduction	35
3.7.2 Droplet cell experimental procedure	37
3.7.3 Linear polarisation resistance	39
3.7.4 Zero resistance ammetry (ZRA)	40
3.7.5 Cathodic polarisation curve	42
3.8 Scanning vibrating electrode technique (SVET)	42
3.8.1 Introduction	42
3.8.2 SVET measurements	43
4. Results	45
4.1 Introduction	45
4.2 Metallographic studies	45

4.3 DC electrochemical measurements	50
4.3.1 Average free corrosion potential	50
4.3.2 Local free corrosion potential	51
4.3.3 Zero resistance ammetry	64
4.3.4 Linear polarisation resistance.....	69
4.3.5 Cathodic polarisation curve.....	87
4.4 SVET measurements.....	92
4.4.1 Calibration of the SVET System.....	92
4.4.2 SVET tests within chloride solution	93
4.4.3 SVET tests within chloride solution with CO ₂ additions.....	99
5. Discussion	104
5.1 Introduction	104
5.2 DC Electrochemical Tests.....	105
5.2.1 Introduction	105
5.2.2 Open circuit potential (OCP) within 3.5% NaCl solution.....	105
5.2.3 OCP within 3.5% NaCl solution with CO ₂ saturation.....	107
5.3 Zero resistance ammetry (ZRA).....	108
5.3.1 ZRA tests within chloride solution	108
5.3.2 ZRA tests within chloride solution with CO ₂ saturation.....	109
5.4 Linear polarisation resistance measurements.....	111
5.4.1 LPR within 3.5% NaCl solution.....	111
5.4.2 LPR within 3.5% NaCl solution with CO ₂ saturation	112
5.5 Cathodic polarisation tests	114
5.6 Effect of microstructure	116
5.7 SVET measurements.....	117
5.7.1 Introduction	117
5.7.2 SVET tests within chloride solution	118
5.7.3 SVET test within chloride solution saturated with CO ₂	119
6. Conclusions.....	120
7. Suggestions for further work.....	122
References	123
Publications.....	128

Abstract

Electrochemical measurements and metallographic studies were performed on welded carbon steel pipeline materials. Corrosion tests were performed within naturally chloride solution with and without CO₂ additions at ambient temperature. The pH within different environments, chloride solution alone and buffered chloride solution with CO₂ additions was measured at 6.3 ± 0.3 and 6.2 ± 0.1 respectively. The objective of this study was to evaluate the corrosion behaviour (rates) of carbon steel welds using both traditional and novel electrochemical scanning techniques within two different chloride environments. Corrosion tests were conducted using DC steady state and scanning electrochemical techniques. These tests consisted of linear polarisation resistance (LPR), corrosion potential (E_{corr}), zero resistance ammetry (ZRA), cathodic polarisation (CP) and the scanning vibrating electrode technique (SVET), which were used to semi-quantitatively assess the corrosion activity of the different microstructures, i.e., weld metal (WM), heat-affected zone (HAZ) and parent plate (PP) respectively. Samples were freshly ground before exposure to the different aqueous chloride solutions. SVET was used during these investigations to evaluate preferential corrosion susceptibilities of weldments. SVET results were compared with results from (long term-immersion) DC-based electrochemical corrosion tests. SVET was found to be a sensitive technique with good resolution allowing differences in corrosion response to be determined within hours as compared to other corrosion tests that require several hours to days.

Acknowledgements

I would like to express my gratitude to my supervisor Professor R. Akid for his invaluable guidance, help and encouragement during my first study within the department.

I am also thankful to my second supervisor Dr N. Farmilo for his sincere advice and help.

Many thanks for the research staff at the Centre for Corrosion Technology especially, Dr D. Greenfield and all the technicians at the Materials and Engineering Research Institute for their cheerful help with the production of this thesis.

The author gratefully acknowledges the Libyan Higher Education Committee for financial support of this research work.

Finally, I would like to express my heartfelt gratitude to my wife for her cheerful help, encouragement during my study and pressing me every day to correct and finish this thesis.

Nomenclature

DC direct current

E_{corr} corrosion potential

i_{corr} corrosion current

OCP open circuit potential

I_a anodic current

I_c cathodic current

LPR or R_p linear polarisation resistance

SVET scanning vibrating electrode technique

Σ summation

WM weld metal

HAZ heat affected zone

PP parent plate

CR corrosion rate

PIS point in space

UTS ultimate tensile stress

YTS yield stress

B linear polarisation resistance constant

CE carbon equivalent value

FCC face centred cubic

CP cathodic polarisation

ZRA zero resistance ammetry

1. Introduction

The production of oil and gas, its transportation and refining and its subsequent use as a fuel and raw materials for chemicals constitute a complex and demanding process. Various problems are encountered in this process, and corrosion is a major one. The costs of lost time, the replacement of materials of construction, and the constant personnel involvement in corrosion control are substantial and, if not controlled, can be financially and socially catastrophic. The control of corrosion through the use of coatings, metallurgy, non-metallic materials of construction, cathodic protection, inhibitors, and other methods has evolved into a science in its own right and has created industries devoted solely to corrosion control in specific areas [1].

Corrosion in the oil field and gas industry appear as leaks in tanks, casings, tubing, pipelines, and other equipment. These processes change the outer surface layers of the base metal to a non-metallic material, i.e., corrosion products (oxide scale). The most corrosive species found in oil field operations include chloride, oxygen, carbon dioxide and hydrogen sulphide, the latter being present in deep oil-well water (formation water) [2].

These types of environment have been found to destroy major items of equipment within several months [3, 4]. Corrosion inhibitors are widely employed in the oil industry to protect iron and steel equipment used in drilling, production, transport and refining of hydrocarbons [5]. Carbon and low-alloy steels are, due to their limited corrosion resistance, expected to corrode in service and frequently fail from this cause.

Uniform corrosion can be predicted with reasonable accuracy in most systems and checked or monitored to prevent unexpected failures [6].

Carbon steels the most widely used engineering material, accounts for over sixty million tons, or approximately 88%, of the annual steel production in the United States. Despite its relatively limited corrosion resistance, carbon steels are used in large tonnages in marine applications, nuclear power, transportation, chemical processing, oil production and refining pipelines, construction and metal processing equipment. The possibilities of application depend upon the corrosion behaviour [1]. In this respect, the necessity to characterise electrochemical properties is the first step to a more extended study of the corrosion problems. The use of electrochemical tests is attractive because they are based upon the corrosion process, e.g., namely anodic oxidation and cathodic reduction [7, 8]. The corrosion of metals in aqueous electrolytes occurs by an electrochemical mechanism and therefore DC techniques offer a simple way to accelerate the corrosion process. Corrosion of carbon steels occurs within a range of aqueous solutions, including chlorides, hydroxides, carbonates and nitrates, but increased acidity at pH levels less than 7 ($\text{pH} < 7$) is also an important contributory factor.

The cost of metallic corrosion to the total economy is measured in hundreds of millions of dollars per year [1, 9]. Carbon steels represent the largest single class of material in use, both in terms of tonnage and total cost and therefore it is easy to appreciate that the corrosion of carbon steel is a problem of enormous (severe) practical importance. In this thesis, only the intrinsic aspects of the corrosion system, primarily the environmental and compositional factors will be addressed. Carbon or mild steels are by their nature of limited alloy content that is less than 2% by weight of alloy additions. These levels of addition do not generally produce any remarkable

changes in general corrosion behaviour. One possible exception to this statement would be the, so called, weathering steels, in which small additions of copper, chromium, nickel, and/or phosphorus produce significant reduction in corrosion rate in certain environments [9]. At the levels present in low alloy steels, the usual impurities have no significant effect on corrosion rate in the atmosphere, neutral waters or soils. Only in the case of acid attack is an effect observed. In this latter case, the presence of phosphorus and sulphur markedly increase the rate of attack [10]. Indeed, in acid systems, the pure irons appear to exhibit the best resistance to attack. In solving a particular corrosion problem, a dramatic change in the rate of attack can often be attained by altering the corrosion environment. The deaeration of water and the addition of corrosion inhibitors are two examples that have broad application in the area of aqueous corrosion control [11].

Oil and gas companies have experienced considerable corrosion in weld zones of hydrocarbon pipeline systems made of carbon steels. In CO₂ containing environments corrosion failures are often explained by the varying tenacity of protective scales on different carbon steel microstructures [12-14]. Preferential corrosion of weld metal and heat affected zone has mostly been explained by galvanic effects caused by differences in chemical content and microstructures [15].

Many failures of welded carbon steel products have been attributed to the selective corrosion of the weld. Corrosion is found in both fusion and electrical resistance welded (ERW) products and occurs in varied environments and is not confined to one region of the weldment [16, 17]. Weld corrosion is often characterised by grooves parallel to the weld. Extensive research [15, 17] on the corrosion of weldments has been performed to formulate corrosion prevention strategies. However, the mechanisms involved in the localised corrosion of the weldments are not fully clear.

Preferential weld corrosion has historically been a major problem and remains of significant concern for the oil and gas industry. The term preferential weld corrosion describes selective attack of the weld itself rather than of the parent plate but it is frequently used in a somewhat loose manner to describe corrosion of other features of a weldment, e.g., the heat affected zone of the parent plate. The origin of preferential attack is usually a combination of a more active weld material (the weld would tend to be more susceptible to corrosion than the parent material) together with galvanic coupling to the parent material. The influence of coupling is accentuated by an unfavourable area ratio, i.e. a small anodic weld / large cathodic parent plate [18].

2. Literature survey

2.1 Carbon steel

2.1.1 Composition and classification

Steel is the general name given to a wide range of alloys of iron and carbon with or without the purposeful addition of other alloying metals. The carbon imparts higher strength to the iron and the ability, over a certain percentage, to permit hardening and a wide range of structural properties by heat treatment. Increasing the carbon content of steel gives increased hardness with higher strength but lower ductility. Tougher steels with superior properties can be achieved by replacing some of the added carbon with other alloying elements such as Cr, Ni, and Mo, modifying the microstructure of the metal. Steel is considered to be carbon steel, when the specified minimum for copper does not exceed 0.4%, or when the maximum content specified for any of the following elements does not exceed the following percentages, namely, 1.65% Mn, 0.60% Si, and 0.60% Cu [19].

Steels can be classified by a variety of different systems depending on:

- 1- The composition, such as carbon, low alloy or stainless steel.
- 2- The finishing method, such as hot rolling or cold rolling.
- 3- The microstructure, such as ferrite, pearlite or martensite.
- 4- The heat treatment, such as annealing, and quenching.
- 5- The required strength level, as specified in ASTM standards.

However, variations in carbon have the greatest effect on mechanical properties, with increasing carbon content leading to increased hardness and strength and decreased

toughness. Carbon steels are generally categorised according to their carbon content, up to 2% C total alloying elements.

2.1.2 Weldability

As a good approximation, the weldability of steel can be estimated from its composition. The formula, which may be used to calculate the equivalent amount of carbon, i.e., the carbon equivalent (CE) equation also known as the International Institute of Welding (IIW) equation [20, 21] is given below;

$$CE = C + \frac{Mn}{6} + \frac{Cr+Mo+V}{5} + \frac{Ni+Cu}{15} \quad (1)$$

Carbon equivalent equations have been developed experimentally to express (or estimate) weldability. The application of the CE expression is empirical, e.g., the IIW Carbon equivalent equation has been used successfully with traditional medium-carbon low alloy steels. Steels with lower CE values (< 0.45 wt %) generally, exhibit good weldability where weld cracking is unlikely. Therefore, steels with the highest CE values, (> 0.45wt %) will be the most difficult to weld [20].

The weldability of steel greatly depends on its carbon and manganese content and impurity levels, and can be subdivided as follows;

- i) Low carbon steels containing from 0.052 to 0.3% C, with up to 0.4% Mn are ductile, easily worked and readily welded by all common welding techniques.

$$CE = 0.30 + \frac{0.4}{6} = 0.36 \text{ wt } \%, (< 0.45 \text{ wt } \%) \quad (2)$$

ii) Medium carbon steels are similar to low carbon steels except that the carbon content ranges from 0.30 to 0.6% C. These steels also usually have a slightly higher manganese content ranging from 0.60 to 1.65% Mn making the steels capable of being through- hardened.

$$CE = 0.30 + \frac{1.65}{6} = 0.58 \text{ wt } \%, (> 0.45 \text{ wt } \%) \quad (3)$$

iii) High carbon steels contain 0.60 to 2.00% C, with various alloy modifications of the plain carbon steel are available giving enhanced specific properties. Steels have a manganese contents ranging from 0.30 to 0.9% Mn [19].

$$CE = 0.6 + \frac{0.9}{6} = 0.75 \text{ wt } \%, (> 0.45 \text{ wt } \%) \quad (4)$$

2.2 Corrosion and localised corrosion

2.2.1 Corrosion

In broad terms, corrosion is defined as the interaction between a material and its environment that results in the degradation of the physical, mechanical, or even aesthetic properties of that material. More specifically, corrosion is usually associated

with a change in the oxidation state of constituent elements within the metal oxide. The presence of an anode, cathode, conducting electrolyte, and an electric circuit between the anode and cathode is essential for electrochemical corrosion processes to take place. The removal of any one of these factors will lead to an arrest in the corrosion process [22].

Modern day society depends upon component structures, which are often constructed using metals and alloys. Engineering metals and alloys, e.g., steel and aluminium, in contact with moist (humid) atmospheres are in most cases chemically unstable. The presence of oxygen and other oxidising agents in the atmosphere or media, with which, metals are in contact, favour metal instability and consequently their degradation. It is recognised that metals are unstable because they show a thermodynamic tendency to revert to a lower energy state oxide or other chemical species from which the metal was extracted. Excluding the noble metals such as gold and platinum, for example, (which are much more expensive), all other metals present some degree of instability under atmospheric conditions.

The stability of metals depends upon the events taking place on their surface when they are in contact with an electrolyte [23]. Corrosion of metals and alloys is generally an electrochemical process, which involves complex mass and charge transfer at the metal-electrolyte interface. These charge transfer reactions at the interface are the origin of the instability of metals. The necessary condition for corrosion is that the metal dissolution (oxidation) reaction and reduction reactions (reactions that consume the electric charge liberated during metal dissolution) proceed simultaneously at the electrode-electrolyte (metal-environment) interface.

For the anodic and cathodic reactions to take place simultaneously, two conditions are necessary;

i) The potential difference across the interface must be more positive than the equilibrium potential of the anodic reaction, represented here in a simplified way as;



Where, M represents any metal, n is the number of interchanged charges and e^{-} represents an electron.

ii) The potential difference across the interface must be more negative than the equilibrium potential of the reduction reaction;



For example,



This involves electron acceptors (represented by A in this equation) contained in the electrolyte.

When the electron sink-site or cathode, and electron source area or anode is stable in time but at different defined places on the corroding metallic surface, local-cell or localised corrosion takes place. On the other hand, when the oxidation and reduction reactions occur randomly over the surface with regard to both, space and time, the Wagner and Traud mixed potential theory of homogeneous corrosion is considered to

be operative [24, 25] and uniform corrosion occurs. The theoretical principles for corrosion as an electrochemical phenomenon were derived from the mixed potential theory [25], which is the basis for corrosion testing. The modern form of this theory is commonly accredited to Wagner and Traud. Corrosion can range from highly uniform attack to highly localised attack, such as occurs during pitting and crevice corrosion and intergranular attack.

The selection of the techniques used to evaluate and study corrosion depends on the kind of corrosion taking place. The principal aim of the corrosion scientist is to determine the mechanism of the corrosion process including intermediate reactions and the kinetics of these processes. Sometimes it is necessary to use intrusive methods (electrochemical methods) in which the system is stimulated externally and the response of the system to that perturbation is measured, e.g., DC steady state electrochemical methods. There are other methods (non-intrusive techniques) which measure electrochemical activity without imposing any kind of external perturbation to the system, such as the scanning reference electrode Technique (SRET) and Scanning Vibrating Electrode Technique (SVET) [26, 27].

The most important aspect of the corrosion assessment of components and structures in real service is the prediction of their residual life when there is a risk of failure by localised attack. In this respect the use of electrochemical methods for studying localised corrosion is an important part of the evaluation of localised corrosion compared to general (uniform) corrosion. In the case of uniform corrosion several electrochemical methods have been developed and are applied to assess the corrosion rate. In both laboratory experiments and in the field, the method of Tafel extrapolation and the measurements of the linear polarisation resistance (LPR) are the DC techniques most frequently used [24, 28].

2.2.2 Localised corrosion

Localised corrosion may be considered in a wide sense to include all types of corrosion except general corrosion e.g., pitting and crevice corrosion. This type of corrosion is characterised by regions of locally severe corrosion, with the general loss of thickness being relatively small. Other types of localised corrosion include galvanic corrosion and stress corrosion cracking, [24, 25].

In the present context, however, localised corrosion will be restricted to pitting and crevice corrosion as both these types of corrosion are closely related to each other and occur in more or less occluded cavities, so-called occluded corrosion cells [29].

Localised corrosion may occur on all metals, but this research work will be restricted to a metal most commonly used in practice, notably carbon steel [30].

In nature, localised corrosion processes often cause major practical problems affecting the performance of technologically important metallic materials, i.e., steels, stainless steels, aluminium alloys, copper and other metals and their alloys in different environments, especially those containing chlorides. It can be considered that the corrosion process results from changes in the nature and composition of metals exposed to environments of homogeneous composition. The established essential principles of corrosion, is that, the sum of the rate of the cathodic reaction must be equal to the sum of the rate of the anodic reaction, irrespective of whether the attack is uniform or localised [24]. So the following equation must be satisfied;

$$\Sigma I_a = -\Sigma I_c \quad (8)$$

Where I_a and I_c denote the anodic and cathodic currents respectively, which has a direct relation with the reaction rate for the electrochemical process.

It is now known that many aqueous corrosion processes of great technical interest occur under conditions in which access of the electrolyte is restricted. This can be due to the geometry of the structure, e.g. flange joints, gaskets and plate rivets. Also it may occur due to the existence of corrosion deposits, such as iron carbonate (FeCO_3) or oxide scales on the metal surface. In the case where corrosion occurs under conditions of restricted diffusion, the chemical composition of the corroding environment inside the occluded cavity may be very different from that of the composition of the bulk solution. One of the most important effects is that of changes in oxygen or ionic concentration in the electrolyte, which give rise to local changes in corrosion potential. Under normal circumstances where the aggressive environment is aerated, the surface of the corroding alloy outside the occluded cavities is often cathodic as a result of the formation of the oxide film. Passivation takes place at these sites because they are in direct contact with the oxygen dissolved within the electrolyte. These surfaces act as aerated cathodes where oxygen takes part in the reduction reaction of the corrosion process. In acidic solutions oxygen is reduced to water (or hydrogen peroxide) with a subsequent increase in pH, according to the following equation [31].



For basic or neutral solutions the cathodic reduction reaction is [23].



The surface, which is inside the occluded cavity, is active and acts as an anode due to the very low oxygen concentration in the solution. At these surfaces the metal undergoes dissolution. Additionally, an a hydrolysis reaction takes place with a decrease in the pH of the solution according to the following reaction sequence;

For aluminium



and,



For iron,



and,



In the chemical processing industries, localised corrosion is a major cause of repeated service failures and is estimated to account for at least 90% of metal damage by corrosion [32].

2.3 Aqueous corrosion within different electrolytes

Carbon steel pipeline and vessels are often required to transport water, oil and gas or are submerged in aqueous environments to some extent during service. This exposure can be under conditions of varying temperature, flow rate and pH, all of which can alter the rate of corrosion. The relative acidity of the solution is probably the most important factor to be considered. At low pH, the evolution of hydrogen tends to eliminate the possibility of protective film formation, so that steel continues to corrode, but in alkaline solutions, the formation of a protective film greatly reduces the corrosion rate. The corrosion of steels in aerated seawater is about the same overall as in aerated freshwater, but this is somewhat misleading because the greatest electrical conductivity of seawater can lead to increased pitting [33], where typical corrosion rates of mild steel from 5 to 10 mils/yr (0.13-0.30 mm/yr) is considered moderate and more than 10 mils/yr is considered severe. Corrosion of metals in an aqueous environment is an electrochemical process and occurs when two or more electrochemical reactions take place on a metal surface. As a result, some of the elements of the metal or alloy change from the metallic state to a non-metallic state. The products of corrosion may be dissolved species or solid corrosion products, in either case; the energy of the system is lowered as the metal converts to a lower energy form. Rusting of steel is an example of the conversion of a metal (iron) into a non-metallic corrosion product (rust). The electrochemical reactions occur uniformly or non-uniformly on the surface of the metal (the electrode), where the ionically conducting liquid is called the electrolyte. As a result of the reaction, the electrode/electrolyte interface acquires a special structure, in which such factors as the separation of charges between the metal and ions in the solution, interaction of ions

with water molecules, adsorption of ions on the electrode and diffusion of species all play important roles. The special layer at the metal surface is called the Helmholtz double layer. One of the important features of the electrified interface between the electrode and the electrolyte is the appearance of a potential difference across the double layer, which allows the definition of the electrochemical potential. The electrode potential becomes one of the most important parameters in both the thermodynamics and the kinetics of corrosion.

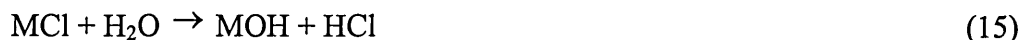
The corrosion of carbon and low alloy steels in CO₂ containing media, denoted sweet corrosion, has been one of the important problems in the oil and gas Industry since 1940 because of both high corrosion rate and severe localised corrosion [34, 35]. CO₂ corrosion affects the materials used in both production and processing. Low cost carbon steels are susceptible to corrosion in CO₂ environments with the severity of corrosion being dependent particularly upon temperature, CO₂ partial pressure, pH, velocity and material composition [27].

Generally, CO₂ corrosion can be controlled using different applications such as epoxy powder coatings inhibitor injection and the use of corrosion resistant alloys, depending on field formation and experience concerning the quantity of fluid produced, gas or the fluid ratio, flow velocity and CO₂ partial pressure. On the other hand experimental work has been carried out by Eilerts et al [36] to determine the effect of metallurgical factors on the corrosion behaviour of carbon and low alloy steels. Furthermore, the effect of CO₂ on the cathodic reaction and the mechanism of CO₂ corrosion are discussed with respect to the behaviour of the corrosion product by Ikeda et al [37] and Riesenfeld and Blohm [38] have suggested that dissolved CO₂ aids iron dissolution by the formation of iron carbonates (FeCO₃) and/or hydrated oxides of iron, such as FeO-H₂O on the surface. The formation of the surface film can

lead to a potential difference between the filmed and unfilmed surface, this potential difference is driving force for corrosion.

2.4 Pitting corrosion

Stated simply, pitting is a type of localised corrosion that produces pits, that is, sites of severe corrosive attack that are relatively small compared to the overall exposed surface. This type of corrosion is usually associated with passive metals e.g., stainless steels although this is not always the case. Pit initiation is usually related to the local breakdown of the passive film and can often be induced by the presence of halide ions in solution [39]. Pitting is one of the most destructive forms of corrosion found in carbon steel pipeline exposed to aqueous solution containing chloride ions. The local environment within a pit can be extremely acidic, resulting in a high rate of corrosion within this small region. For the common situation of a metal in salt water, the dissolution of metal within the pit results in the formation of metal chlorides (MCl). These salts are then hydrolysed to form hydrochloric acid (HCl) within the pit, as shown in the reaction;



The decrease in pH within the pit caused by acid formation further increases the rate of metal dissolution [40]. Pitting corrosion represents an important limitation to the safe and reliable use of many alloys in various industries. Pitting is a very serious type of corrosion damage because of the rapidity with which metallic sections might be

perforated. The unanticipated occurrence of pitting and its unpredictable propagation rate make it difficult to take it into consideration in practical engineering design.

Deterioration by pitting is one of the most dangerous and

common types of localised corrosion encountered in aqueous environments [30, 41].

Pitting is the most common cause of premature corrosion related failure encountered in the carbon and low alloy steels. Any condition that removes the moderately protective oxide film normally present on these materials may allow pitting corrosion to occur. Pitting of metals is extremely localised corrosion such that it generally produces sharply defined holes. The attack on the interior walls of the hole is usually reasonably uniform, but may be irregular where there are specific additional contributions to attack such as secondary intergranular attack. Pitting occurs when one area of a local site or the metal surface becomes anodic with respect to the rest of the surface. Pitting on clean surfaces ordinarily represents the start of breakdown of passivity or local breakdown of inhibitor-produced protection.

Pitting is one of the most insidious forms of corrosion; it can cause failure by perforation while producing only a small weight loss of the metal. In addition, pits are generally small, and often remain undetected [28, 42] and therefore pitting is sometimes difficult to detect in laboratory tests and in service, because there may be a period of months or years, depending on the metal and the corrodent, before the pits initiate and develop to a readily visible (detectable) size.

2.5 Crevice corrosion

Historically, crevice corrosion was used to describe only the attack upon oxide passivated alloys by aggressive ions such as chloride in crevices or other shielded areas of a metal surface [43]. This type of corrosion occurs in restricted or occluded regions, such as at bolted joints, and is often associated with solutions that contain halide ions. Crevice corrosion is initiated by a depletion of dissolved oxygen in the restricted region. The supply of oxygen within the crevice is depleted, because of cathodic oxygen reduction, the metal surface within the crevice becomes activated, and the anodic current is balanced by cathodic oxygen reduction from the region adjacent to the crevice. The reactions occurring within the crevice are the same as those described for pitting corrosion [44]. Thus crevice attack is very much associated with the geometry of the structures, for example, riveted plates, welded structures, threaded components, contact of metal with non-metallic solids such as glass and plastic or corrosion products (scale). The common factor is the initial geometrical arrangement of the solid elements of the system, arising from the way in which the solid components of the system have been assembled or through the surface accumulation of solid debris [45, 46]. This leads to heterogeneous distribution of species dissolved in the electrolyte, which in turn provides conditions for localised attack. Considerable research has been devoted to the electrochemistry within crevices, mainly because of advances in technology, which enable accurate measurements to be made within the extremely small confines of a crevice [43, 47]. Thus, this form of localised attack starts at defects formed at the surface of the metal e.g. scratches, cracks or contact joints with other components or contaminant deposits.

Because of the nature and characteristics of this type of localised attack, it can be considered that pitting and crevice corrosion are virtually identical, i.e. a pit is a form of crevice that is self-initiating. Stainless steel that undergoes pitting corrosion can also be expected to suffer crevice corrosion. On a passive metal, for example stainless steel, crevice corrosion occurs when the cathodic reaction, that sustains the dissolution in the passive state, becomes insufficient due to depletion of the oxidising species in the solution within the cavity [48].

2.6 Corrosion of weldments

2.6.1 Introduction

Since welding is the most common method of joining metals, it is important to be able to effectively evaluate weld corrosion. Therefore, this subject has been the matter of much controversy in past years. A particular concern for carbon steel weldments is preferential corrosion of the weld metal or the heat-affected zone. This may occur if either of these regions is more susceptible to corrosion than the parent plate. Weld corrosion is a much-researched form of corrosion damage, which may occur on the weld metal (WM), heat affected zone (HAZ) or parent plate (PP) regions.

Corrosion in welds has always been a problem due to local variations in material composition and microstructure. Initiated localised corrosion will reduce lifetime significantly and may cause failures, which may be a threat to safety in the oil and gas production. During the welding process a mixture of parent plate and welding rod is rapidly heated to a high temperature and then cooled. Phase changes with precipitation and grain growth occur as a result of the extreme temperature during the

joining process. A controlled thermal process is important to avoid producing local microstructures, which are susceptible to localised corrosion. Figure 1 shows a schematic of time temperature transformation diagram [49], which shows some of the possible structures, which may form during the welding process. Cooling curve 1 is slow enough to give complete transformation from austenite to ferrite and pearlite. Curve 2 gives a mixture of ferrite, bainite and martensite. Curve 3 gives bainite and/or martensite whilst curve 4 gives only martensite phase.

In virtually all cases, corrosion attack has been attributed to local galvanic difference between the parent plate (PP), heat affected zone (HAZ) and weld metal (WM). The effect of composition, inclusion type and distribution, metallographic structure, degree of the stress and the galvanic effects of neighbouring areas must be taken into account [50]. Advanced techniques, such as the scanning vibrating electrode technique, may be used to map out the corrosion activity of carbon steel weldments. Weldments sometimes exhibit preferential corrosion of the weld metal, heat affected zone or the parent plate.

The localised nature of attack limits the usefulness of standard weight loss corrosion tests. Corrosion of weldments is a complex subject but there have been considerable advancements in standardisation during the past decade [51].

There are different types of welding; two of the most familiar processes are electric arc welding and gas welding. All types of welding can render the product susceptible to weld corrosion, however only these two welding processes will be discussed. In the gas welding process, a combination of oxygen and a fuel, e.g., oxy-acetylene flames are burned to create the temperature required to melt the edges of the parent metal. The advantage of this type of welding is that the equipment needed is normally

portable. However, in order to quickly melt the metal, the flame must reach very high temperatures (e.g. 3100 °C), thus oxidation becomes a large problem. The other main welding process is electric arc welding which has the advantage of being faster than gas welding because it occurs at higher temperatures; however this can lead to a greater heat affected zone [52, 53].

Weld deterioration (decay) is a major problem in stainless steel during the welding process. Mechanical stress can build up as the welded area cools. Intergranular corrosion can occur at the area of intermediate temperature in the parent plate (PP) known as the heat affected zone (HAZ), causing the loss of Cr in the HAZ for example, of stainless steels. If the coefficient of thermal expansion for the filler material and the weld metal (WM) differ to a large extent, cracking can occur as a result of the residual stress built up during cooling. The microstructure of the weld metal can also be affected. In austenitic stainless steels, Ti or Nb can react with carbon to form carbides to prevent weld decay. These carbides build up next to the weld bead and are not able to diffuse due to rapid cooling of the WM. The remedy for avoiding knife line attack is to heat the completed structure after welding process to around 1065 °C. These types of process can prevent or minimise weld corrosion in most applications. Corrosion occurs in many forms and can be difficult to predict when combined with variables introduced by welding. For example, welds can be made with or without adding filler metal. In many cases, the corrosion resistance of the WM exceeds that of the PP. In other applications, the WM corrodes at a faster rate than the PP [54]. One common rule for minimising problems of weldments is to make sure that the weld metal has a higher corrosion potential than the surrounding parent metal, so that the weld metal will be the cathode and the large area, surrounding metal will be the anode in a galvanic circuit.

2.7 Metallurgy of welding

The main effect of the heat input is the effect on the microstructure of the WM and the HAZ. In broad terms the longer the time spent above the grain coarsening temperature of the alloy the coarser the structure of the WM and HAZ. The variation of steel microstructure as a function of cooling rate for eutectoid steel is depicted in Figure 1. The extent width of the HAZ into parent plate depends on the heat input and on the cooling rate. The cooling rate is also dependent on the capacity of the component to act as a heat sink.

2.7.1 Transformation and microstructure of carbon steel

Steel consists predominantly of two elements, iron and carbon, ignoring inclusions that are present in steel. It is true that steels will contain e.g., Mn, Al, Si, and other alloying elements such as Nb, V, Cr and Ni. These elements may modify the overall microstructure; however, it is the iron-carbon ratio that is always the predominating influence. The room temperature structure of steels has not been rapidly quenched to form martensite / bainite phases depend on chemical compositions and cooling rate. Carbon and low alloy steel can contains a combination of iron (ferrite) and iron carbide (cementite, Fe_3C), the relative proportion and distribution of each phase being controlled by the cooling conditions from the high temperature (austenite) phase. Austenite is a homogeneous phase consisting of a solid solution of carbon in the iron form (FCC) and only exists at temperatures above 723°C . The steel is cooled below, 723°C , ferrite forms with the solid solution carbon forming cementite (Fe_3C , 93.3%,

Fe, 6.67%C). When steel containing approximately 0.80% C is cooled, all the ferrite and cementite precipitate together at one temperature to form a lamellar structure called pearlite. This is a eutectoid structure and at carbon contents below and above the excess ferrite or cementite is known as pro-eutectoid iron or α -ferrite.

The expected ferrite and cementite structures can be predicted via the Iron-Carbon Equilibrium Diagram, is shown in Figure 2.

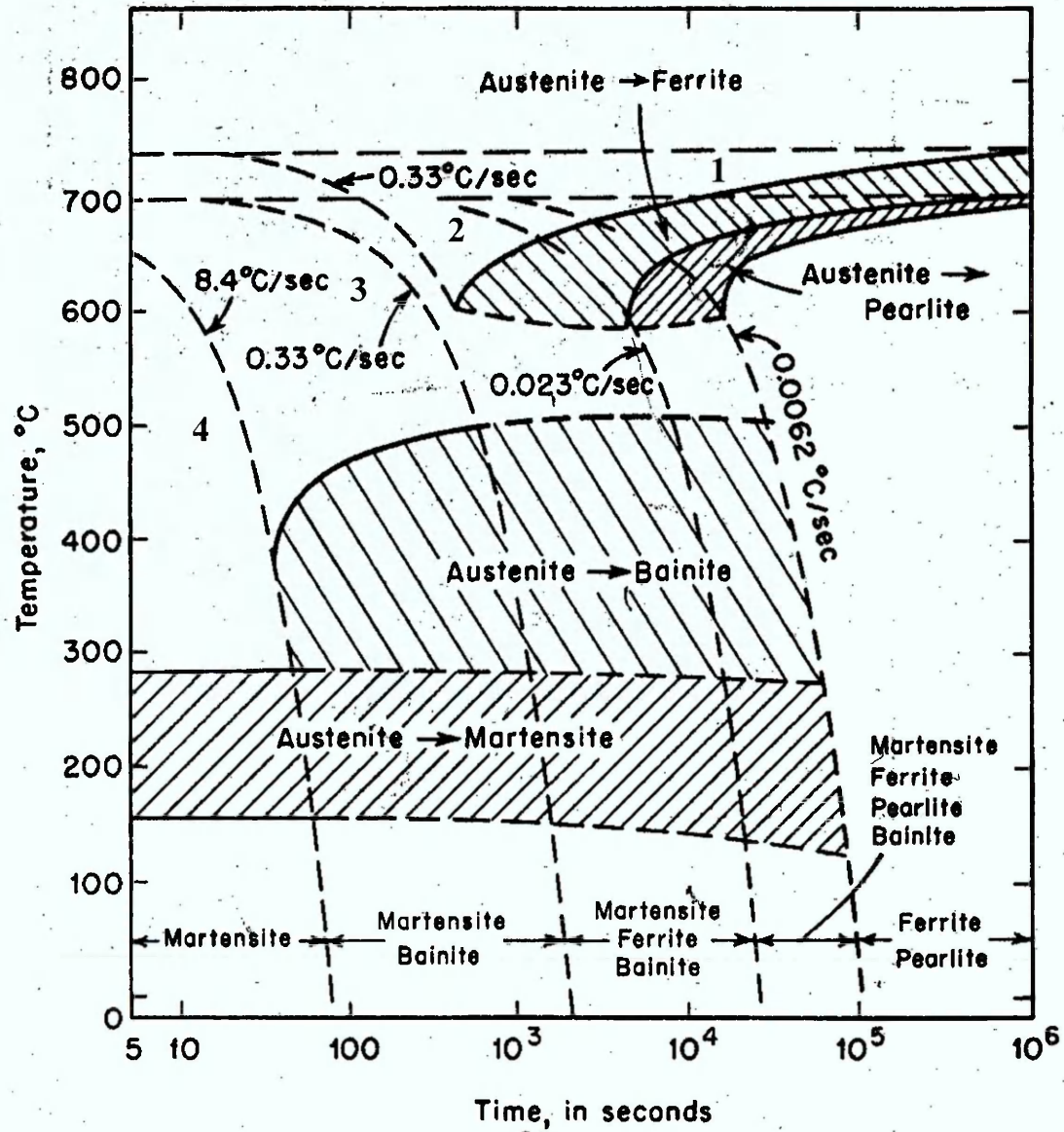


Figure 1 TTT diagram with four cooling rates including the phases, austenite (A), bainite (B), ferrite (F), pearlite (P) and martensite (M) [49].

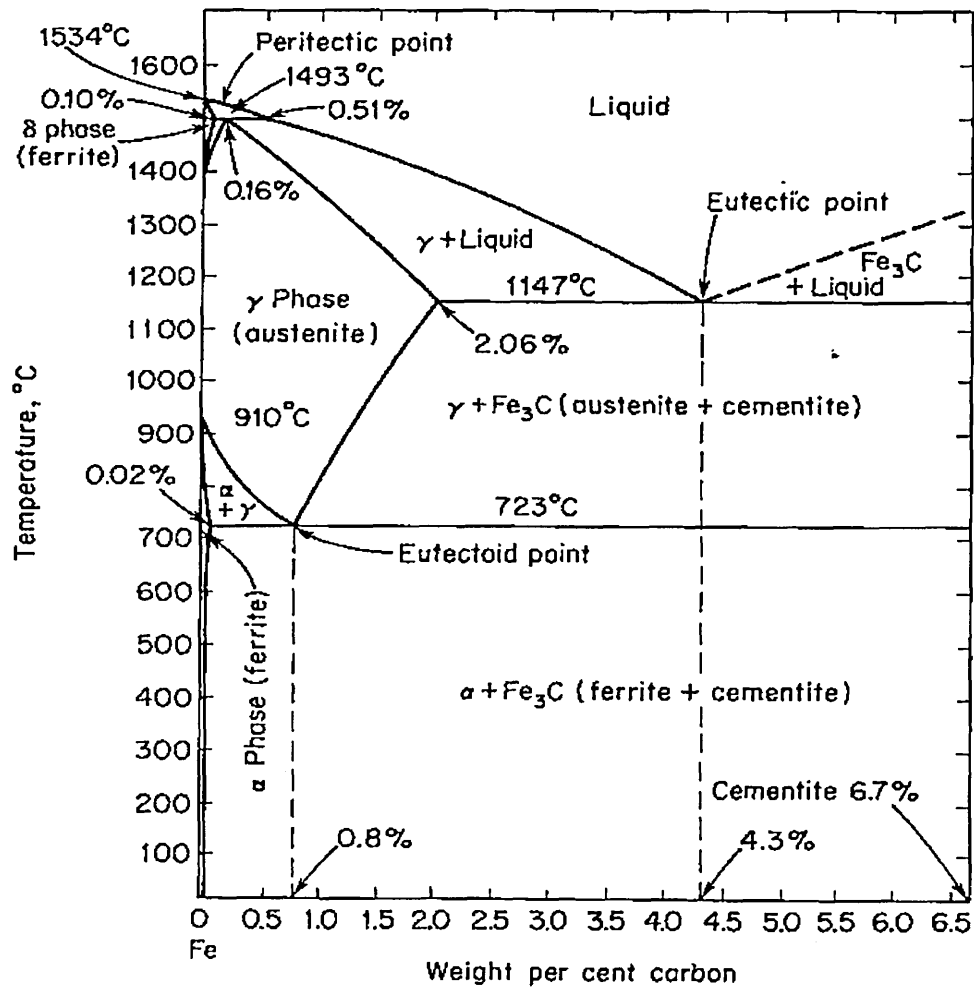


Figure 2 Phase diagram for Iron-Carbon system showing the metastable Fe-Fe₃C equilibrium [55]

2.7.2 Microstructure of the WM

In low carbon steel the first phase to form is pro-eutectoid ferrite, which occurs as a network of parallel lathes. In between the lathes the austenite transforms depending upon the cooling rate and weld composition. For a low carbon consumable (filler rod) this usually transforms to acicular ferrite with fine pearlite, bainite and martensite between the grains. Increasing the alloy content of the consumable replaces the acicular ferrite with bainite or martensite [55].

2.7.3 Microstructure of the HAZ

The metallurgical process of the HAZ is one of a thermal cycle and its associated effect on the microstructure. In simple terms the HAZ can be separated into two regions, the grain growth and grain refined regions. At circa 1200 °C the austenite grains grow rapidly and this results in the grain growth region. Below this temperature the thermal cycle will usually produce a refined grain structure. The microstructure of the grain growth region is controlled by two factors, the austenite grain size and the transformation structure within the region. The grain size is controlled by grain coarsening temperature of the steel and weld thermal cycle. The higher the heat input the coarser the grains. In this region the structure of low carbon steel will be of pro-eutectoid ferrite at the prior austenite grain boundaries with a ferrite / pearlite or ferrite / bainite structure within the grains. Higher cooling rates result in the loss of the pro-eutectoid ferrite with acicular structures of bainite or martensite developing [55, 56].

2.8 Effect of microstructure and composition

It is difficult to assess separately the individual effect of either the microstructure of the weld or the composition on corrosion behaviour. Changes in the alloy content of a consumable alters parameters such as grain coarsening temperature and transformation temperature and different heat inputs may be necessary to successfully lay different welds. Some workers [50, 57] have studied preferential weld corrosion and they have concluded that electrochemical differences between PP, WM and HAZ lead to selective corrosion. The electrochemical difference between the components is due to the presence of bainite, manganese sulphide (MnS) inclusions, retained austenite and macro slag inclusions [57]. Massive ferrite on the grain growth of the HAZ has been found to lead to accelerate corrosion rates over the normalised ferrite and pearlite structure.

The main compositional effects on the above structures are the carbon and manganese content and so it is possible to state that increasing the C and Mn content of the weld consumable will make the WM more anodic [58]. Correspondingly, increasing the C and Mn content of the parent steel may accelerate attack of the PP at the parent plate / weld interface.

2.9 Corrosion susceptibility of welds

Failures due to corrosion and environment assisted cracking often occur at weldments (WM and HAZ). For example, 18 % of the corrosion failures experienced by a major oil industry were caused by preferential weld corrosion, with a large number of stress corrosion cracking and pitting corrosion failures also occurring at weldments [59]. Welding may reduce the resistance to corrosion and environment assisted cracking by altering the composition and microstructure, modifying the mechanical properties, introducing residual stress and creating physical defects. When weldments are selected for use in an aggressive environment, corrosion and stress corrosion tests are conducted to ensure that the proposed welding procedure is satisfactory. However, in practice, a welding operator may deviate from the specified welding procedure and produce a poor quality weldment. Physical defects, such as porosity, undercut, slag inclusions and lack of fusion, can be detected using methods such as visual examination using radiography and ultrasonic probe testing [20].

Preferential corrosion of the weld area of carbon steel fabrications has occurred on ships and chemical plant for over sixty five years [60, 61] and, more recently Dawson et al [62] found that preferential corrosion of the heat affected zone (HAZ) may be mitigated by modifying the alloy composition of the parent plate (PP) to a more noble potential and by control of microstructure through specification of the thermal cycle. Also they found that typical morphologies of preferential weld corrosion are influenced by several factors, such as the environment, flow conditions, the PP composition, weld metal (WM) composition and the weld procedure with changes in any one causing a significant difference in corrosion behaviour. Early weld corrosion

failures due to galvanic effects were overcome by additions of Cu, Cr, Ni and Mo to the weld consumable (filler rod) to produce a cathodic (noble) weld [62].

Weld joint corrosion is much researched [57, 59] from the point of view of corrosion damage, which may occur on the parent plate (PP), heat affected zone (HAZ) or weld metal (WM) regions. The effect of composition, inclusion type and distribution, metallographic structure and the galvanic effects of neighbouring areas must be taken into account.

The microstructure of the WM depends on a number of factors;

- a) Heat input,
- b) Alloy composition-hardenability,
- c) Degree of preheat treatment of work piece and,
- d) Reactions with the shielding gas.

Whilst the microstructure of the HAZ, depends on;

- a) Heat input,
- b) Alloy composition of the PP,
- c) Distribution of inclusions,
- d) Preheat treatment and,
- e) Cooling rate dependent on heat sink of work piece and preheat temperature.

2.10 Summary

The term welding encompasses a wide variety of different fusion joining techniques. Each particular welding technique must be considered separately although the basic guidelines hold for all processes.

Welding is a dynamic process with the rapid formation and solidification of a molten metal joint occurring due to the transient application of a heat source. The majority of widely used processes use a filler metal to bridge a pre-set gap between the two items to be joined. The austenite phase transforms depending up on the cooling rate and weld composition. For low carbon consumable this usually transforms to acicular ferrite with fine pearlite, bainite and martensite and retained austenite between the grains. The metallurgical process of the heat affected zone is one of the thermal cycle and its associated effect on the microstructure. The structure of low carbon steel will be of proeutectoid ferrite at the prior austenite grain boundaries with a ferrite / pearlite or ferrite / bainite structures.

The electrochemical differences between parent plate, heat affected zone and weld metal lead to selective corrosion. However electrochemical difference elements are due to the presence of bainite, manganese sulphide inclusions, retained austenite and macro slag inclusions.

3. Experimental work

3.1 Introduction

The aim of this research project was to conduct an electrochemical study in order to further understand the corrosion behaviour of carbon steel welded pipeline within different aggressive environments, e.g. 3.5% NaCl solution alone and buffered chloride solution with CO₂ saturation.

The materials used in this study are carbon steel welded joints, designated type Y8R27 (St-1), Y8R26 (St-2), Y8R24 (St-3) and 4Y2BJ (St-4).

Emphasis was given to the use of traditional DC steady-state electrochemical techniques such as linear polarisation resistance (LPR), cathodic polarisation and zero resistance ammetry (ZRA). In addition a novel technique e.g. the scanning vibrating electrode technique (SVET) was applied to semi-quantitatively assesses the general corrosion activity of the three different microstructures present from the welding process. In order to achieve these objectives several activities were carried out in the experimental programme. These included a metallographic characterisation study, electrochemical tests and SVET measurements.

3.2 Materials

The carbon steel welded pipeline materials used in this experimental work were sectioned to provide samples having three different microstructures namely, WM, HAZ, and PP respectively. These samples were then used as the reference microstructures used to perform the traditional DC steady state and SVET experiments.

3.3 Chemical composition

The actual chemical compositions of these steels are given in Table 1 as reported by the manufacturer.

Table: 1 Chemical compositions of the welded steels (Wt %)

Materials	C	Si	Mn	P	S	Ni	Cr	Mo	Cu
St-1	0.076	0.324	1.67	0.008	0.0007	0.025	0.023	0.004	0.011
St-2	0.081	0.201	1.62	0.008	0.0005	0.270	0.021	0.008	0.11
St-3	0.081	0.293	1.46	0.01	0.002	0.136	0.027	0.003	0.147
St-4	0.052	0.30	1.40	0.012	0.003	0.04	0.08	0.02	----

The compositions of the weld metal depend on the kind of welding procedures adopted and the composition of the electrodes used. Unfortunately no information on the procedures was available at the time the welds were investigated.

3.4. Mechanical properties

The mechanical properties of the four welded steels are presented in Table 2.

Table 2 Mechanical properties of steels welded pipeline

Materials	Transverse Tensile Properties			Body Charpy, +J	Hardness Hv	CEV
	σ_{uts} , MPa	σ_{ys} , MPa	%El			
St-1	626	516	55.5	274 (-40)	219	0.376
St-2	585	480	51.6	249 (-40)	203	0.382
St-3	632	541	38	149 (-40)	189	0.361
St-4	-----	-----	-----	-----	182	0.310

3.5 Sample preparation

Specimens were prepared by cutting welded joints to give samples having three different microstructures representing; WM, HAZ and PP. Sections taken from weldments for testing are shown in Figure 3. Each one of these specimens consisting of a 1.0 cm^2 cross-section area, was embedded in non-conducting epoxy resin. Electrical contact between the specimen and the electrochemical equipment was made using a steel wire fixed by spot welding to the rearside of the sample, see Figure 4. The wire was isolated with a polymeric material to avoid contact with the electrolyte. Before testing these specimens were mechanically, ground with 320, 400, 600, 800 and finally 1200 grit SiC papers to produce a clean surface finish for every test.

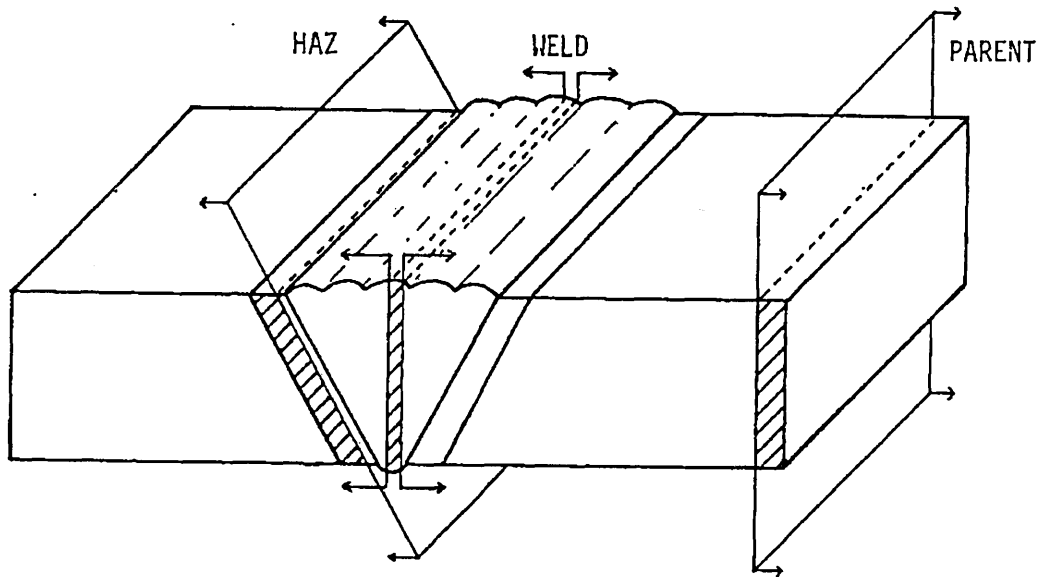


Figure 3 Sections taken from weldments for testing.

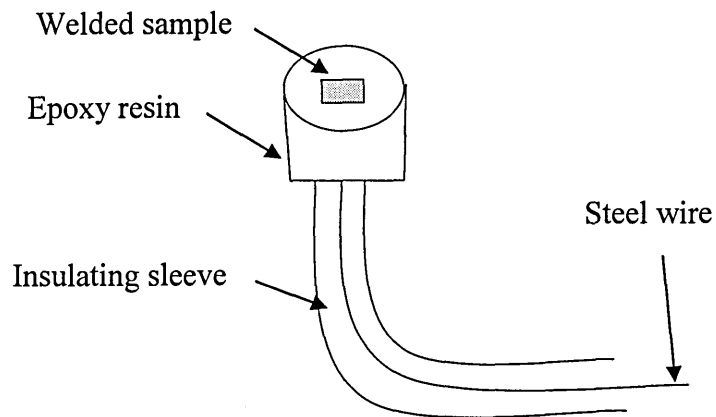


Figure 4 Schematic of the specimen configuration, used in DC corrosion test.

3.6 Microstructural characterisation

General characterisation of the microstructures for the welded steels was performed using an optical light microscope. However detailed weld metal/ heat affected zone characterisation e.g., heat input and consumable materials was beyond the scope of the project because no information was available regarding the welding procedure or the weld consumable.

Specimen grinding was performed using water-cooled silicon carbide papers of 320, 400, 600 and finally with 1200 grit size. Polishing was performed in two steps, starting with an initial diamond paste polish with 6 μm and finally with 1 μm . Samples were then washed with fresh water and finally dried using acetone and hot air. The selected etching method used to develop the microstructure for WM, HAZ and PP segments of the different welded steels was 2% Nital (2 ml HNO_3 + 98 ml $\text{C}_2\text{H}_5\text{OH}$) to reveal the microstructure. Etching of the samples was carried out immediately after the polished samples had been washed and dried.

3.7 Electrochemical tests

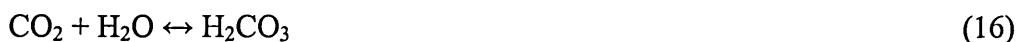
3.7.1 Introduction

Electrochemical tests were performed on samples to assess the electrochemical parameters namely, E_{corr} and LPR, associated with the corrosion performance of these types of steels. The equipment used for these tests include a Thompson Ministat, a PC controlled EG&G Potentiostat and a UNISCAN SVET (SVP100).

Corrosion investigations were performed on the four carbon steels using both individual and coupled sections, e.g., PP/HAZ, HAZ/WM and WM/PP. Individual and coupled samples were exposed to different aqueous environments e.g. 3.5% NaCl (0.6 M) solution with and without CO₂ additions. Carbon dioxide saturated solutions were prepared as follows;

- i) Carbon dioxide was bubbled through the chloride solution about one hour until the solutions were saturated and the pH was stabilised at 6.2.
- ii) Immersion all the samples in the solution with CO₂ bubbling through the solutions throughout the duration of the corrosion tests.

When CO₂ dissolves in the presence of a water phase, carbonic acid forms, which is corrosive to carbon steel. So the cathodic reaction in this case;



At room temperature only about one in a thousand molecules dissociates. For this reason, it is unlikely (usually combined with carbonic acid) to form bicarbonate ion as the major corrosive species.

A simple experimental cell comprising of a glass beaker of 1000 ml capacity was used for all DC electrochemical tests. All measurements were taken within 5 min after immersion of the test sample.

Corrosion potentials are quoted relative to the saturated calomel electrode (SCE). Corrosion potentials have been performed using microelectrode probe droplets to measure changing the E_{corr} across different section for steel welded joints.

The test arrangement for LPR measurements consisted of a counter electrode of platinum wire along with the carbon steel specimens as the working electrode,

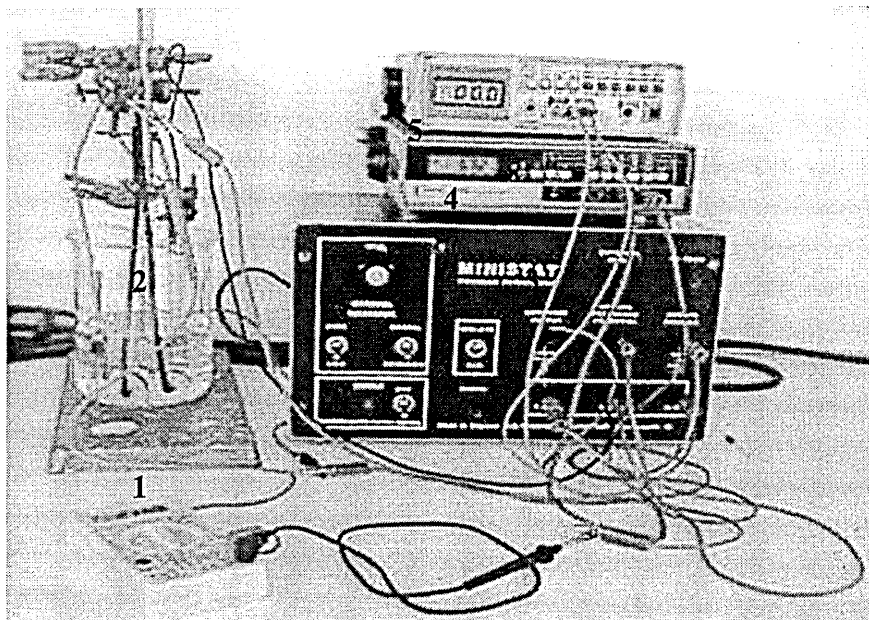
connected with the reference electrode in a conventional three electrodes test cell arrangement, as shown in Figure 5.

The electrochemical system was then left at free corrosion potential for 72 hours to allow the corrosion potential (E_{corr}) to stabilise.

The samples for each new electrochemical test was subject to the surface preparation procedure previously mentioned; therefore every test was conducted with a sample having the same surface finish.

3.7.2 Droplet cell experimental procedure

Electrochemical tests were performed on cross section of the samples taken from different welded carbon steels to assess the electrochemical parameter namely, corrosion potential (E_{corr}) associated with corrosion performance of these types of steels. The technique used for these tests include a microelectrode probe cell.



- 1- Digital voltmeter for measure E_{corr}
- 2 -Three electrodes for corrosion cell (WE, RE and AUX)
- 3 -Potentiostat connected with three electrodes
- 4- Multimeter used for change potential from E_{corr}
- 5- Multimeter used to measure current.

Figure 5 Arrangement of the electrochemical apparatus used to conduct DC-based LPR corrosion tests.

3.7.3 Linear polarisation resistance

Linear polarisation resistance (LPR) is an electrochemical technique for determining corrosion rates. It originated from empirical observations by Simmons [63] and Skold and Larson [64]. It is a widely used technique applied to corrosion monitoring. The polarisation resistance of a material is defined as the slope of the potential-current density ($\Delta E/\Delta i$) curve at the free corrosion potential, yielding the linear polarisation resistance (LPR) that can itself be related to the corrosion current based on the following approximation;

$$\frac{(\Delta E)}{(\Delta i)} = R_p = \frac{B}{i_{corr}} \quad (17)$$

Where;

R_p is the polarisation resistance, $\Omega \cdot \text{cm}^2$.

i_{corr} is the corrosion current, μA .

B an empirical polarisation resistance constant that can be related to the anodic (b_a) and cathodic (b_c) Tafel slopes [65, 66] i.e.

$$B = \frac{b_a \cdot b_c}{2.3(b_a + b_c)} \quad (18)$$

The Tafel slopes themselves can be evaluated experimentally using real polarisation plots. Also, the resistance of the sample can then be calculated using Ohm's law, which is given as;

$$R_p = \frac{\Delta V}{\Delta i} \quad (19)$$

A potentiostat was used to control the applied potential (E_{app}) between the working electrode (sample) and reference electrode (SCE). Changes in potential from E_{corr} were made manually, e.g. ± 5 mV Vs SCE above and below the free corrosion potential. The potential was changed at a rate of 2.5 mV/min. Both current (via a resistor of 2.2 k Ω) and potential were then measured using a digital voltmeter. The linear polarisation resistance measurements were repeated at selected intervals up to a 72 hours period.

3.7.4 Zero resistance ammetry (ZRA)

Experiments were performed using an EG&G Potentiostat connected with a computer within 3.5% NaCl solution alone and buffered chloride solution with CO₂ additions at room temperature for 48 hours. Couples of different microstructures for different steels i.e., PP/HAZ, HAZ/WM and WM/PP respectively were allowed to corrode freely while the current passing between them was measured by connecting a zero resistance ammetry (ZRA) into the circuit, depicted in Figure 6.

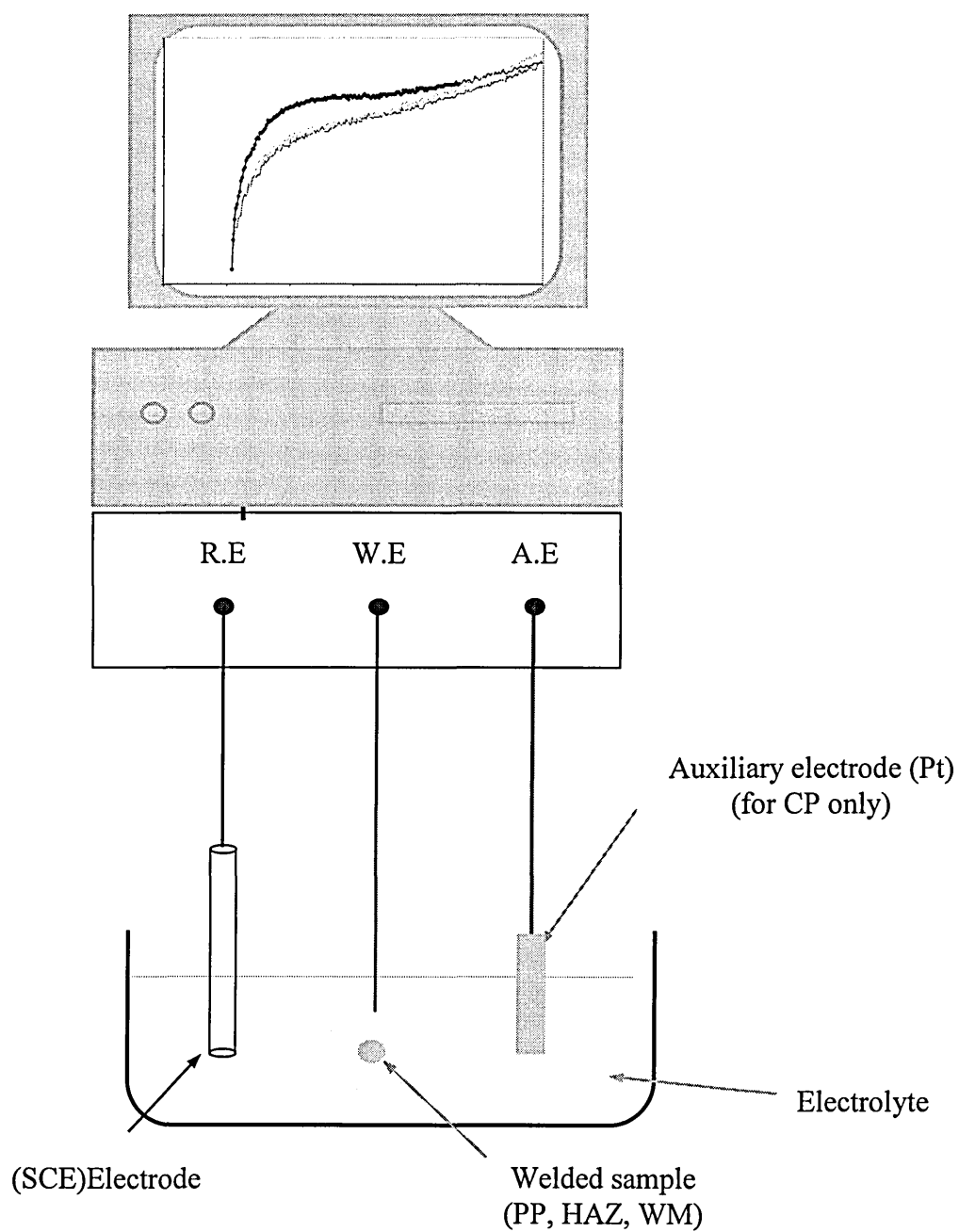


Figure 6 Schematic diagram of the EG&G Potentiostat apparatus used to conduct cathodic polarisation and to connect two samples and reference electrode for ZRA measurements.

3.7.5 Cathodic polarisation curve

Experiments were performed using an EG&G Potentiostat connected with a computer within buffered 0.35% NaCl solution saturated with CO₂ environments at room temperature for five minutes, one hour and four hours respectively. Cathodic polarisation tests were performed to investigate the effect of different immersion times on the development of a protective film on each of the different welded steel microstructures, i.e., WM, HAZ and PP respectively.

3.8 Scanning vibrating electrode technique (SVET)

3.8.1 Introduction

The scanning vibrating electrode technique also, known as, SVP is an electrochemical method, which is able to resolve and quantify highly localised corrosion currents occurring at the metal-electrolyte interface [67]. It consists of a platinum microelectrode tip at the end of insulated wire thinned down to a fine point, positioned close to the surface to be scanned. A schematic of the SVET arrangement is given in Figure 7. The SVET microtip electrode is vibrated mechanically at a constant amplitude and frequency using a simple electromagnetic or piezoelectric driver [68, 69]. The SVET has found a wide range of applications in the study of localised corrosion phenomena [70, 71].

The scanning microtip electrode is vibrated relative to the scanned surface and registers an alternating potential at the vibration frequency, this potential being proportional to electrical field strength or potential gradient in the direction of the

vibration. The alternating potential arises from the oscillation of the microtip in the potential field generated ohmically by the ionic current flux passing through the electrolyte.

3.8.2 SVET measurements

The scanning vibrating electrode technique that is a relatively new technique offers the opportunity to obtain information concerning corrosion activity on a small scale. However, its utilisation to investigate the corrosion of welds has been limited.

SVET experiments were carried out on specimens of different welded sections in two different electrolytes, 0.35% NaCl solution alone and buffered 0.35% NaCl solution saturated with CO₂. Samples were prepared by cutting welded steel pipeline to give specimens having three different segments representing, WM, HAZ and PP combined together on the same sections. Before testing these specimens were mechanically, ground with 400, 600, 800 and finally 1200 grit SiC paper to product clean surface finish for every test and finally coated all other sides from the cross sections of weldments and etched using Nital to obtain three different microstructures. The configuration of the welded samples used in the SVET tests is shown in Figure 8.

The parameters used to conduct the SVET tests were; scan speed of 500 $\mu\text{m}/\text{sec}$, X-Y scan ranges as 51-42 mm, 52-42 mm, 43-29 mm and 35-27 mm for different welded steels 1-4 respectively. The Vibrating Amplitude (VA) used was 30 μm , samples per line was 128 using a sweep scan mode and area scan experiment mode. The probe-sample distance was 100 μm . The SVET measurements have been used to investigate the localised corrosion activity of the four welded steels.

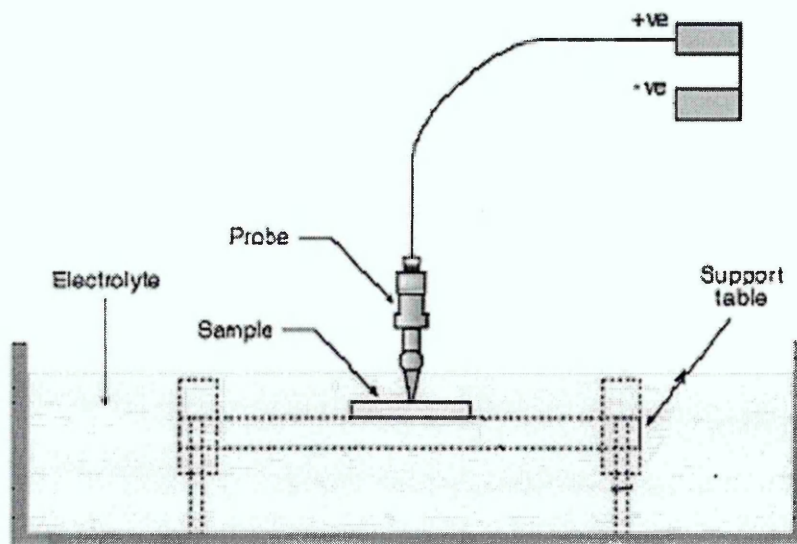


Figure 7 Schematic diagram shows SVET circuit used for measuring corrosion activity of the welded steel samples.

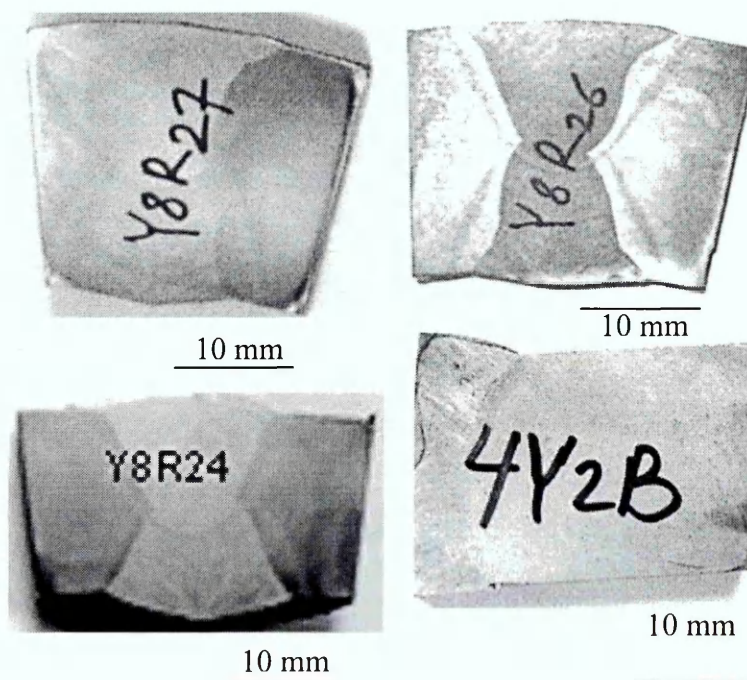


Figure 8 Schematic illustrations of the welded specimens used in the SVET tests.

4. Results

4.1 Introduction

This chapter presents the results obtained from the experiments carried out on Y8R27 (St-1), Y8R26 (St-2), Y8R24 (St-3) and 4Y2BJ (St-4) carbon steel welded pipeline samples. The microstructural features of the three different segments e.g., WM, HAZ and PP for the four welded steels are described in section 4.2.

The results of the electrochemical tests, namely LPR, cathodic polarisation and ZRA methods for each of the four welded steels are given in section 4.3.

Section 4.4 is dedicated to the presentation of the results of SVET measurements within 0.35% NaCl solution alone and buffered chloride solution saturated with CO₂ at open circuit potential (E_{corr}).

4.2 Metallographic studies

To determine the microstructure for different welded steels, metallographic analysis was carried out using an optical light microscope.

The different microstructures of the St-1 is given in Figure 9, i.e., PP, HAZ and WM respectively, Figure 10 shows the individual microstructures of the St-2, whilst the microstructures of the St-3 and St-4 steels are given in Figures 11 and 12 respectively.

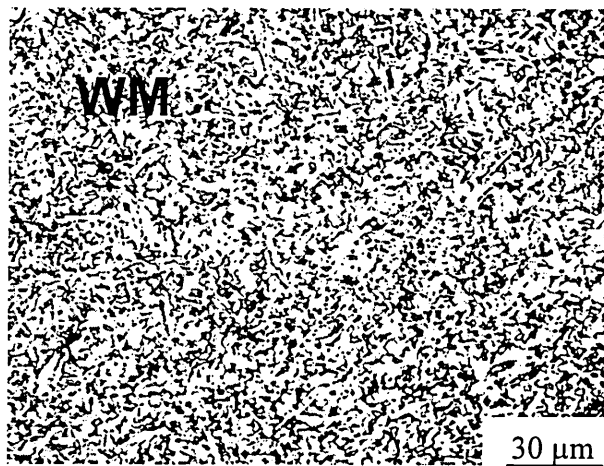
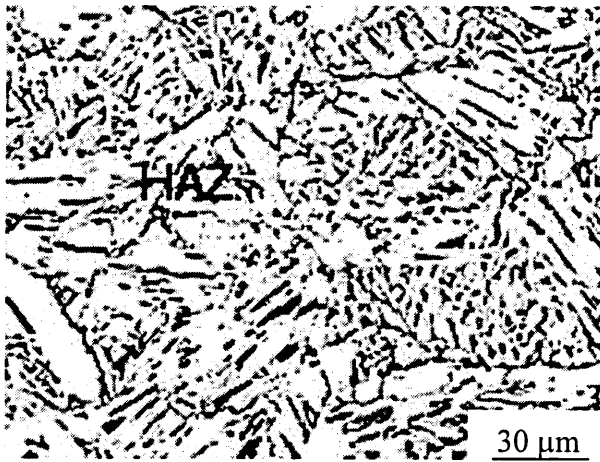
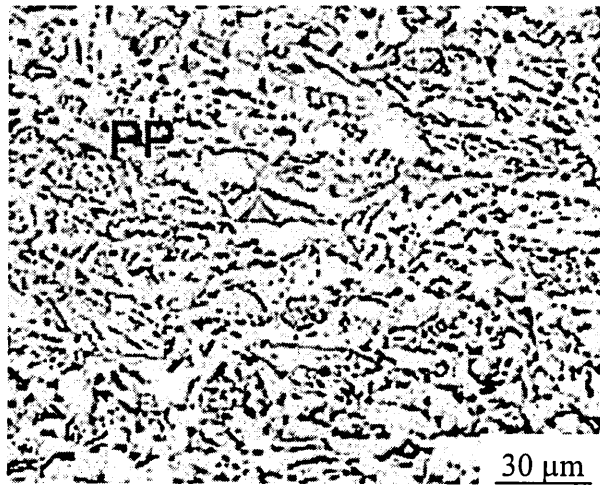


Figure 9 Photo-micrographs showing the general microstructural features of the St-1 welded pipeline steel, 500X.

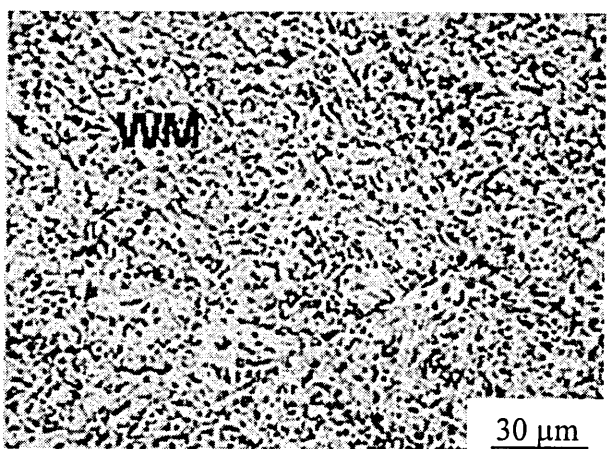
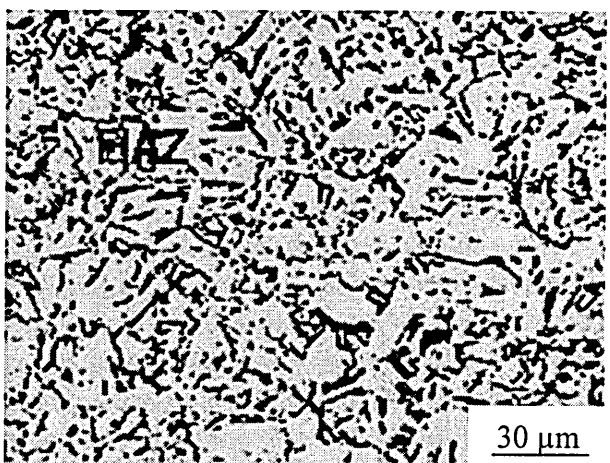
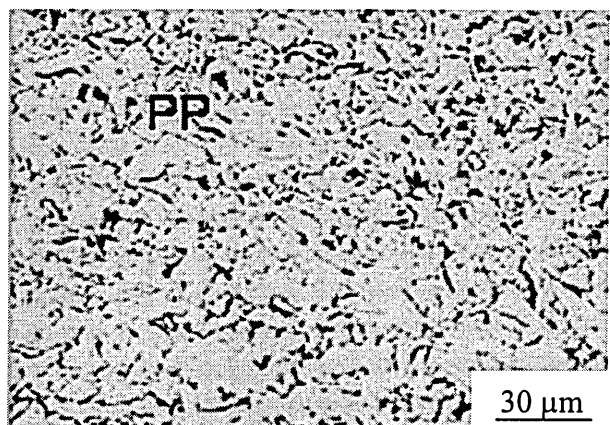


Figure 10 Photo-micrographs showing the general microstructural features of the St-2 welded pipeline steel, 500X.

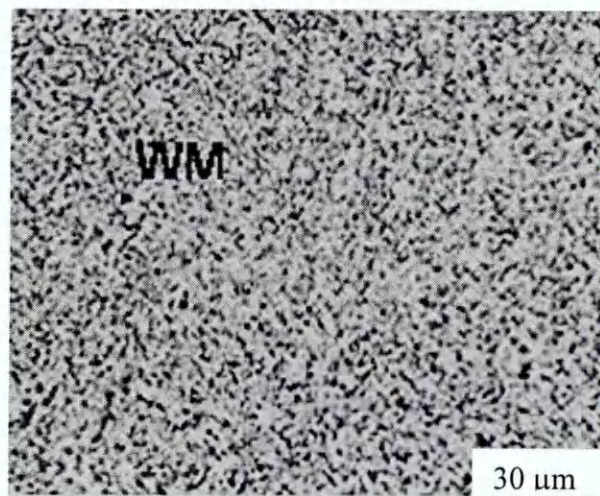
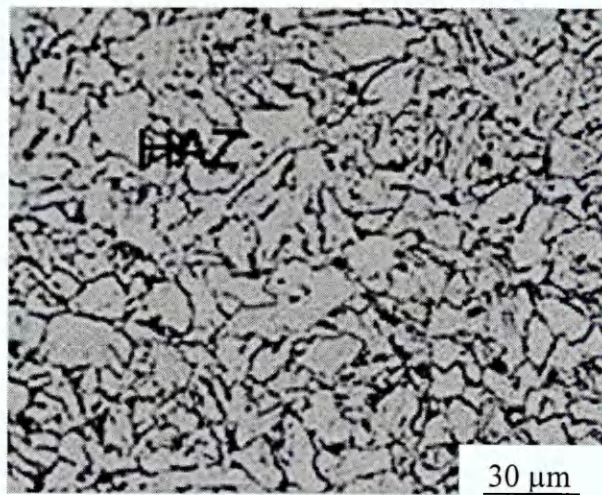
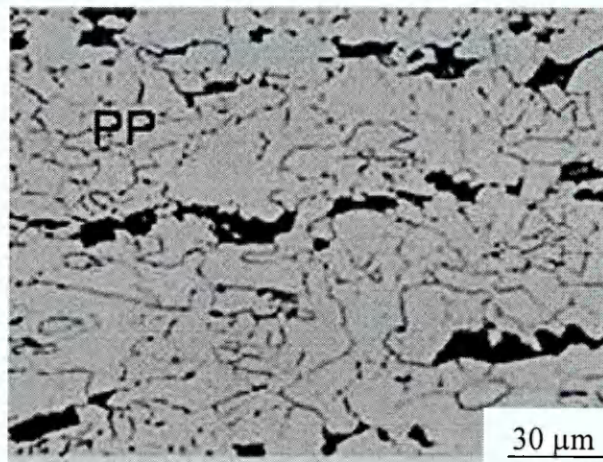


Figure 11 Photo-micrographs showing the general microstructural features of the St-3 welded pipeline steel, 500X.

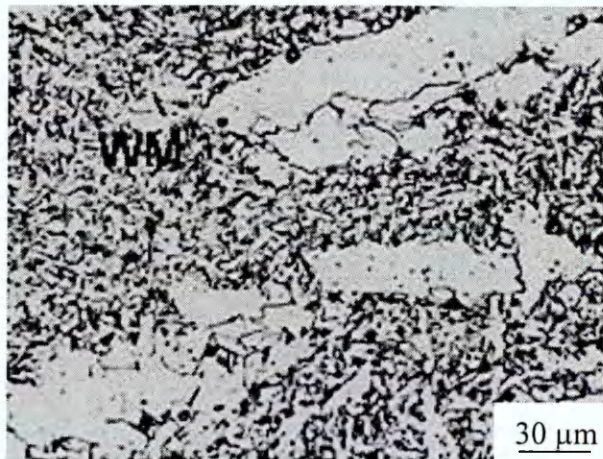
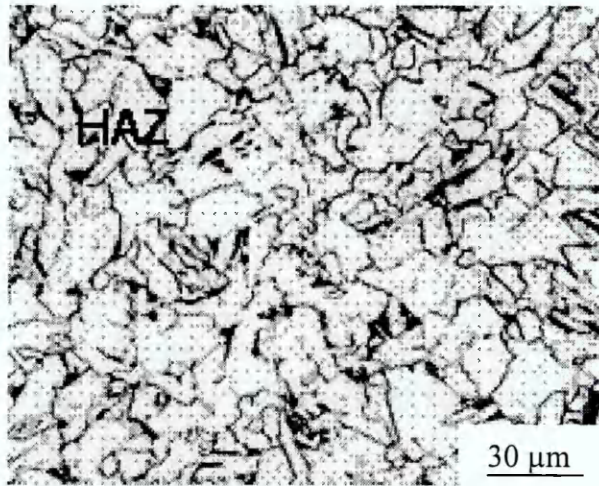
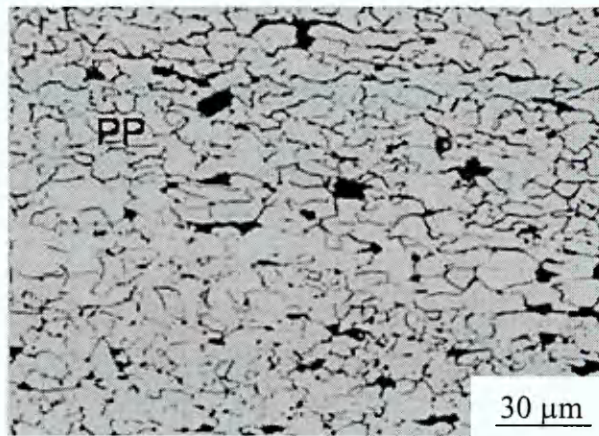


Figure 12 Photo-micrographs showing the general microstructural features of the St-4 welded pipeline steel, 500X.

4.3 DC electrochemical measurements

4.3.1 Average free corrosion potential

Experiments were carried out at room temperature using the ground surface finish for the three different microstructures of welded carbon steels pipeline to determine the corrosion behaviour of carbon steel welded joints after 72 hours immersion within 3.5% NaCl solution and buffered chloride solution with CO₂ saturation respectively. The pH of these solutions was 6.3 ± 0.3 and 6.2 ± 0.1 respectively.

Corrosion potentials measurements of welded samples varied from the cathodic potential to the highest potential for uncoupled and coupled microstructures respectively i.e., WM, HAZ, PP, PP/HAZ, HAZ/WM and WM/PP respectively for Steels 1-4. These values are considered to represent an average value of E_{corr} across the microstructures. All these results have been given after immersed different microstructures for different steels within 3.5% NaCl solution alone and buffered 3.5% NaCl solution with CO₂ saturation for 72 hours are given in Tables 3, 4.

Therefore corrosion potential values for different uncoupled and coupled microstructures of the different welded steels as a function of immersion time have been reported in Tables 5 and 6 for chloride solution alone and Tables 7 and 8 for buffered chloride solution saturated with CO₂ for 72 hours. Thereafter all the results are presented graphically in Figures 13 a and b for uncoupled and coupled different three microstructures respectively for the St-1. Figures 14 a and b present individual and coupled microstructures of the St-2 whilst Figures 15 a and b for different microstructures of the St-3 steel. Finally, Figures 16 a and b present uncoupled and

coupled microstructures of the St-4 steel respectively. All these results have been conducted within 3.5% NaCl solution.

The results for the tests conducted within buffered 3.5% NaCl solution saturated with CO₂ for 72 hours are shown in Figures 17 a and b present different microstructures of the St-1. Figures 18 a and b present different microstructures of the St-2 whilst Figures 19 a and b present different microstructures of the St-3. Finally, Figures 20 a and b present different microstructures of the St-4 welded steel.

4.3.2 Local free corrosion potential

E_{corr} measurements have also been performed using a microelectrode in an attempt to measure the E_{corr} values of the local PP, WM and HAZ regions. The results of these measurements are given in Table 9 for each of the four steels. These measurements were obtained to investigate how the corrosion potential changes across each weldment for the individual steel microstructures.

The consideration of the error values have been estimated ± 10 mV.

Table 3 represents the highest and the lowest potential values, mV Vs (SCE) for uncoupled and coupled different steel microstructures within 3.5% NaCl solution.

materials/segments		maximum potential	minimum potentials
St-1	uncoupled segments	-580	-717
	coupled segments	-580	-727
St-2	uncoupled segments	-527	-713
	coupled segments	-527	-720
St-3	uncoupled segments	-550	-727
	Coupled segments	-557	-728
St-4	uncoupled segments	-554	-734
	coupled segments	-568	-729

Table 4 represents the highest and the lowest potential values, mV Vs (SCE) for the uncoupled and coupled different steel microstructures within buffered 3.5% NaCl solution with CO₂ saturation.

materials/segments		maximum potential	minimum potentials
St-1	uncoupled segments	-739	-766
	coupled segments	-740	-760
St-2	uncoupled segments	-729	-751
	coupled segments	-730	-754
St-3	uncoupled segments	-720	-752
	Coupled segments	-723	-748
St-4	uncoupled segments	-726	-754
	coupled segments	-725	-755

Table 5 represents E_{corr} , mV Vs (SCE) values for individual different welded steel microstructures within 3.5% NaCl solution at pH 6.3 ± 0.3 .

Materials	Time, hrs	5 min	1.0	2.0	8.0	24	48	72
St-1	WM	-580	-651	-678	-670	-714	-715	-715
	HAZ	-584	-650	-647	-679	-705	-702	-700
	PP	-588	-657	-664	-668	-717	-712	-710
St-2	WM	-541	-579	-621	-700	-703	-709	-711
	HAZ	-527	-547	-660	-698	-713	-706	-705
	PP	-531	-652	-585	-650	-702	-703	-696
St-3	WM	-552	-589	-673	-686	-709	-704	-707
	HAZ	-550	-610	-637	-692	-707	-710	-712
	PP	-580	-613	-571	-727	-721	-720	-710
St-4	WM	-554	-565	-590	-640	-706	-710	-708
	HAZ	-582	-646	-648	-642	-734	-729	-721
	PP	-596	-611	-647	-645	-701	-714	-695

Table 6 represents E_{corr} , mV Vs (SCE) values for coupled different welded steel microstructures within 3.5% NaCl solution.

Materials	Time, hrs	5 min	1.0	2.0	8.0	24	48	72
St-1	PP/HAZ	-585	-645	-676	-683	-725	-715	-712
	HAZ/WM	-593	-658	-662	-664	-727	-722	-715
	WM/PP	-580	-621	-657	-680	-708	-706	-704
St-2	PP/HAZ	-527	-555	-651	-690	-720	-715	-713
	HAZ/WM	-558	-590	-650	-684	-706	-704	-699
	WM/PP	-531	-580	-634	-678	-712	-706	-707
St-3	PP/HAZ	-562	-627	-665	-690	-728	-723	-715
	HAZ/WM	-559	-639	-660	-689	-720	-721	-711
	WM/PP	-557	-602	-651	-669	-718	-709	-708
St-4	PP/HAZ	-597	-629	-668	-679	-723	-719	-709
	HAZ/WM	-594	-603	-630	-697	-711	-713	-711
	WM/PP	-568	-584	-602	-675	-729	-722	-721

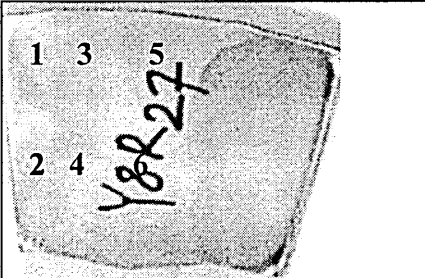
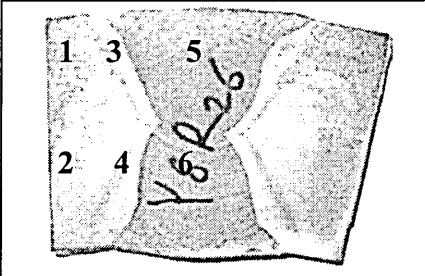
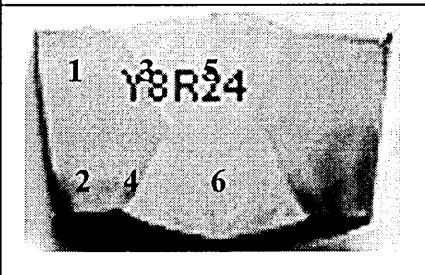
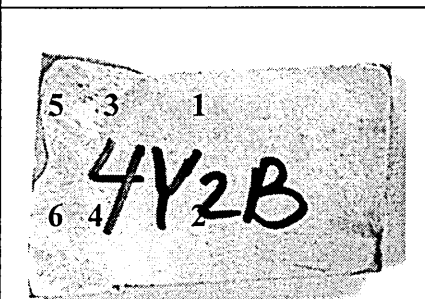
Table 7 represents E_{corr} , mV Vs (SCE) values for individual of welded steel microstructures within buffered 3.5% NaCl solution + CO₂ saturation at pH 6.2 ± 0.1.

Materials	Time, hrs	5 min	1.0	2.0	8.0	24	48	72
St-1	WM	-757	-751	-751	-750	-750	-747	-746
	HAZ	-755	-751	-740	-739	-742	-739	-740
	PP	-766	-753	-748	-749	-745	-751	-750
St-2	WM	-729	-738	-740	-739	-734	-736	-734
	HAZ	-743	-751	-739	-740	-742	-737	-737
	PP	-732	-734	-735	-738	-740	-744	-743
St-3	WM	-740	-742	-742	-738	-739	-736	-735
	HAZ	-720	-726	-728	-729	-728	-731	-730
	PP	-752	-748	-746	-743	-742	-745	-744
St-4	WM	-737	-740	-735	-730	-726	-729	-727
	HAZ	-753	-754	-750	-745	-740	-736	-735
	PP	-740	-736	-742	-739	-728	-731	-730

Table 8 represents E_{corr} , mV Vs (SCE) values for different coupled welded steel microstructures within buffered 3.5% NaCl solution + CO₂ saturation.

Materials	Time, hrs	5 min	1.0	2.0	8.0	24	48	72
St-1	PP/HAZ	-760	-755	-755	-751	-750	-750	-749
	HAZ/WM	-751	-747	-743	-742	-743	-748	-747
	WM/PP	-758	-751	-741	-743	-744	-740	-741
St-2	PP/HAZ	-744	-746	-753	-754	-745	-745	-744
	HAZ/WM	-740	-741	-740	-748	-740	-740	-738
	WM/PP	-730	-737	-730	-745	-739	-734	-733
St-3	PP/HAZ	-738	-736	-726	-723	-724	-726	-725
	HAZ/WM	-723	-729	-735	-732	-727	-729	-728
	WM/PP	-748	-748	-747	-740	-742	-737	-736
St-4	PP/HAZ	-755	-743	-732	-731	-730	-726	-725
	HAZ/WM	-740	-734	-738	-739	-733	-732	-731
	WM/PP	-741	-750	-750	-752	-736	-728	-726

Table 9 represents the local E_{corr} measurements using a microelectrode probe for cross-sections of the different welded steel microstructures.

	<table><tr><th>points</th><th>E_{corr} NaCl</th><th>E_{corr} NaCl/CO₂</th></tr><tr><td>1</td><td>-586 mV</td><td>-600 mV</td></tr><tr><td>2</td><td>-644 mV</td><td>-630 mV</td></tr><tr><td>3</td><td>-659 mV</td><td>-585 mV</td></tr><tr><td>4</td><td>-645 mV</td><td>-625 mV</td></tr><tr><td>5</td><td>-620 mV</td><td>-604 mV</td></tr><tr><td>6</td><td>-632 mV</td><td>-615 mV</td></tr></table>	points	E_{corr} NaCl	E_{corr} NaCl/CO ₂	1	-586 mV	-600 mV	2	-644 mV	-630 mV	3	-659 mV	-585 mV	4	-645 mV	-625 mV	5	-620 mV	-604 mV	6	-632 mV	-615 mV
points	E_{corr} NaCl	E_{corr} NaCl/CO ₂																				
1	-586 mV	-600 mV																				
2	-644 mV	-630 mV																				
3	-659 mV	-585 mV																				
4	-645 mV	-625 mV																				
5	-620 mV	-604 mV																				
6	-632 mV	-615 mV																				
	<table><tr><th>points</th><th>E_{corr} NaCl</th><th>E_{corr} NaCl/CO₂</th></tr><tr><td>1</td><td>-564 mV</td><td>-502 mV</td></tr><tr><td>2</td><td>-590 mV</td><td>-521 mV</td></tr><tr><td>3</td><td>-580 mV</td><td>-500 mV</td></tr><tr><td>4</td><td>-600 mV</td><td>-500 mV</td></tr><tr><td>5</td><td>-610 mV</td><td>-500 mV</td></tr><tr><td>6</td><td>-620 mV</td><td>-504 mV</td></tr></table>	points	E_{corr} NaCl	E_{corr} NaCl/CO ₂	1	-564 mV	-502 mV	2	-590 mV	-521 mV	3	-580 mV	-500 mV	4	-600 mV	-500 mV	5	-610 mV	-500 mV	6	-620 mV	-504 mV
points	E_{corr} NaCl	E_{corr} NaCl/CO ₂																				
1	-564 mV	-502 mV																				
2	-590 mV	-521 mV																				
3	-580 mV	-500 mV																				
4	-600 mV	-500 mV																				
5	-610 mV	-500 mV																				
6	-620 mV	-504 mV																				
	<table><tr><th>points</th><th>E_{corr} NaCl</th><th>E_{corr} NaCl/CO₂</th></tr><tr><td>1</td><td>-505 mV</td><td>-510 mV</td></tr><tr><td>2</td><td>-509 mV</td><td>-530 mV</td></tr><tr><td>3</td><td>-620 mV</td><td>-511 mV</td></tr><tr><td>4</td><td>-648 mV</td><td>-519 mV</td></tr><tr><td>5</td><td>-501 mV</td><td>-503 mV</td></tr><tr><td>6</td><td>-503 mV</td><td>-507 mV</td></tr></table>	points	E_{corr} NaCl	E_{corr} NaCl/CO ₂	1	-505 mV	-510 mV	2	-509 mV	-530 mV	3	-620 mV	-511 mV	4	-648 mV	-519 mV	5	-501 mV	-503 mV	6	-503 mV	-507 mV
points	E_{corr} NaCl	E_{corr} NaCl/CO ₂																				
1	-505 mV	-510 mV																				
2	-509 mV	-530 mV																				
3	-620 mV	-511 mV																				
4	-648 mV	-519 mV																				
5	-501 mV	-503 mV																				
6	-503 mV	-507 mV																				
	<table><tr><th>points</th><th>E_{corr} NaCl</th><th>E_{corr} NaCl/CO₂</th></tr><tr><td>1</td><td>-620 mV</td><td>-535 mV</td></tr><tr><td>2</td><td>-650 mV</td><td>-555 mV</td></tr><tr><td>3</td><td>-623 mV</td><td>-523 mV</td></tr><tr><td>4</td><td>-631 mV</td><td>-565 mV</td></tr><tr><td>5</td><td>-532 mV</td><td>-537 mV</td></tr><tr><td>6</td><td>-568 mV</td><td>-543 mV</td></tr></table>	points	E_{corr} NaCl	E_{corr} NaCl/CO ₂	1	-620 mV	-535 mV	2	-650 mV	-555 mV	3	-623 mV	-523 mV	4	-631 mV	-565 mV	5	-532 mV	-537 mV	6	-568 mV	-543 mV
points	E_{corr} NaCl	E_{corr} NaCl/CO ₂																				
1	-620 mV	-535 mV																				
2	-650 mV	-555 mV																				
3	-623 mV	-523 mV																				
4	-631 mV	-565 mV																				
5	-532 mV	-537 mV																				
6	-568 mV	-543 mV																				

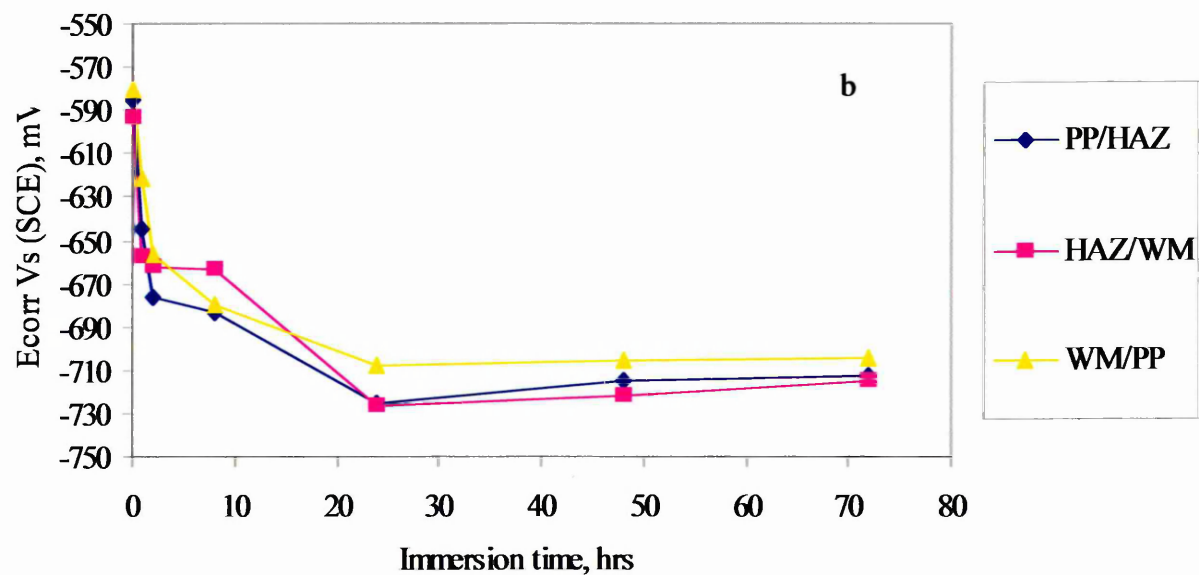
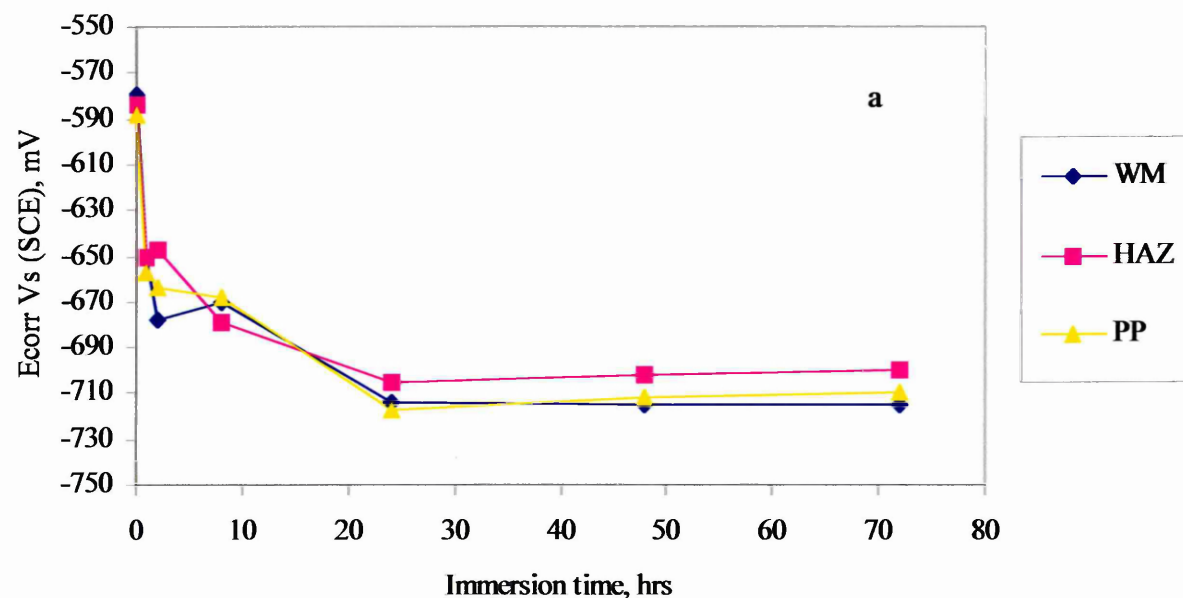


Figure 13 Graph showing, E_{corr} Vs (SCE) versus immersion time for (a) individual and (a) coupled microstructures of the steel St-1 within chloride solution.

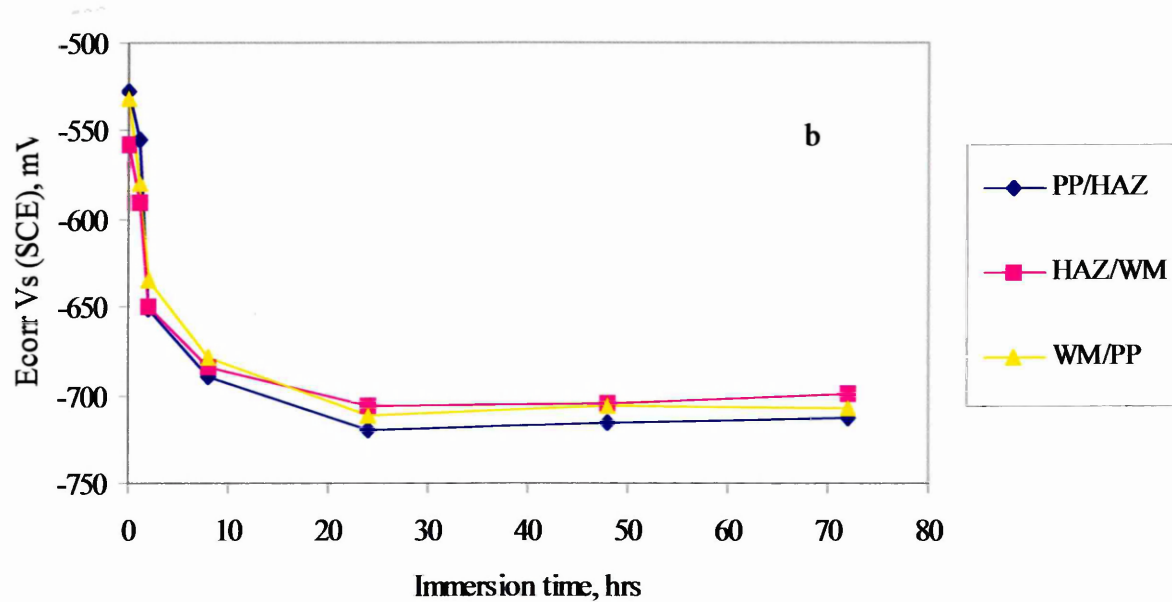
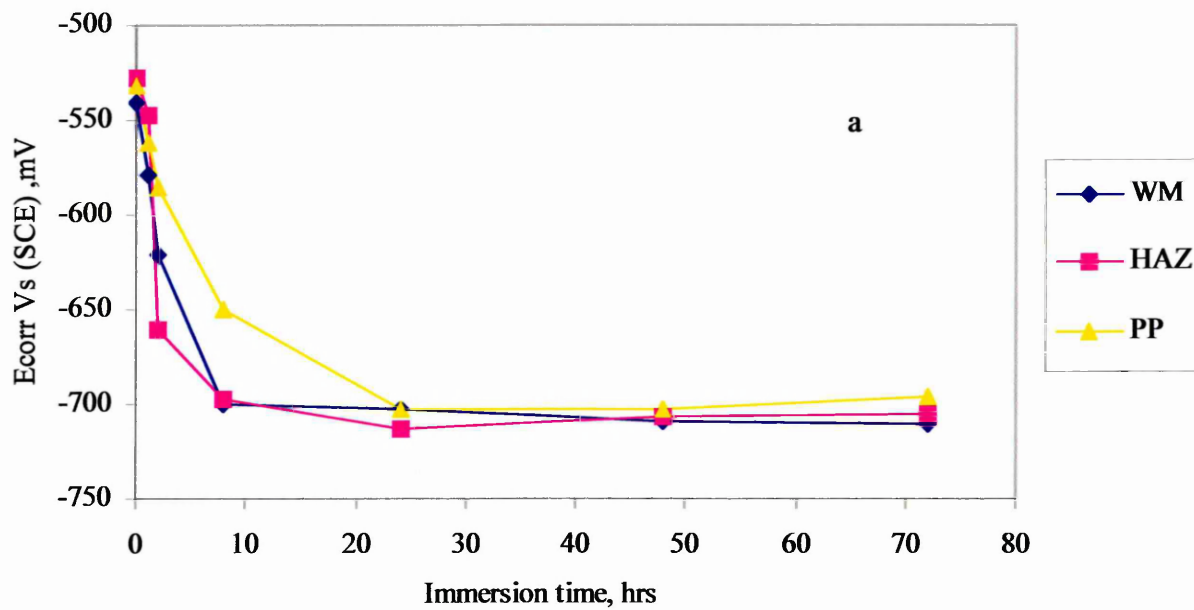


Figure 14 Graph showing, E_{corr} Vs (SCE), versus immersion time for (a) individual and (b) coupled microstructures of the steel St-2 within chloride solution.

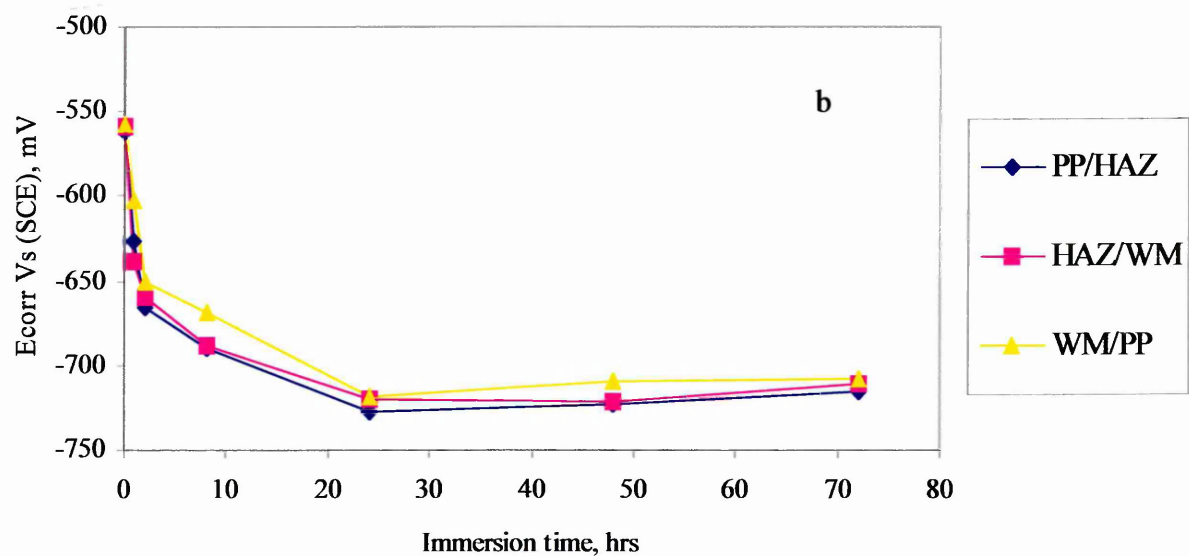
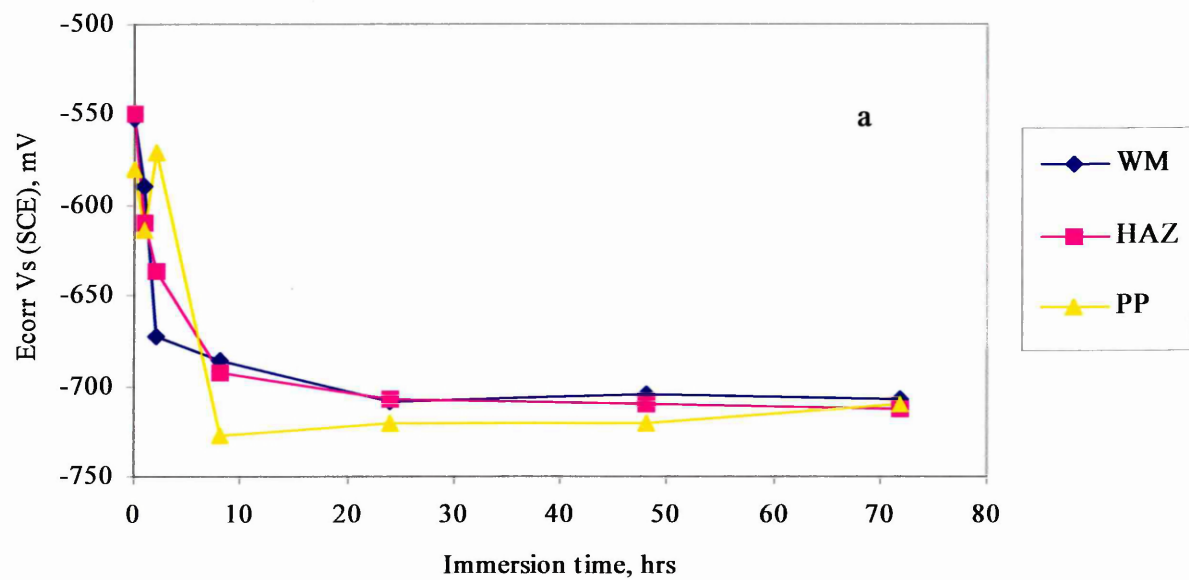


Figure 15 Graph showing, E_{corr} Vs (SCE) as a function of immersion time for (a) individual and (b) coupled microstructures of the steel St-3 within chloride solution.

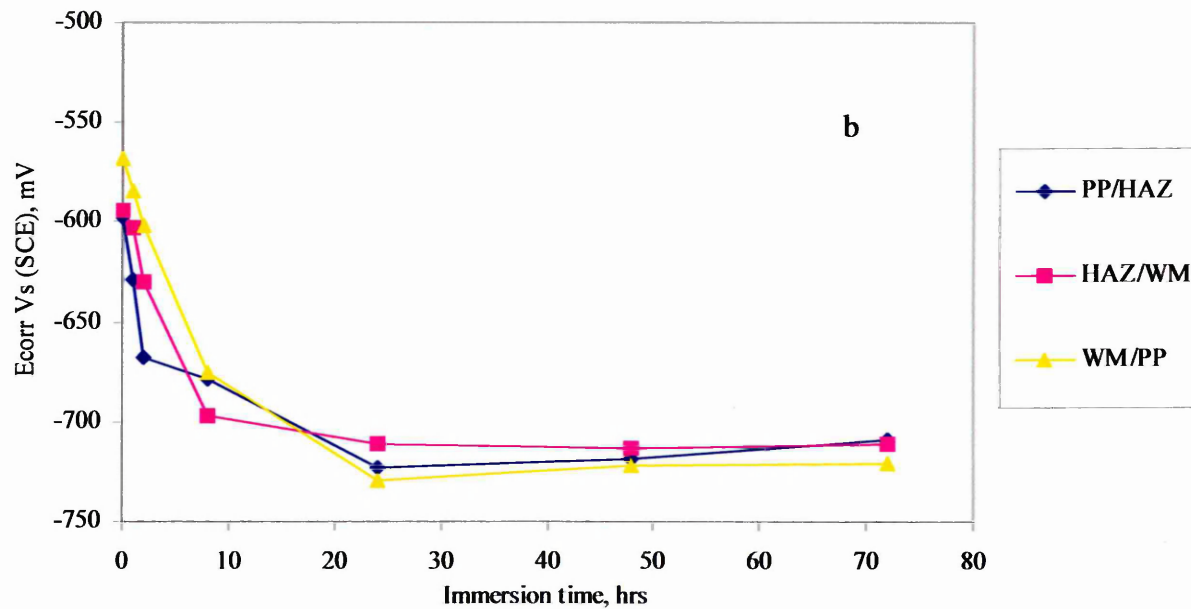
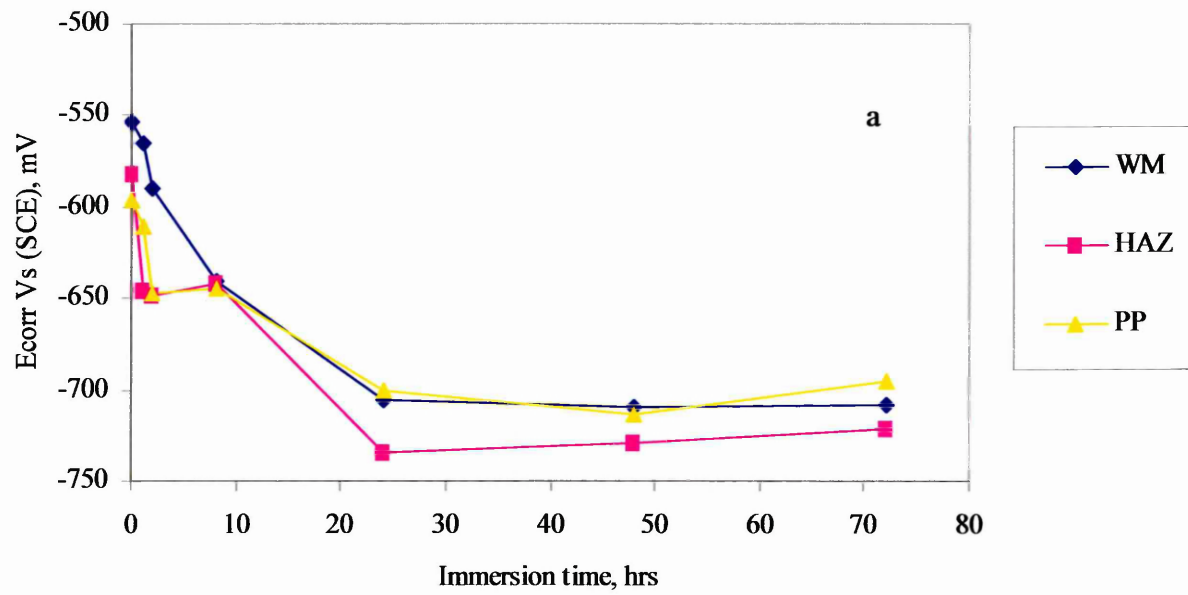


Figure 16 Graph showing, E_{corr} Vs (SCE) as a function of immersion time for (a) individual and (b) coupled microstructures of the steel St-4 within chloride solution.

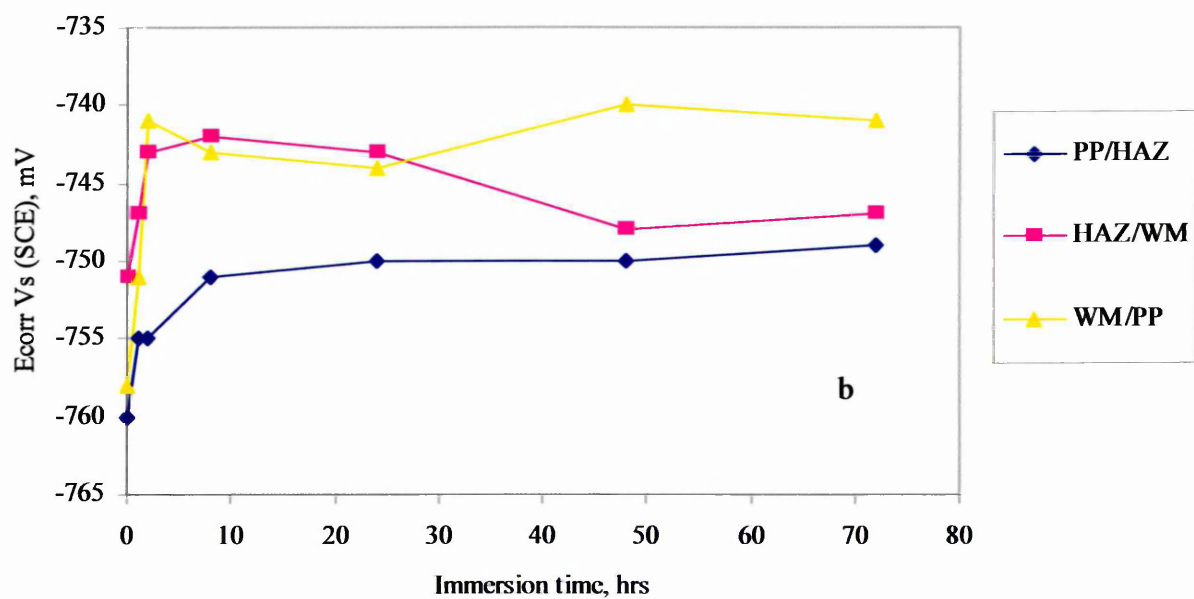
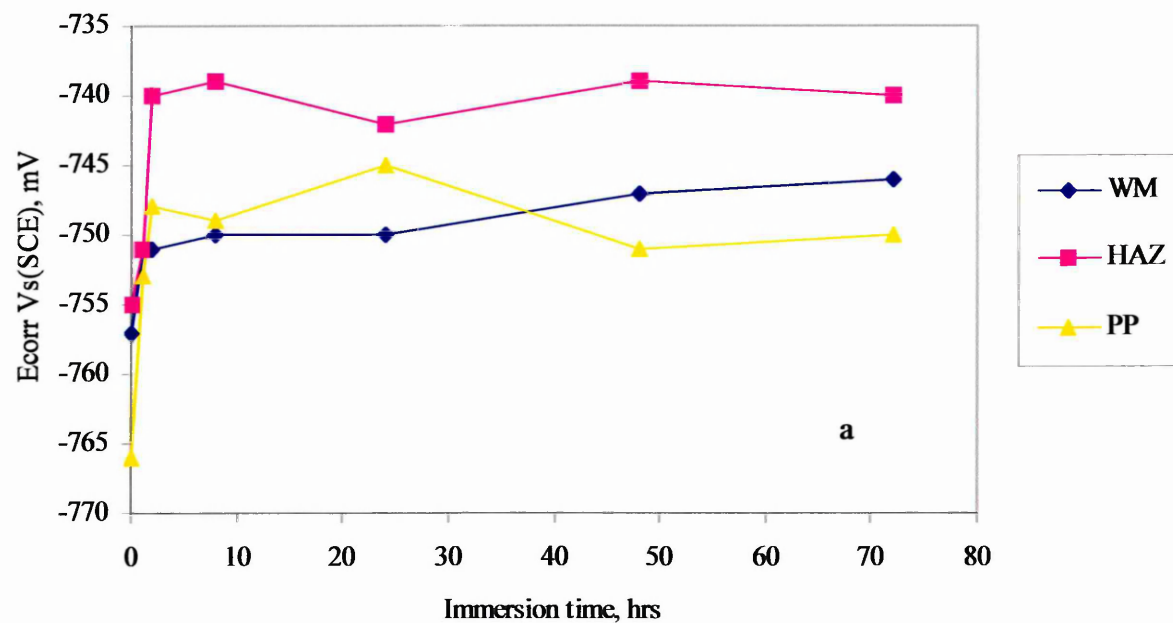


Figure 17 Graph showing, E_{corr} Vs (SCE), versus immersion time for (a) individual and (b) coupled microstructures of the steel St-1 within buffered chloride solution with CO_2 saturation.

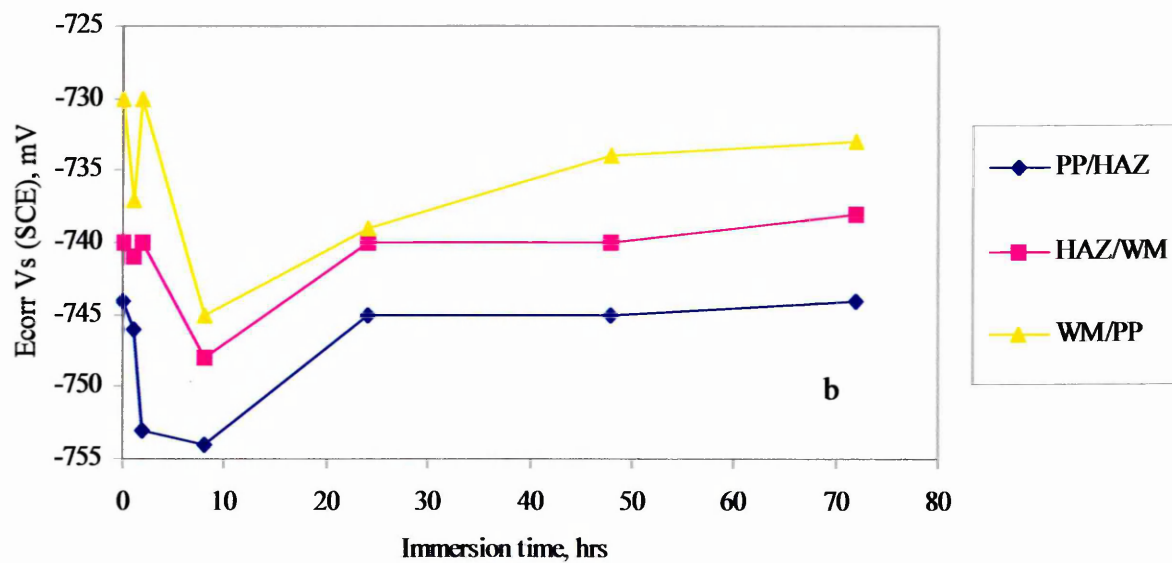
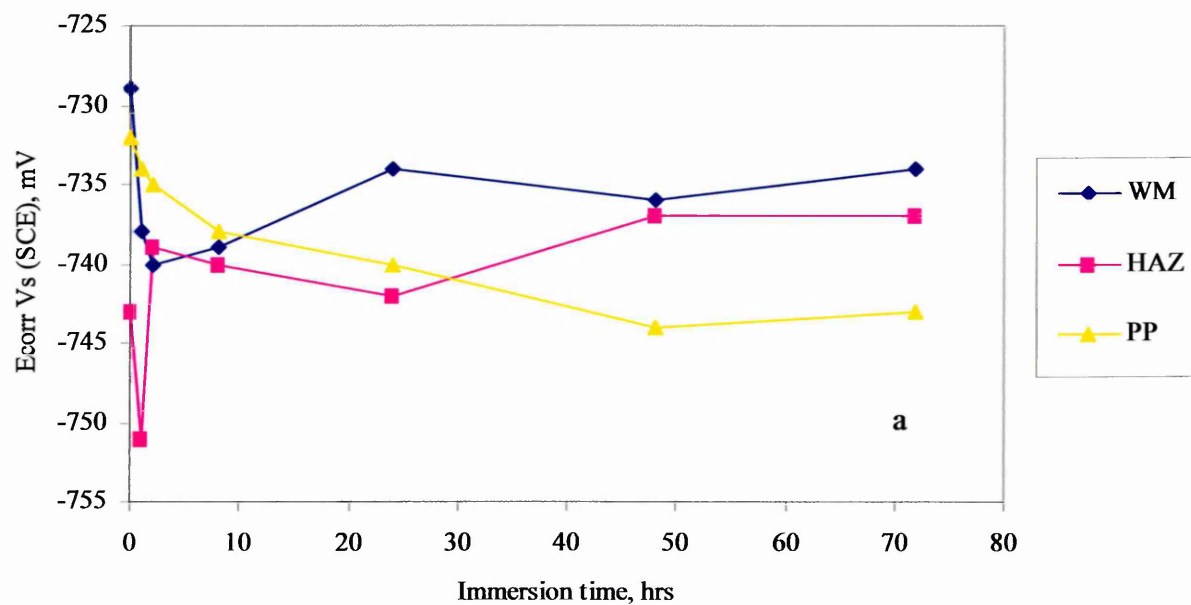


Figure 18 Graph showing, E_{corr} Vs (SCE) versus immersion time for (a) individual and (b) coupled microstructures of the steel St-2 within buffered chloride solution with CO_2 saturation.

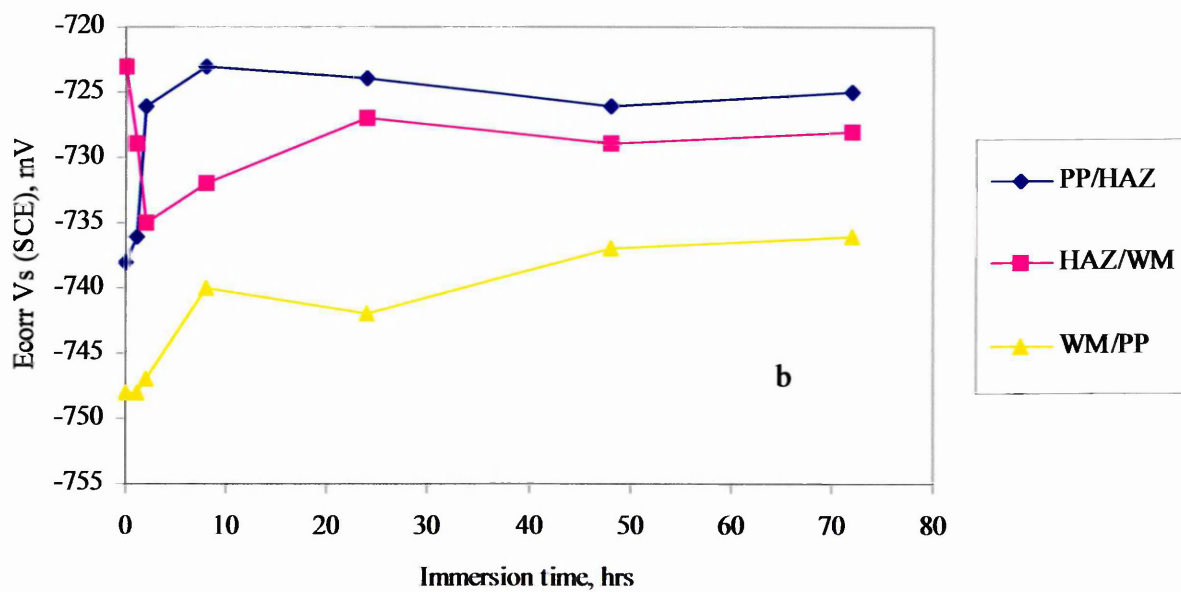
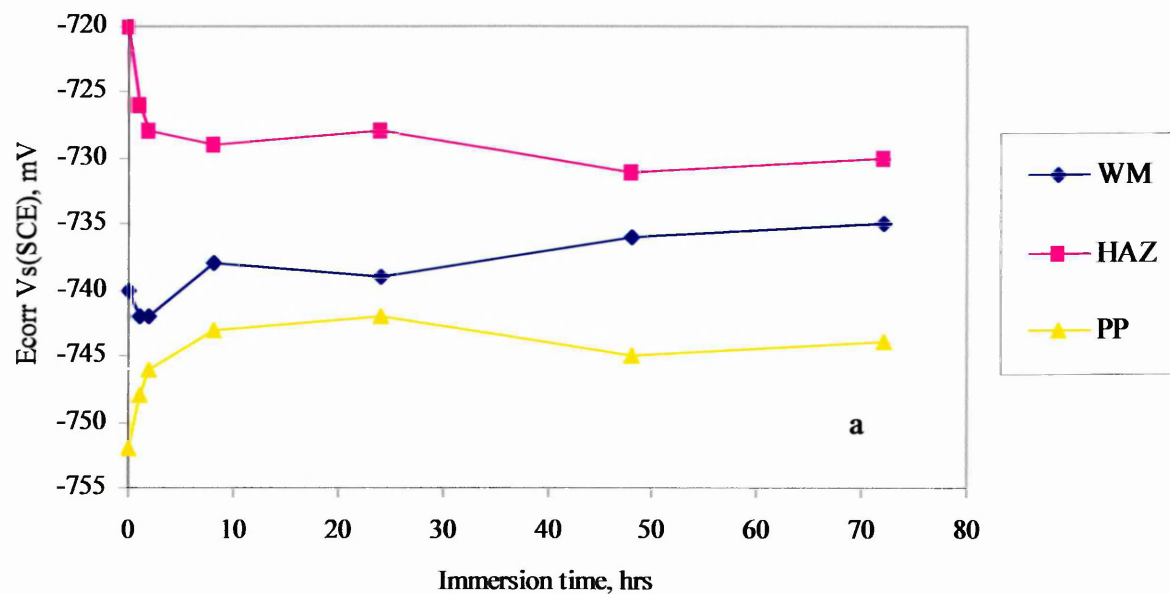


Figure 19 Graph showing, E_{corr} Vs (SCE), versus immersion time for (a) individual and (b) coupled microstructures of the steel St-3 within buffered chloride solution saturated with CO_2 .

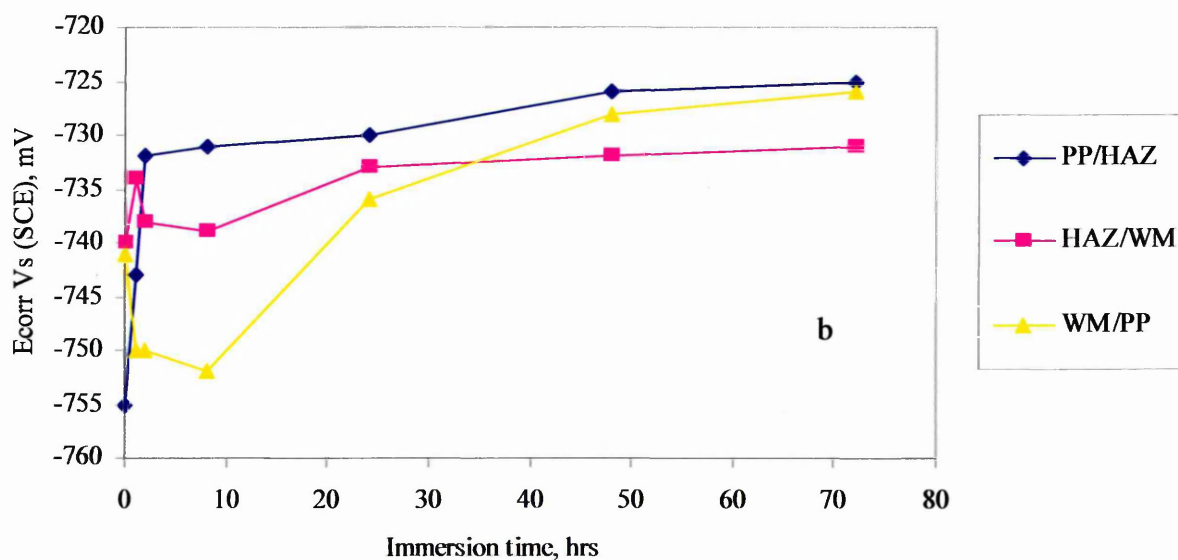
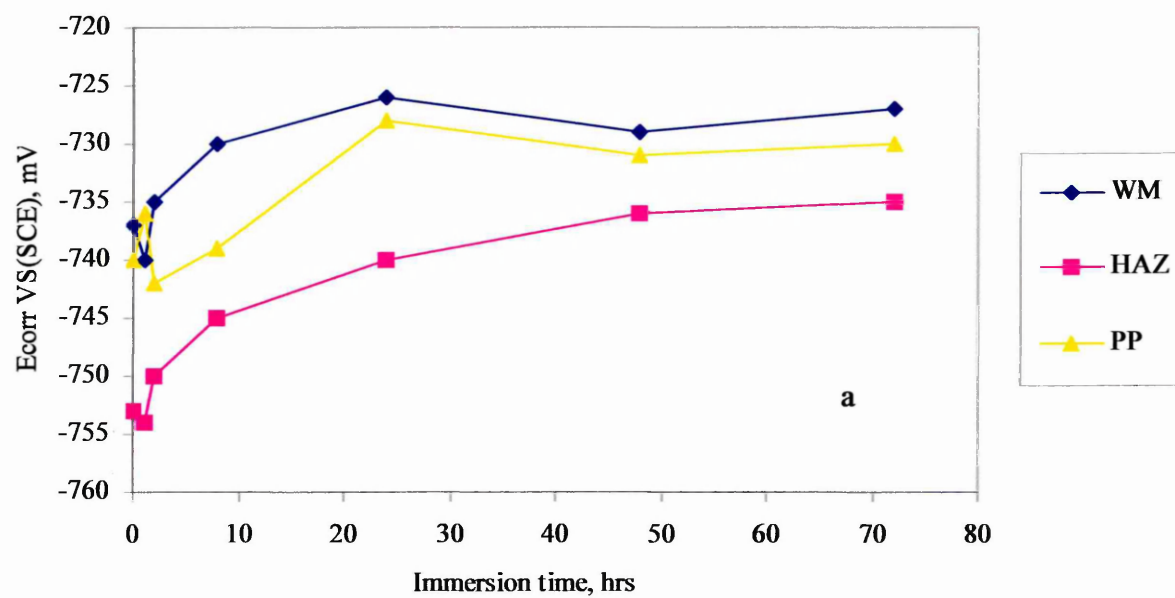


Figure 20 Graph showing, E_{corr} Vs (SCE), versus immersion time for (a) individual and (b) coupled microstructures of the steel St-4 within buffered chloride solution saturated with CO_2 .

4.3.3 Zero resistance ammetry

The average galvanic currents between different microstructures i.e., PP/HAZ, HAZ/WM and WM/PP for welded steels such as St-1, St-2, St-3 and St-4 as a function of immersion time are presented in Figures 21-24 respectively. All these tests have been conducted within different chloride solutions for 48 hours.

For comparison galvanic current values versus immersion time within 3.5% NaCl solution alone and buffered chloride solution saturated with CO₂ for different welded steel microstructures are given in Figures 25-28 respectively. Current flows between two electrodes namely, anode (negative values) and cathode (positive values).

In addition the current density values at 48 hours for coupled different welded steel microstructures with ZRA within different environments have been reported in Tables 10 and 11 respectively.

Table 10 represents current density ($\mu\text{A}/\text{cm}^2$) values from ZRA tests at 48 hrs immersions for coupled steel microstructures within 3.5% NaCl solution.

segments	St-1	St-2	St-3	St-4
PP/HAZ	12.1	12.2	22	13.8
HAZ/WM	-10.8	-5.45	-15.6	9.9
WM/PP	2.71	2.73	8.5	-12.3

Table 11 represents current density ($\mu\text{A}/\text{cm}^2$) values for ZRA tests at 48 hrs immersions for coupled steel microstructures within 3.5% NaCl saturated with CO₂.

segments	St-1	St-2	St-3	St-4
PP/HAZ	3.5	2.4	0.8	1.8
HAZ/WM	11.4	20.7	11.5	8.6
WM/PP	-2.7	-16.4	-15	-2.1

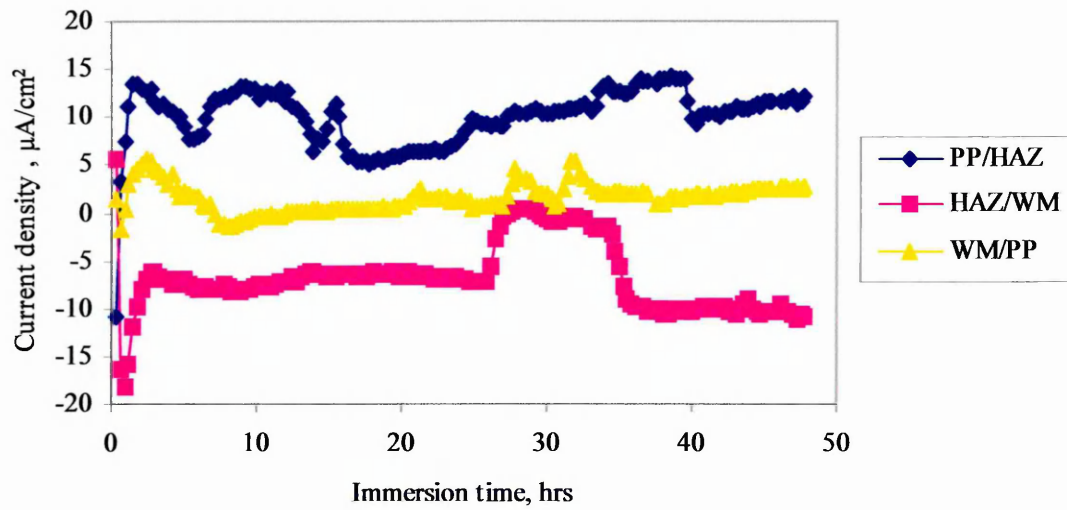


Figure 21 Profile curve showing galvanic current versus immersion time for different microstructures of the St-1 welded steel coupled with ZRA within chloride solution.

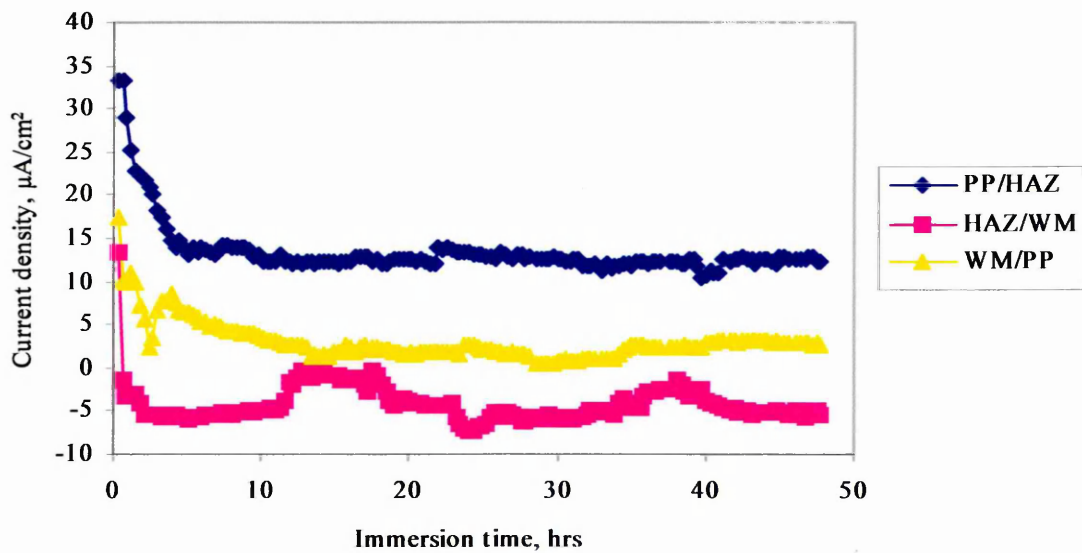


Figure 22 Profile curve showing galvanic current versus immersion time for different microstructures of the St-2 welded steel coupled with ZRA within chloride solution.

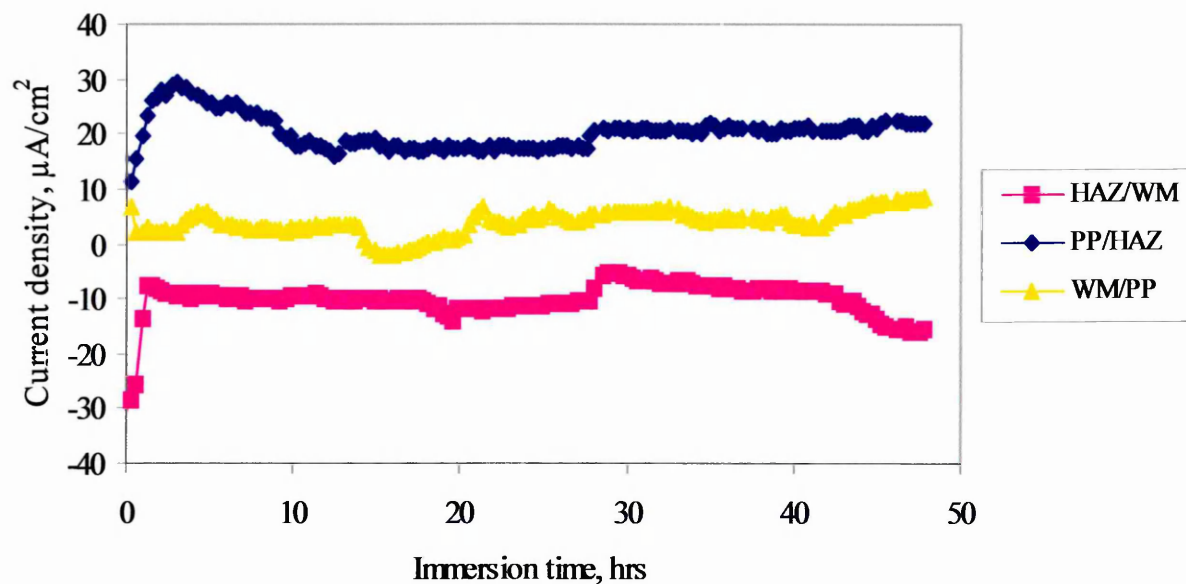


Figure 23 Profile curve showing galvanic current versus immersion time for different microstructures of the St-3 welded steel coupled with ZRA within chloride solution.

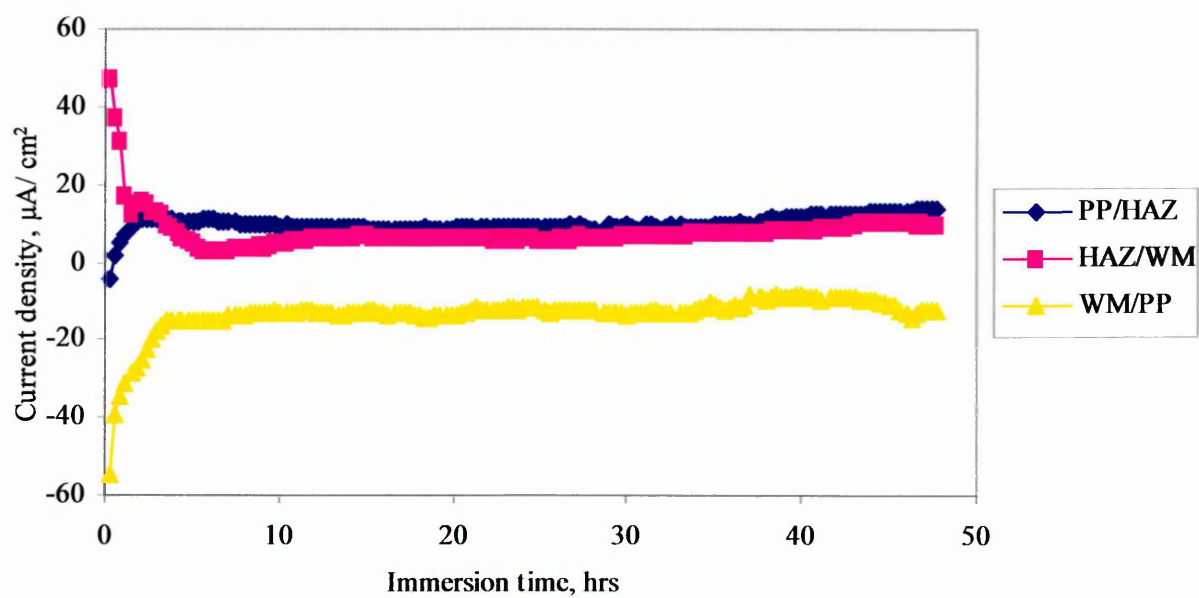


Figure 24 Profile curve showing galvanic current versus immersion time for different microstructures of the St-4 welded steel coupled with ZRA within chloride solution.

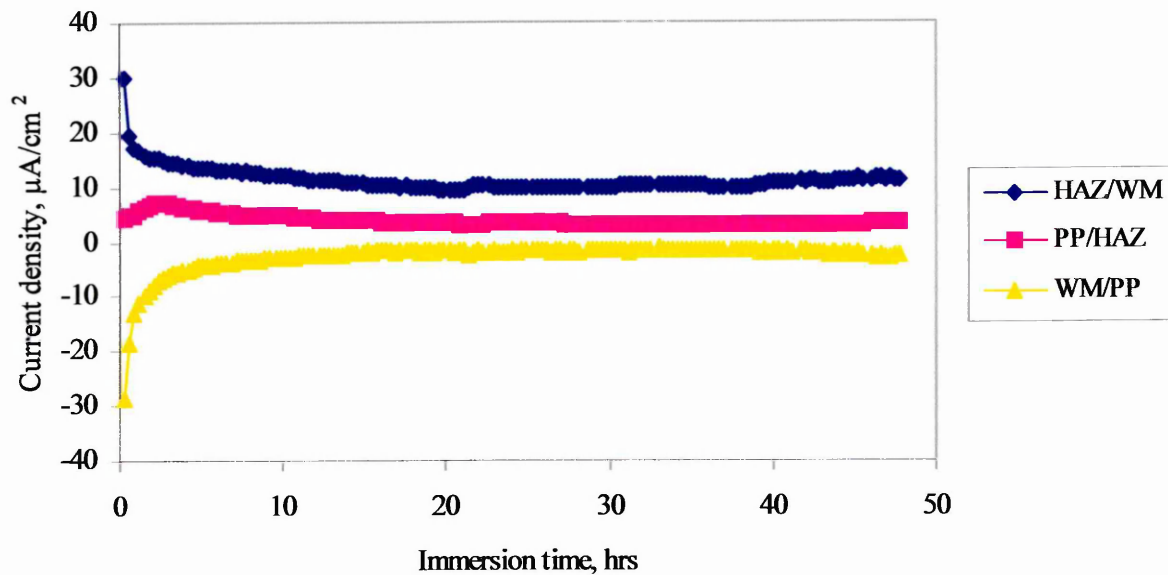


Figure 25 Profile curve showing galvanic current versus immersion time for different microstructures of the St-1 steel coupled with ZRA within buffered chloride solution saturated with CO₂.

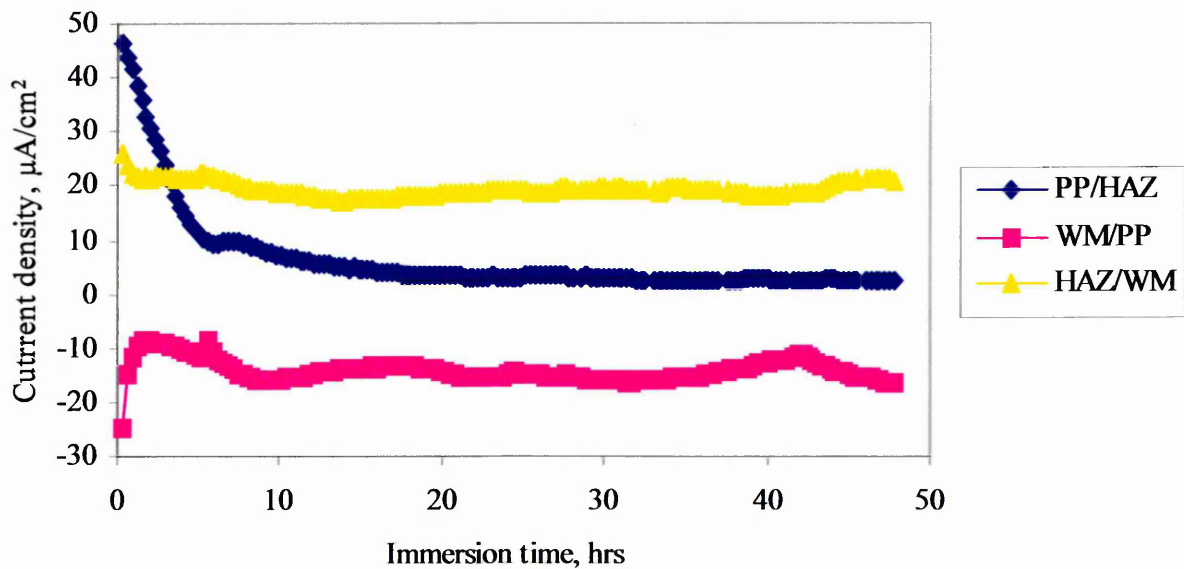


Figure 26 Profile curve showing galvanic current versus immersion time for different microstructures of the St-2 steel coupled with ZRA within buffered 3.5% NaCl solution saturated with CO₂.

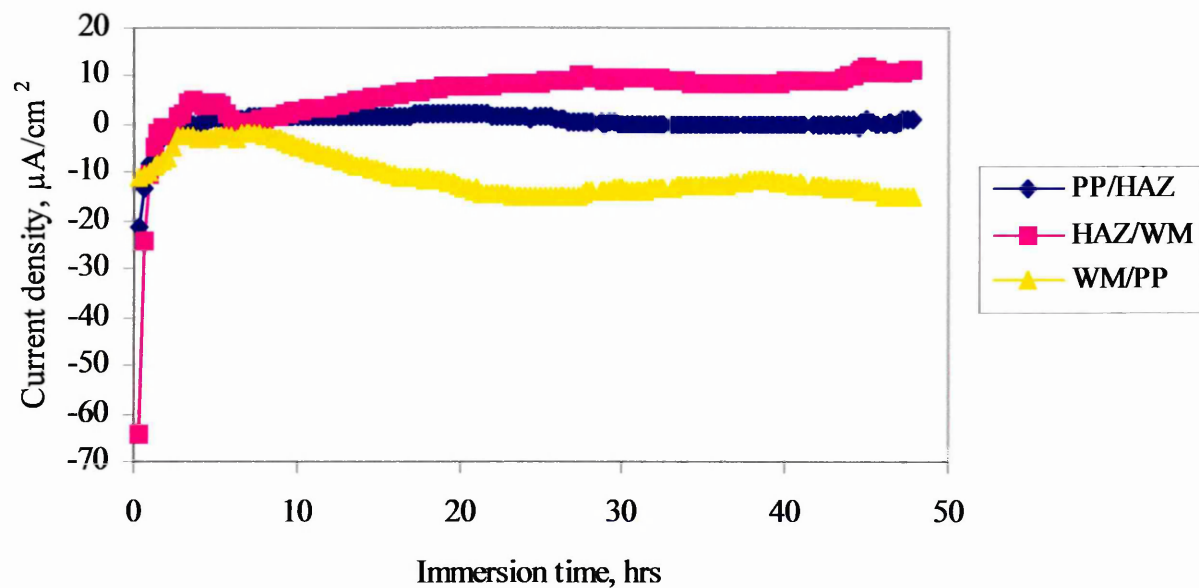


Figure 27 Graph plots showing galvanic current versus immersion time for different microstructures of the St-3 steel coupled with ZRA within buffered 3.5% NaCl solution with CO_2 saturation.

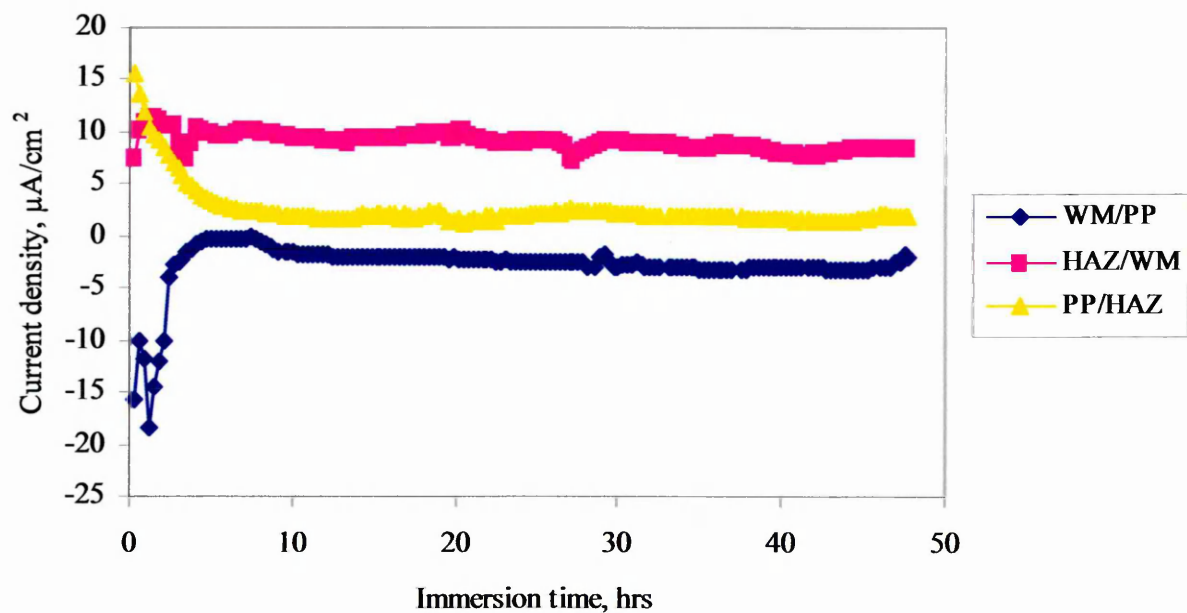


Figure 28 Graph plots showing galvanic current versus immersion time for different microstructures of the St-4 steel coupled with ZRA within buffered 3.5% NaCl solution with CO_2 saturation.

4.3.4 Linear polarisation resistance

The corrosion rate has been directly related to the LPR and can therefore be calculated from its value [44]. The LPR value allows us to assess the relative ability of a material to resist corrosion. Since LPR is inversely proportional to I_{corr} , the materials with the highest LPR value exhibit the lowest corrosion rate. Based on this it can discuss the data obtained from the LPR tests, which are listed in Tables 12 and 13 for individual and coupled different microstructures of the four steels within aqueous 3.5% NaCl solution. Tables 14 and 15 show the equivalent results for the four different microstructures of welded steels within buffered chloride solution with CO_2 saturation. Corrosion rates of each region are calculated using equation 17, where LPR Tafel slopes b_a and b_c for carbon steel welded joints were reported by Gulbrandsen et al [72] for CO_2 containing environments and Sephton and Pistoruis [73] for chloride solution only, where $b_a = 62 \text{ mV/decade}$ and $b_c = 166 \text{ mV/decade}$. The LPR constant B calculated using equation 18 is 20 mV. This value was used in the corrosion current calculation in equation 16 for both environments for all microstructures of the welded steels. The average LPR constant B for this experimental work within chloride solution saturated with CO_2 calculated based upon an analysis of the cathodic polarisation tests was 23 mV, i.e., only 3 mV difference from the literature value.

LPR values as a function of immersion time for individual and coupled different microstructures, are given experimentally in Figures 29 a and b for St-1, Figures 30 a and b for St-2, Figures 31 a and b for St-3 and Figures 32 a and b for St-4. LPR values as a function of immersion time are given in Figures 33-36 (a and b) for individual

and coupled different microstructures within buffered 3.5% NaCl solution with CO₂ saturation. Comparison of the LPR values within 3.5% NaCl solution alone for coupled and uncoupled samples are given in Figures 38-41 for steels 1-4 and Figures 42-45 present graphs of the LPR values for individual and coupled different welded steel microstructures versus immersion time for steels 1-4 within buffered 3.5% NaCl solution with CO₂ saturation.

The stationary current values were measured after one-minute duration of polarisation. Polarisation measurements were conducted at a scan rate of 2.5 mV/min (0.15 V/h) from potential just ± 5 mV above and below E_{corr} . Generally two runs every 1-minute was sufficient to establish the parameters for a particular test condition until a constant current is established. Corrosion rates were determined using the linear polarisation resistance technique using a manual mode potentiostat.

Experiments were conducted for the three different welded steel microstructures for immersion times up to 72 hours. During the linear polarisation resistance measurements, a controlled potential scan over a small range (± 5 mV with scan rate 2.5 mV/min) with respect to the corrosion potential (E_{corr}) was applied.

This programme is based on the work of Wagner and Traud [74] and Stern and Geary [75]. The steady state currents obtained from the anodic and cathodic regions are plotted against overall potential and the slope of the curve obtained at $i = 0$ gives the LPR according to equation 18. LPR is determined simply by taking the slope of the potential current density curve at free corrosion potential. Once measured a value of LPR may be used to estimate the corrosion rate according to the equation 16.

Table 12 LPR, ($\Omega \cdot \text{cm}^2$) values for individual different welded steel microstructures within chloride solution (3.5%NaCl).

Materials	Time, hrs	1.0	8.0	24	48	72
St-1	WM	209	1698	1047	1096	955
	HAZ	1698	1148	1096	1047	832
	PP	851	1905	1698	1820	1995
St-2	WM	646	1047	1047	851	813
	HAZ	851	1820	1698	1820	1950
	PP	759	1000	1148	1096	1230
St-3	WM	631	1698	1096	1288	1413
	HAZ	316	1585	427	501	550
	PP	457	1820	1230	1047	1288
St-4	WM	562	437	661	724	759
	HAZ	759	1122	1148	1047	1096
	PP	245	398	741	955	912

Table 13 LPR, ($\Omega \cdot \text{cm}^2$) values for coupled different welded steel microstructures within chloride solution (3.5% NaCl).

Materials	Time, hrs	1.0	8.0	24	48	72
St-1	PP/HAZ	617	589	1288	1175	1122
	HAZWM	646	661	891	813	891
	WM/PP	550	603	776	1023	1047
St-2	PP/HAZ	1288	741	1479	1413	1380
	HAZ/WM	363	550	933	1096	1096
	WM/PP	661	708	1096	977	1023
St-3	PP/HAZ	316	1096	912	891	851
	HAZ/WM	398	1479	741	933	912
	WM/PP	513	871	1380	1148	1023
St-4	PP/HAZ	437	871	1023	1072	933
	HAZ/WM	363	741	933	891	832
	WM/PP	468	631	724	708	676

Table 14 LPR, ($\Omega \cdot \text{cm}^2$) values for individual different welded steel microstructures within buffered chloride solution (3.5% NaCl) with CO_2 saturation.

Materials	Time, hrs	1.0	8.0	24	48	72
St-1	WM	240	257	316	245	234
	HAZ	501	427	550	479	427
	PP	447	389	372	468	398
St-2	WM	234	219	251	200	182
	HAZ	501	589	447	398	355
	PP	447	437	472	468	417
St-3	WM	200	240	229	224	195
	HAZ	219	490	347	316	372
	PP	347	513	437	407	398
St-4	WM	224	363	234	347	339
	HAZ	331	468	631	776	832
	PP	170	437	407	447	425

Table 15 LPR, ($\Omega \cdot \text{cm}^2$) values for coupled welded steel microstructures within buffered chloride solution (3.5% NaCl) with CO_2 saturation.

Materials	Time, hrs	1.0	8.0	24	48	72
St-1	PP/HAZ	339	398	437	398	380
	HAZ/WM	257	275	301	257	275
	WM/PP	363	288	363	347	363
St-2	PP/HAZ	339	398	436	407	427
	HAZ/WM	257	251	316	269	281
	WM/PP	363	324	363	339	372
St-3	PP/HAZ	275	363	331	324	339
	HAZ/WM	240	295	363	363	363
	WM/PP	295	257	457	437	457
St-4	PP/HAZ	398	275	407	363	437
	HAZ/WM	229	295	339	316	398
	WM/PP	316	275	490	537	617

Table 16 represents corrosion rates obtained from LPR measurements after 72 hours for individual and coupled different welded steel microstructures within chloride solution alone (3.5% NaCl).

Materials	segments	LPR ($\Omega \cdot \text{cm}^2$)	mA/cm^2	mm/yr
St-1	WM	955	0.021	0.24
	HAZ	832	0.024	0.28
	PP	1995	0.010	0.12
St-2	WM	813	0.025	0.29
	HAZ	1950	0.010	0.12
	PP	1230	0.016	0.19
St-3	WM	1413	0.014	0.16
	HAZ	550	0.036	0.42
	PP	1288	0.016	0.19
St-4	WM	759	0.026	0.30
	HAZ	1096	0.018	0.21
	PP	912	0.022	0.26

Materials	segments	LPR ($\Omega \cdot \text{cm}^2$)	mA/cm^2	mm/yr
St-1	PP/HAZ	1122	0.018	0.21
	HAZ/WM	891	0.022	0.26
	WM/PP	1047	0.019	0.22
St-2	PP/HAZ	1380	0.014	0.16
	HAZ/WM	1096	0.018	0.21
	WM/PP	1023	0.020	0.23
St-3	PP/HAZ	851	0.024	0.28
	HAZ/WM	912	0.022	0.26
	WM/PP	1023	0.020	0.23
St-4	PP/HAZ	933	0.021	0.24
	HAZ/WM	832	0.024	0.28
	WM/PP	676	0.030	0.35

Table 17 represents corrosion rates obtained from LPR measurements after 72 hours for individual and coupled different welded steel microstructures within buffered chloride solution (3.5% NaCl) with CO₂ saturation.

Materials	segments	LPR ($\Omega \cdot \text{cm}^2$)	mA/cm^2	mm/yr
St-1	WM	234	0.085	1.0
	HAZ	427	0.047	0.55
	PP	398	0.050	0.58
St-2	WM	182	0.11	1.28
	HAZ	355	0.056	0.65
	PP	417	0.048	0.56
St-3	WM	195	0.10	1.16
	HAZ	372	0.054	0.63
	PP	398	0.050	0.58
St-4	WM	339	0.059	0.68
	HAZ	832	0.024	0.28
	PP	425	0.047	0.54

Materials	segments	LPR ($\Omega \cdot \text{cm}^2$)	mA/cm^2	mm/yr
St-1	PP/HAZ	380	0.053	0.61
	HAZ/WM	275	0.073	0.85
	WM/PP	363	0.055	0.64
St-2	PP/HAZ	427	0.047	0.54
	HAZ/WM	281	0.071	0.82
	WM/PP	372	0.054	0.62
St-3	PP/HAZ	339	0.059	0.68
	HAZ/WM	363	0.055	0.64
	WM/PP	457	0.044	0.51
St-4	PP/HAZ	437	0.046	0.53
	HAZ/WM	398	0.050	0.58
	WM/PP	617	0.032	0.37

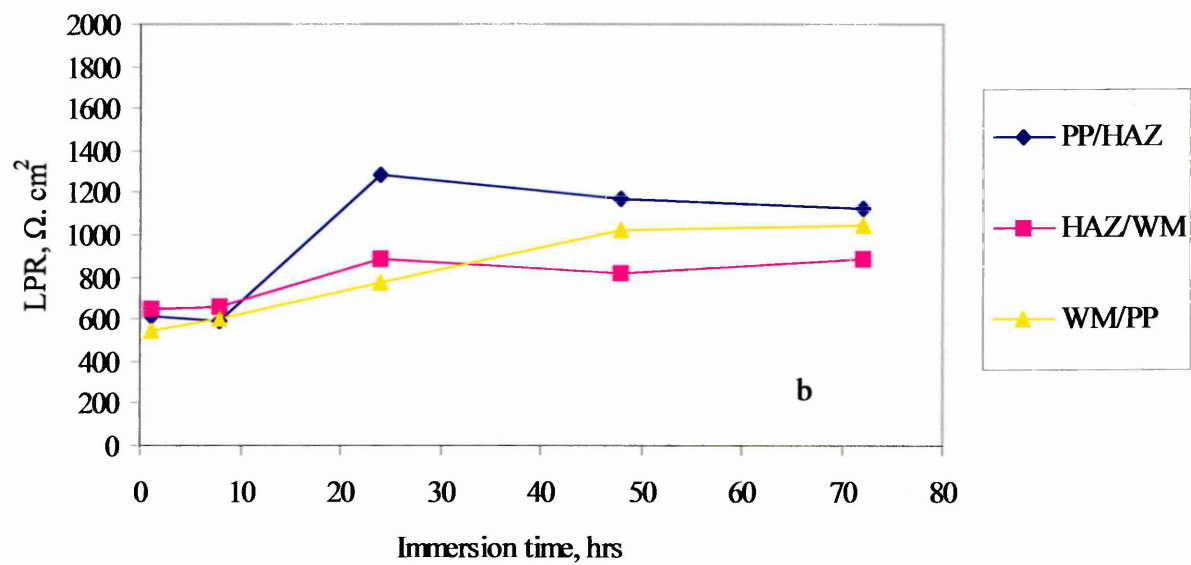
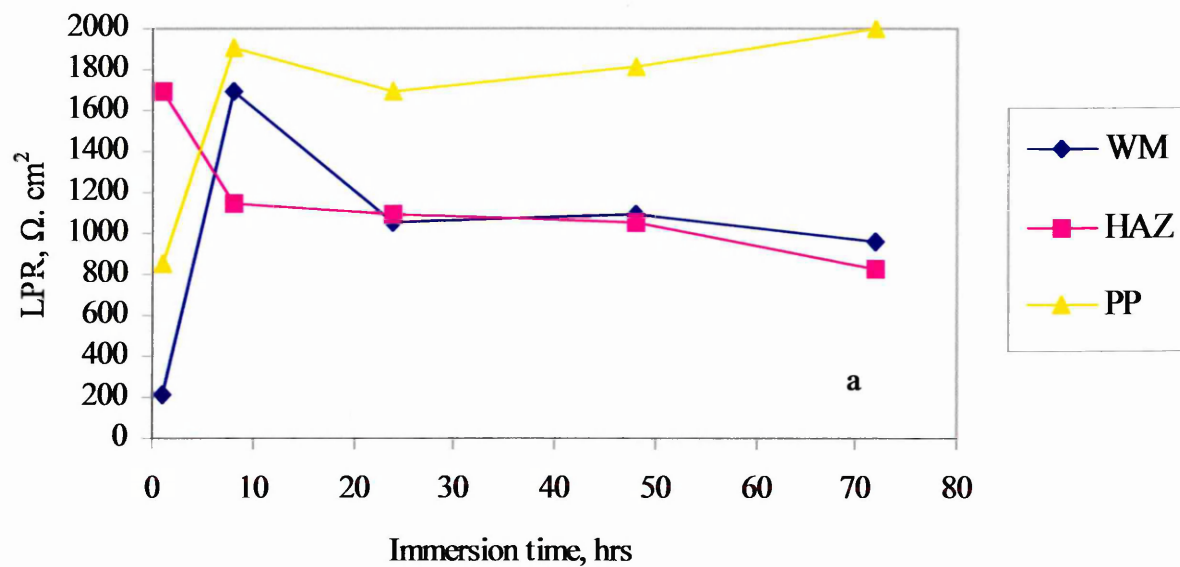


Figure 29 Graph showing LPR values versus immersion time for (a) individual and (b) coupled microstructures of the welded steel St-1 within chloride solution.

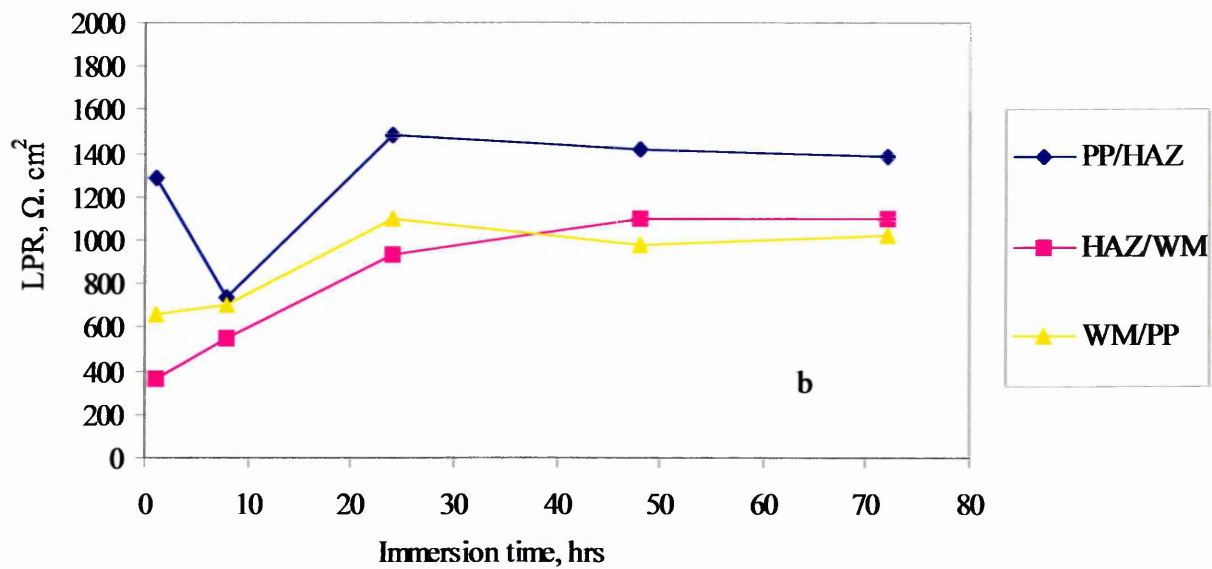
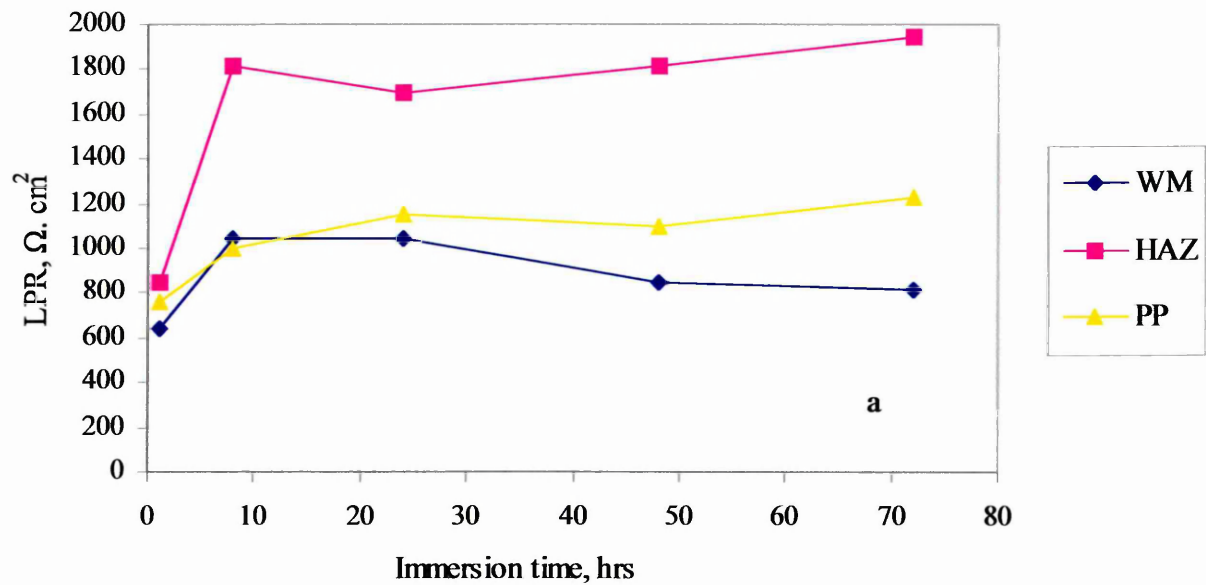


Figure 30 Profile curve showing LPR values versus immersion time for (a) individual and (b) coupled microstructures of the welded steel St-2 within chloride solution.

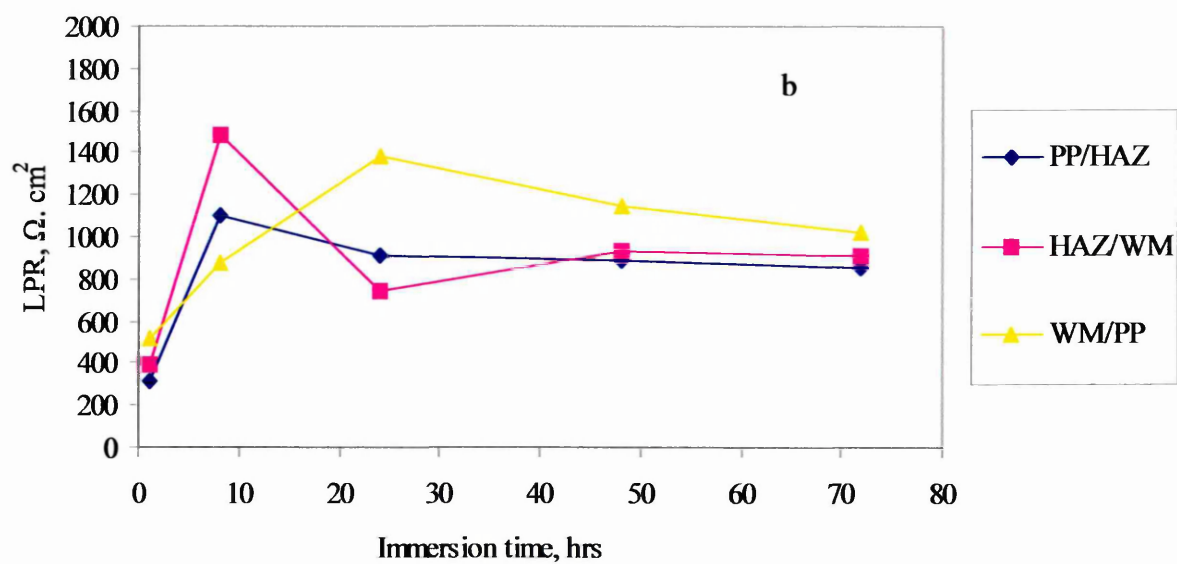
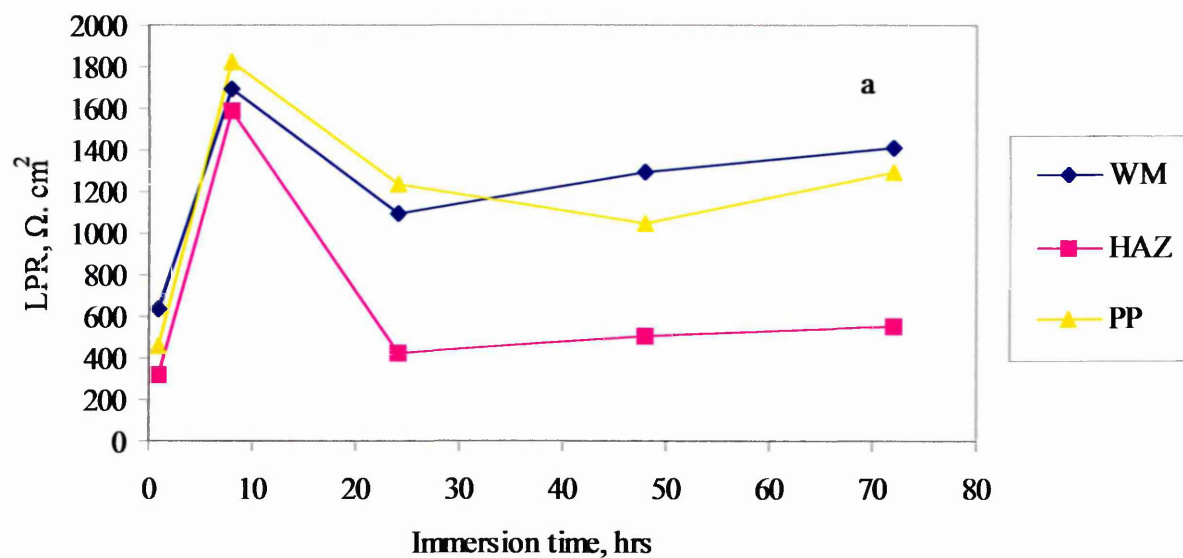


Figure 31 Profile curve showing LPR values versus immersion time for (a) individual and (b) coupled microstructures of the welded steel St-3 within chloride solution.

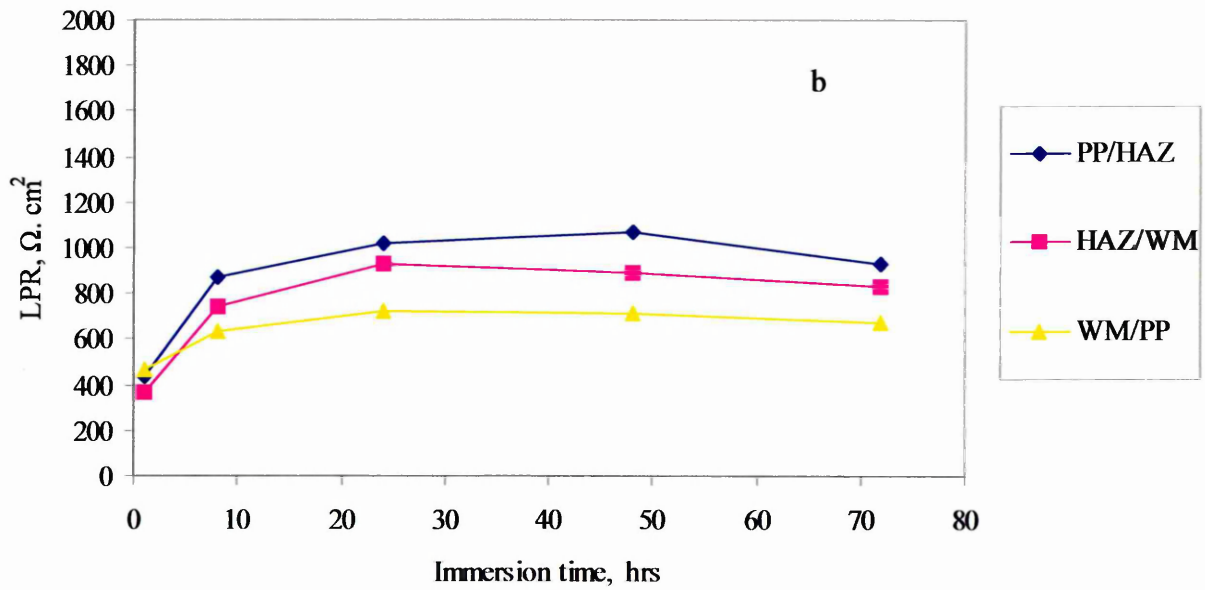
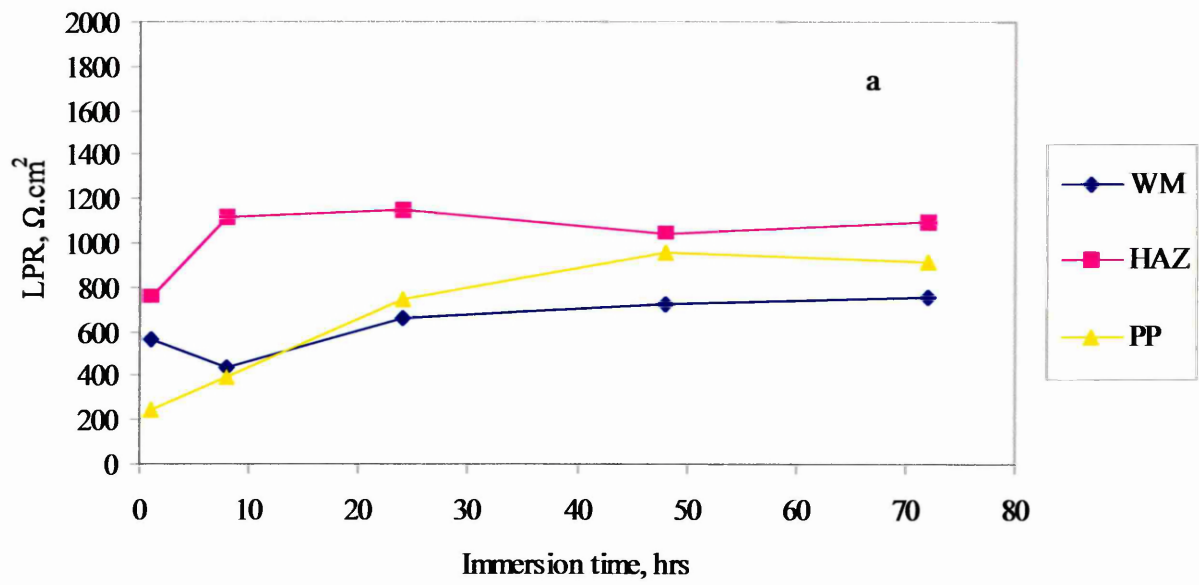


Figure 32 Profile curve showing LPR values versus immersion time for (a) individual and (b) coupled microstructures of the welded steel St-4 within chloride solution.

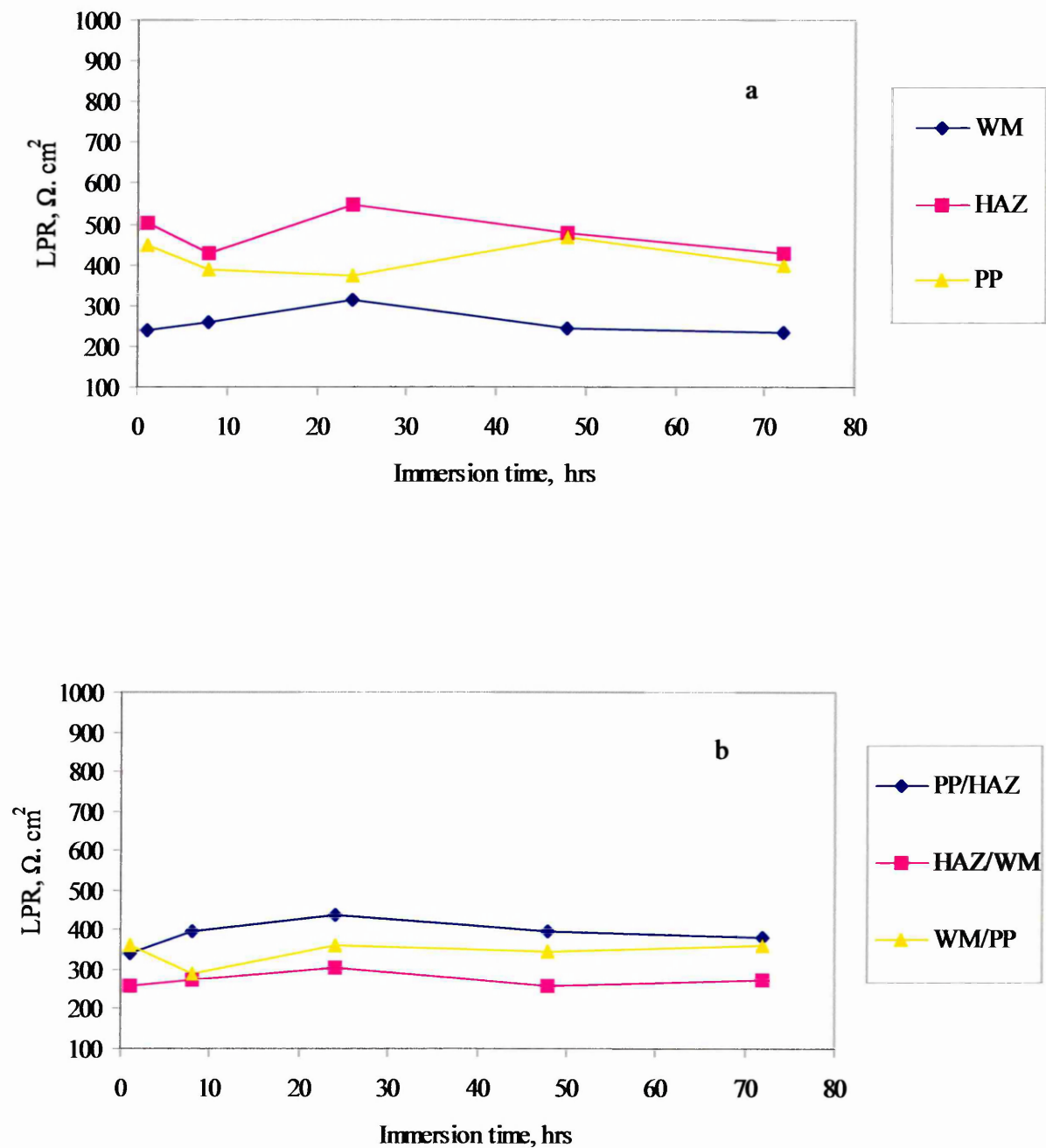


Figure 33 Profile curves showing LPR values versus immersion time for (a) individual and (b) coupled microstructures of the welded steel St-1 within buffered chloride solution with CO_2 saturation.

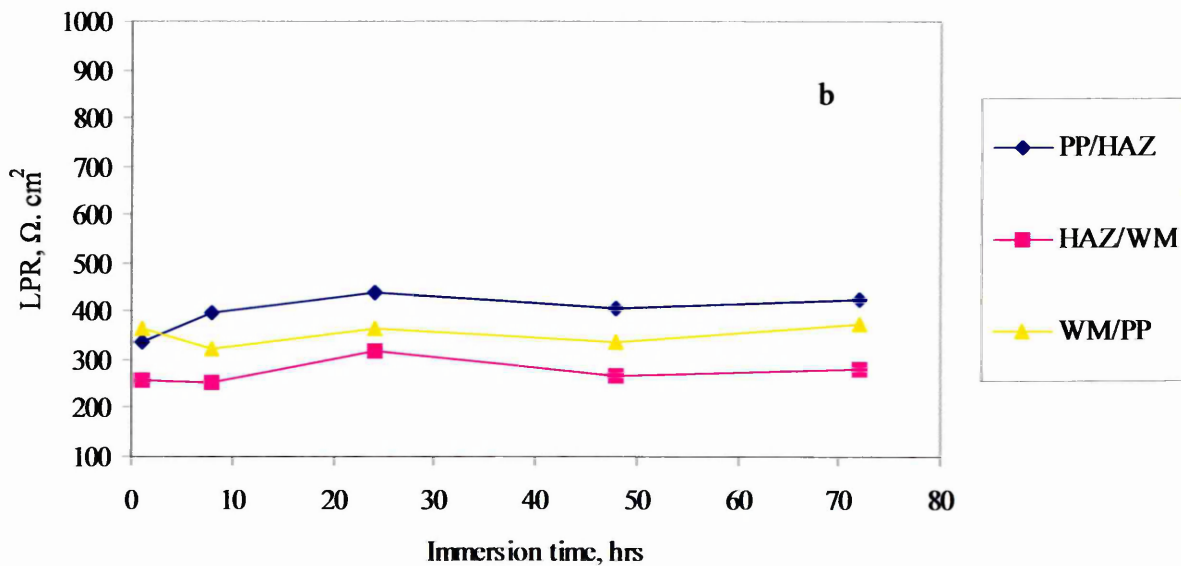
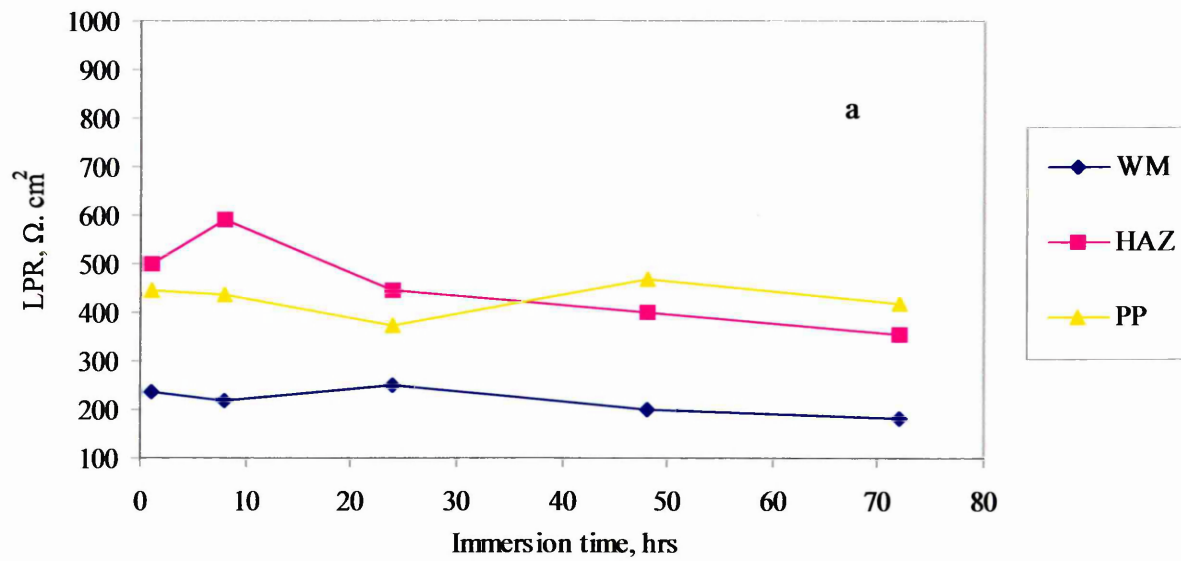


Figure 34 Profile curves showing LPR values versus immersion time for (a) individual and (b) coupled microstructures of the welded steel St-2 within buffered chloride solution with CO_2 saturation.

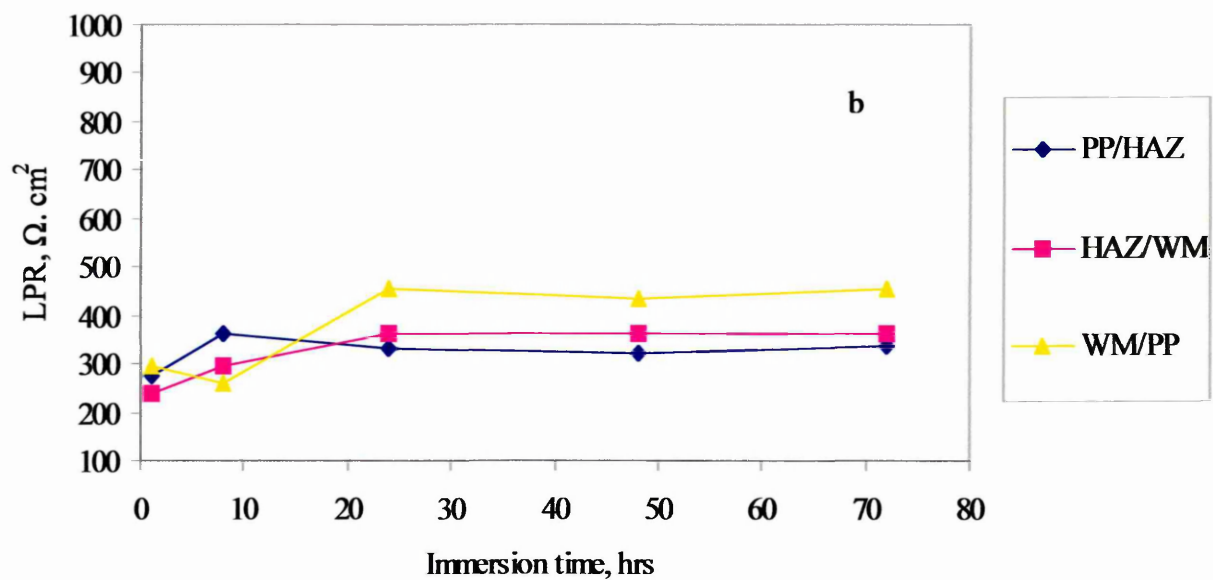
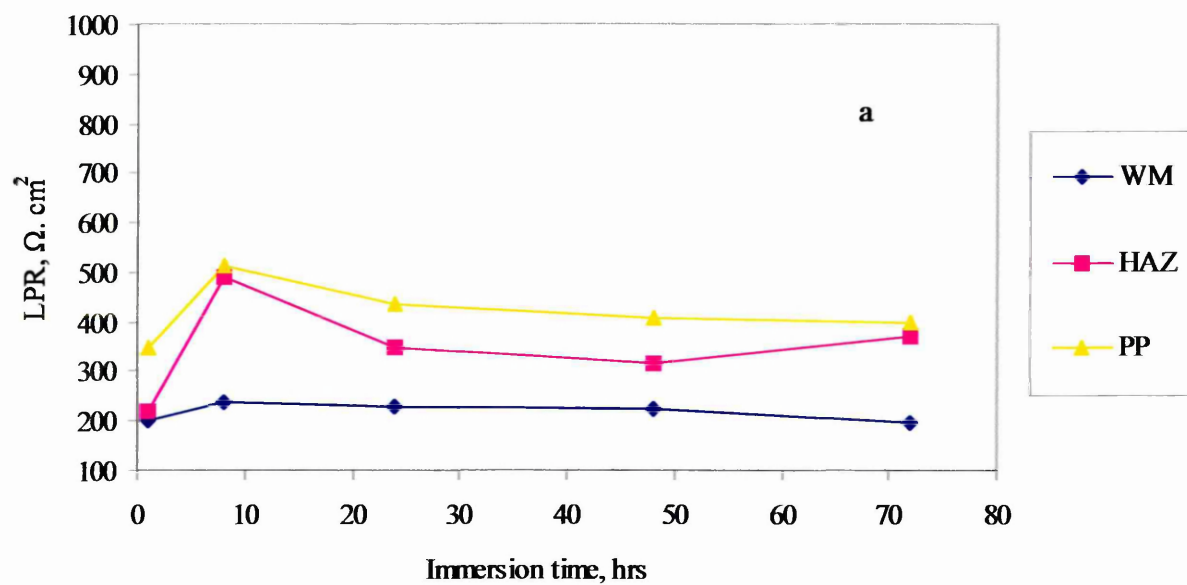


Figure 35 Profile curves showing LPR values versus immersion time for (a) individual and (b) coupled microstructures of the welded steel St-3 within buffered chloride solution saturated with CO_2 .

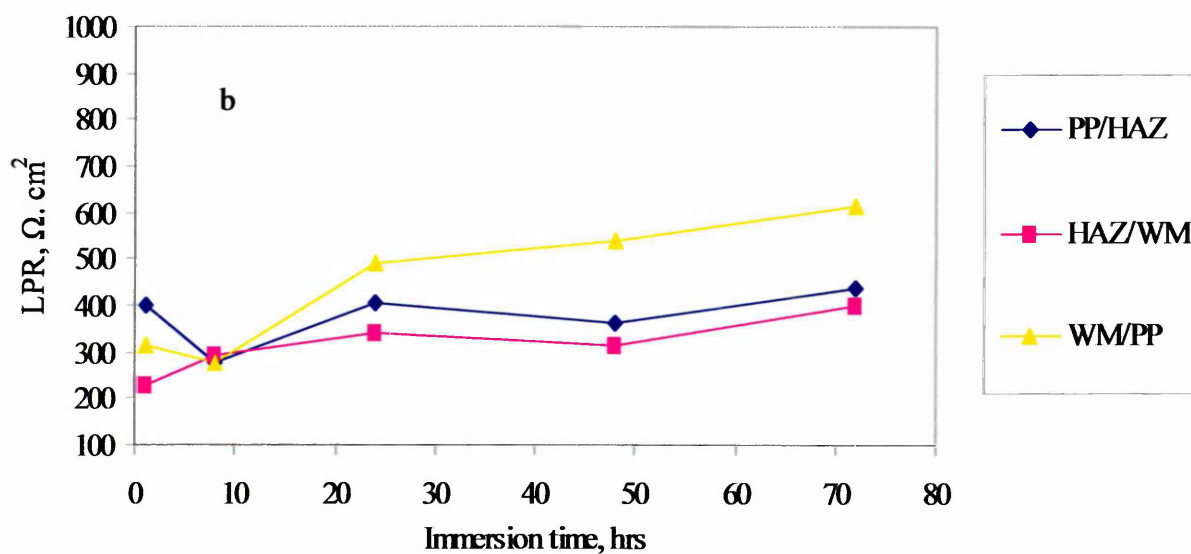
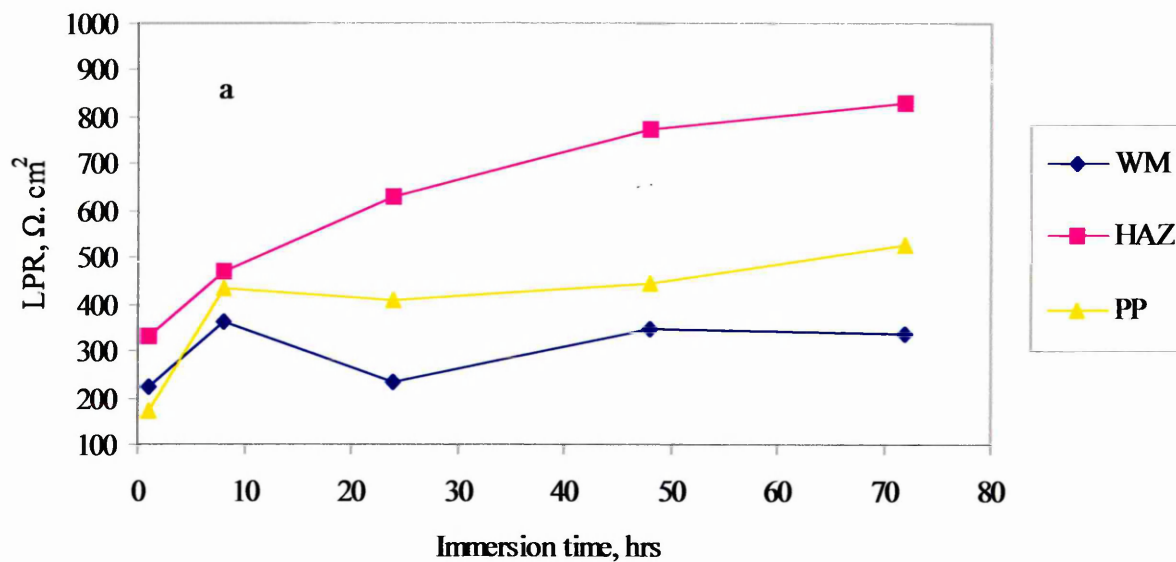


Figure 36 Profile curves showing LPR values versus immersion time for (a) individual and (b) coupled microstructures of the welded steel St-4 within buffered chloride solution saturated with CO_2 .

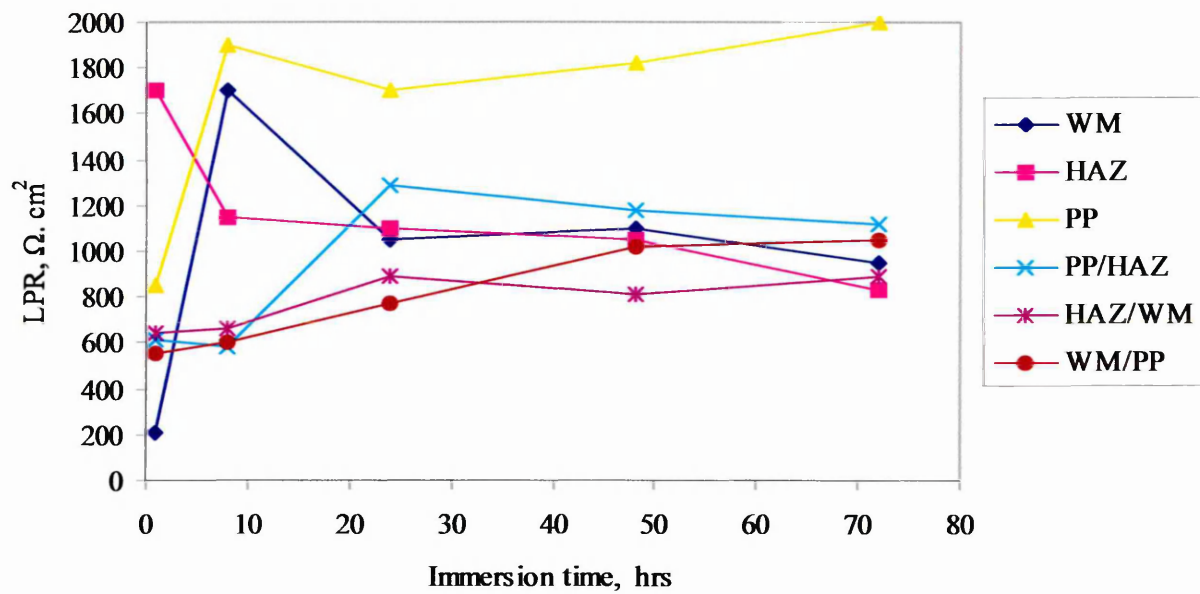


Figure 37 Profile plots showing comparison LPR data for both coupled and uncoupled microstructures versus immersion time for steel St-1 within chloride solution.

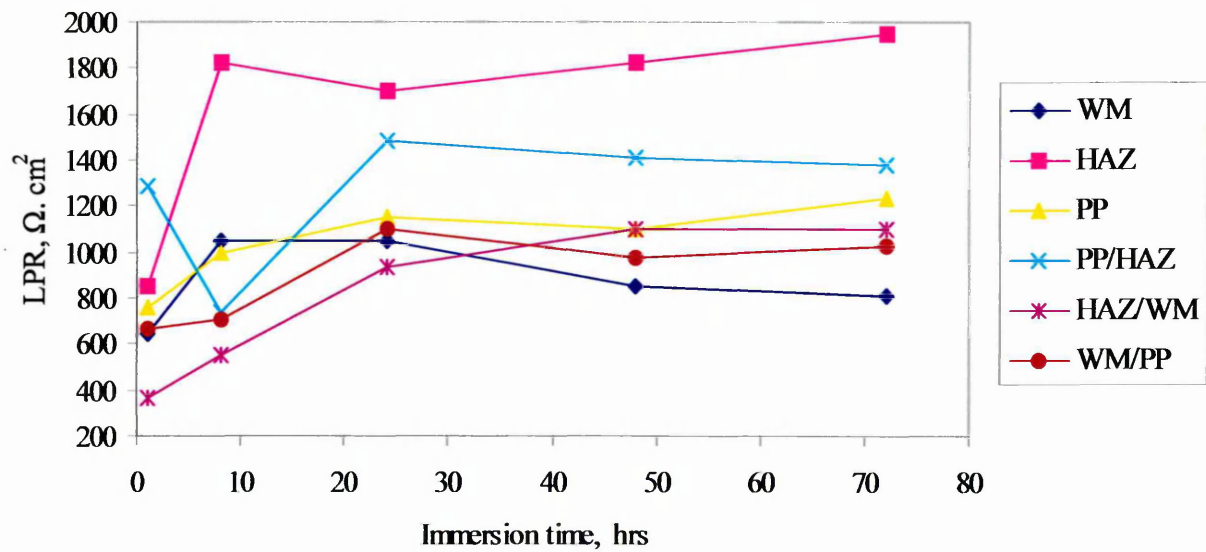


Figure 38 Profile plots showing comparison LPR data for both coupled and uncoupled microstructures versus immersion time for steel St-2 within chloride solution.

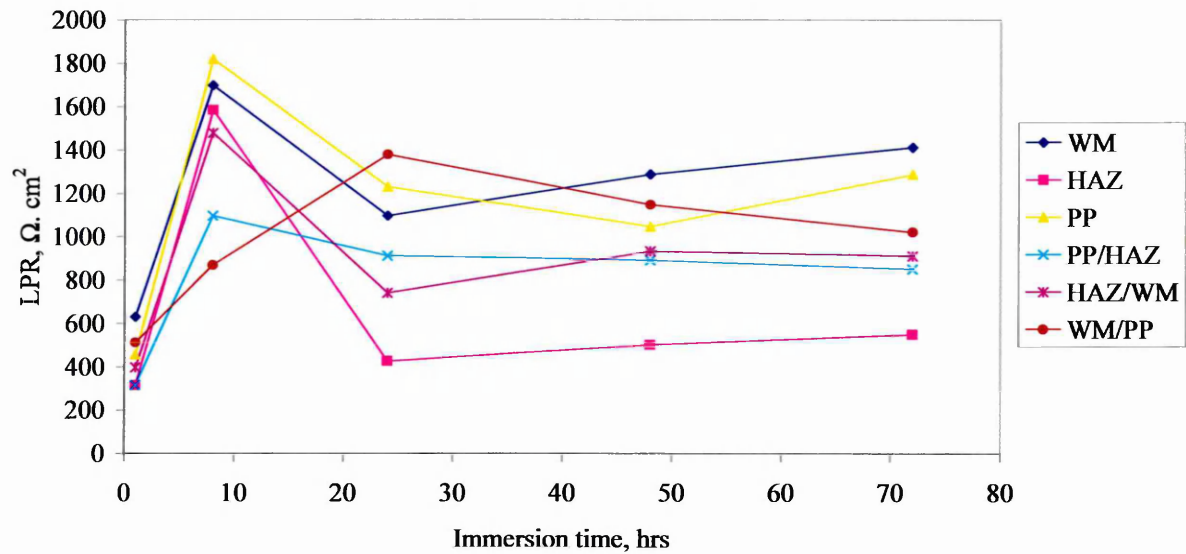


Figure 39 Profile plots showing comparison LPR data for both individual and coupled microstructures versus immersion time for steel St-3 within chloride solution.

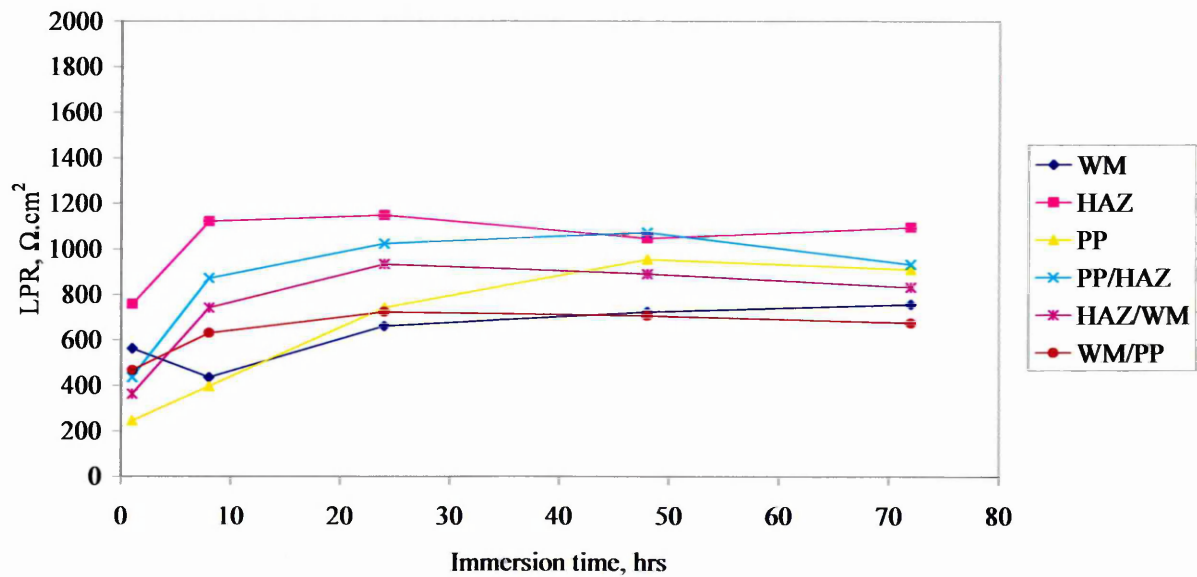


Figure 40 Profile plots showing comparison LPR data for both individual and coupled microstructures versus immersion time for steel St-4 within chloride solution.

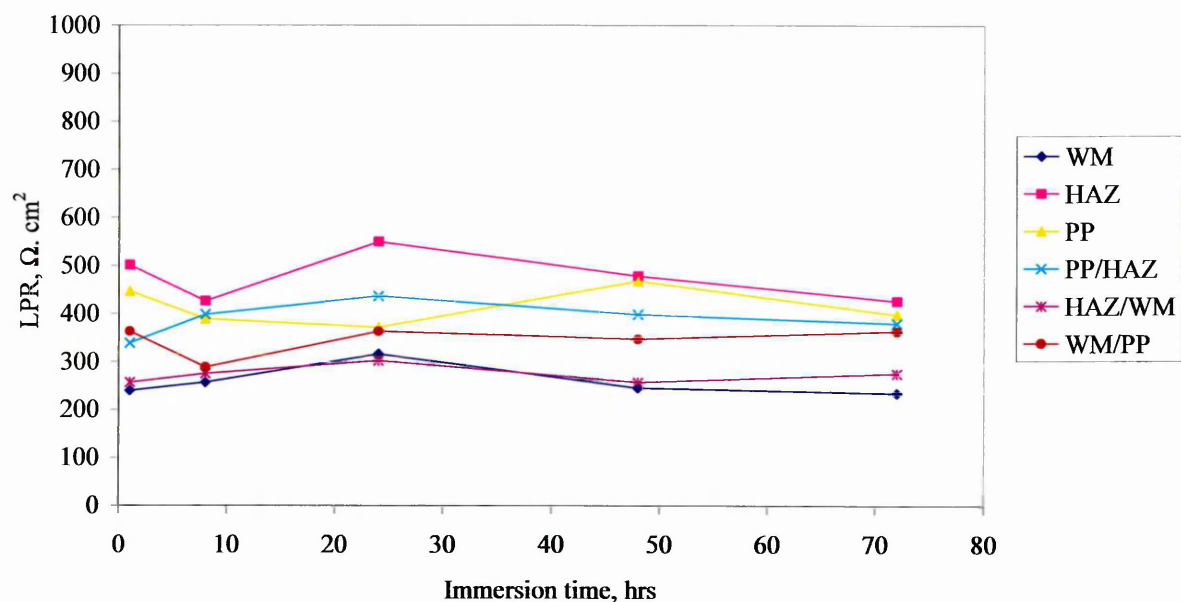


Figure 41 Graph showing comparison the LPR values for both individual and coupled microstructures versus immersion time for welded steel St-1 within buffered chloride solution saturated with CO₂.

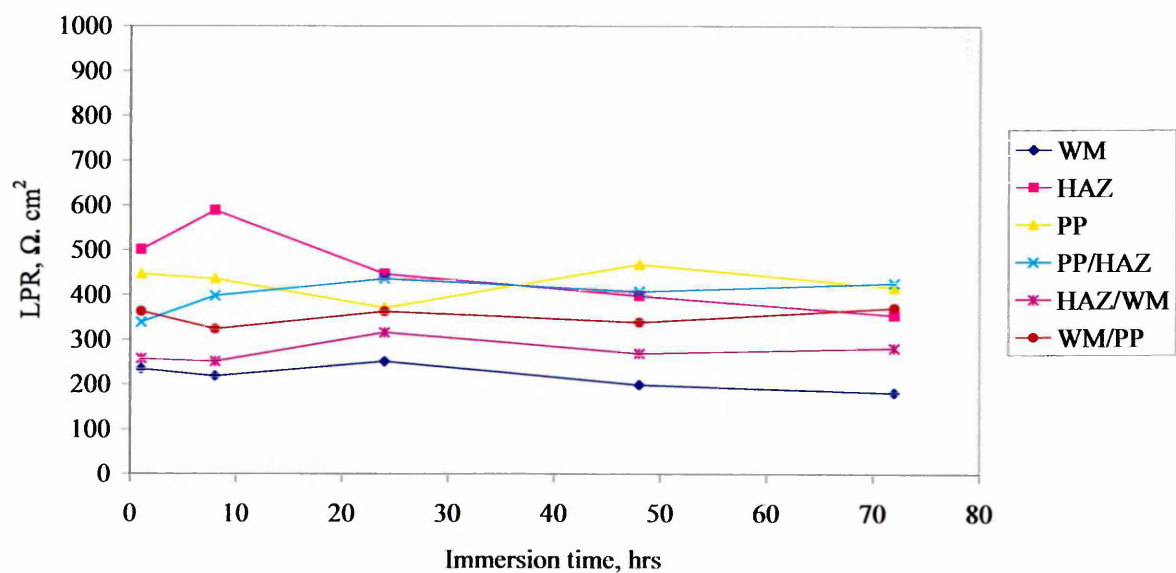


Figure 42 Graph showing comparison the LPR values for both individual and coupled microstructures versus immersion time for welded steel St-2 within buffered chloride solution saturated with CO₂.

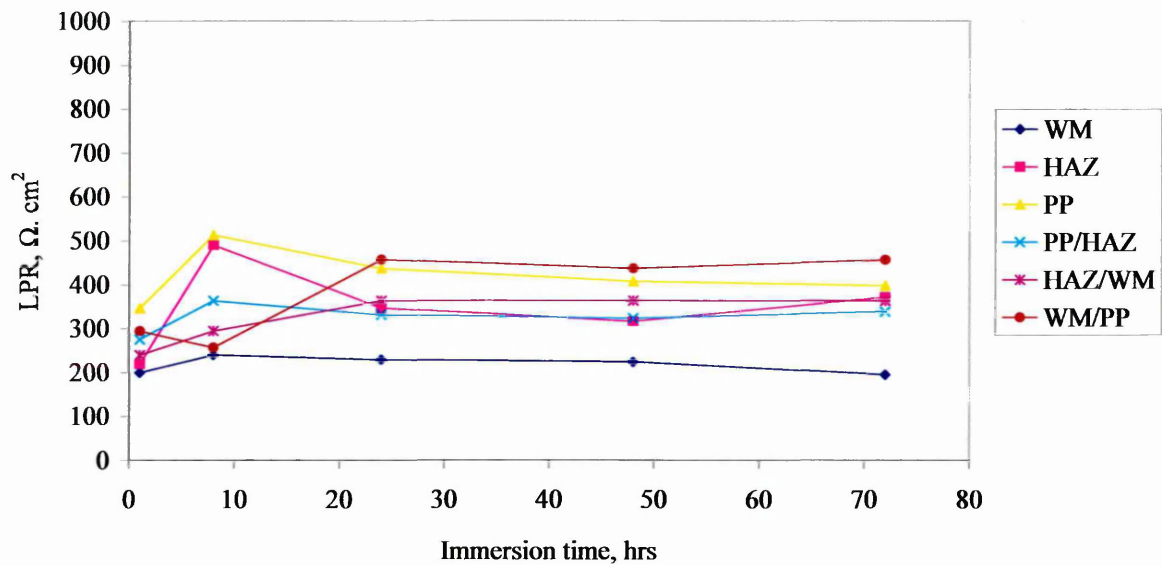


Figure 43 Graph showing the comparison LPR data for both coupled and uncoupled microstructures versus immersion time for welded steel St-3 within buffered chloride solution with CO₂ saturation.

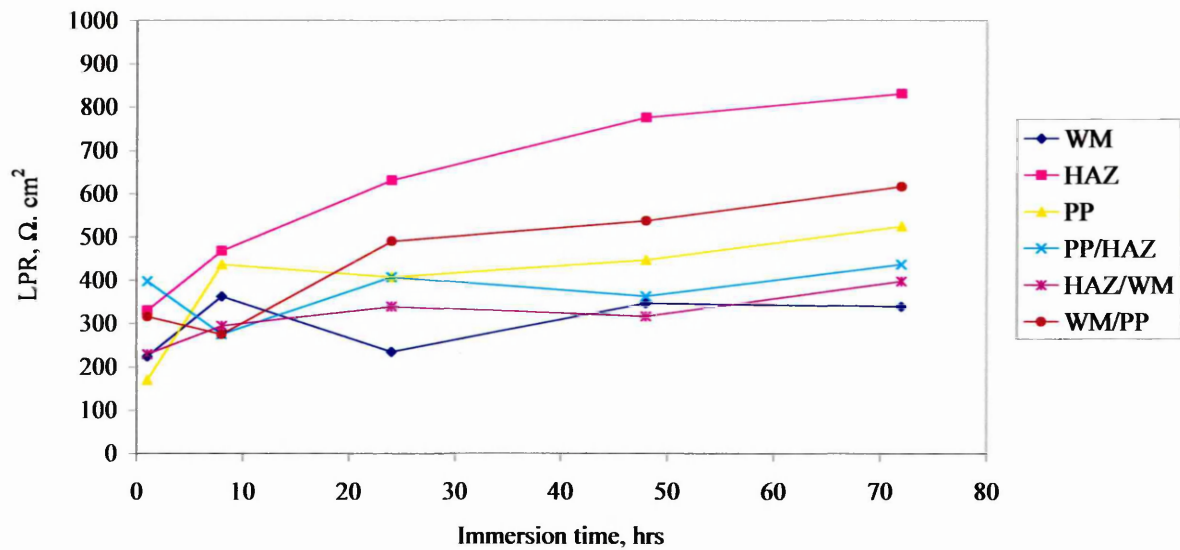


Figure 44 Graph showing the LPR values for both coupled and uncoupled microstructures versus immersion time for welded steel St-4 within buffered chloride solution with CO₂ saturation.

4.3.5 Cathodic polarisation curve

Conventional cathodic polarisation curve results for three individual microstructures of the four different steels are given in Figures 45-48 respectively.

The results are given after immersion of samples within buffered 0.35% NaCl solution saturated with CO₂ for 5 min, 1 hour and 4 hours respectively. The different current densities obtained at a fixed potential of -950 mV Vs SCE are given in Table 18.

Table 18 Current density ($\mu\text{A}/\text{cm}^2$) values for different steel microstructures at a fixed potential of -950 mV for cathodic polarisation tests for different time.

materials	PP			HAZ			WM		
	5 m	1 hr	4 hr	5 m	1hr	4hr	5 m	1 hr	4 hr
St-1	229	158	132	224	182	151	169	208	204
St-2	132	123	135	267	209	132	275	229	234
St-3	123	83	87	324	209	170	195	209	234
St-4	174	151	132	214	174	145	224	200	182

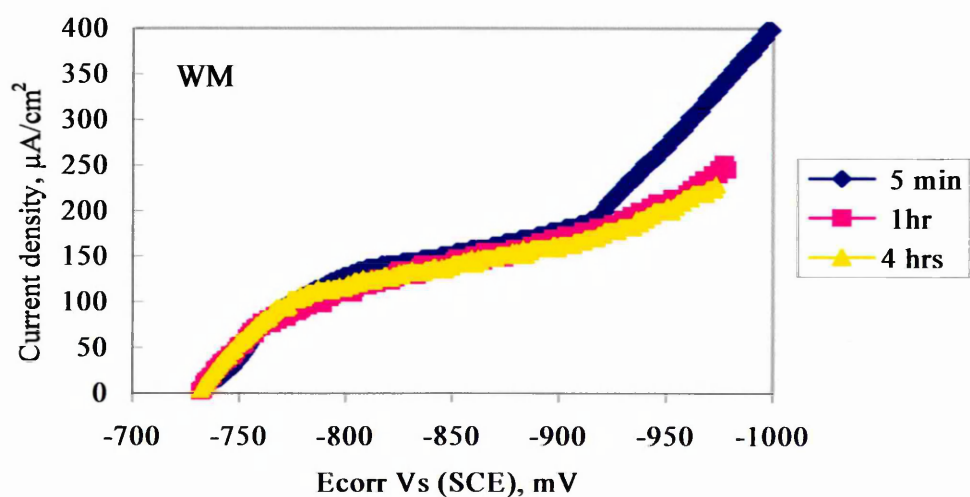
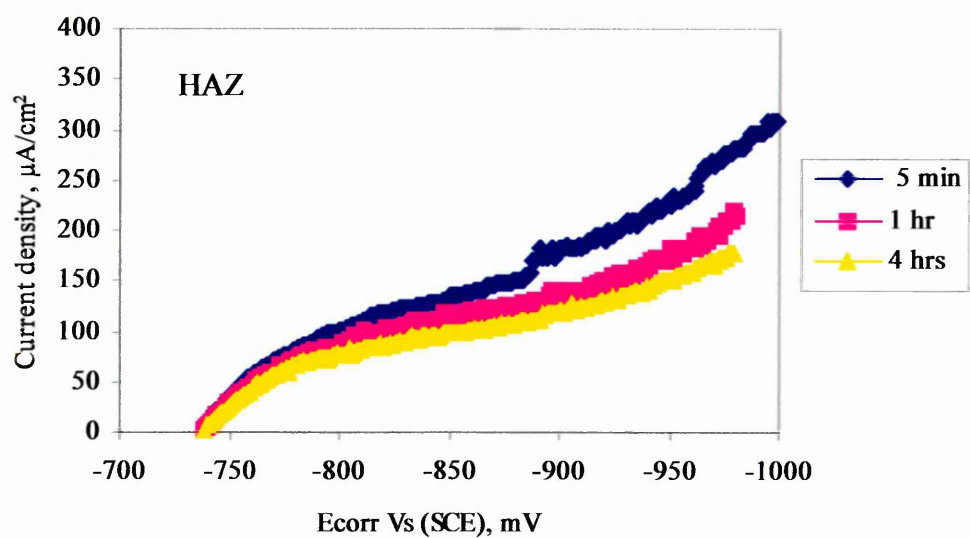
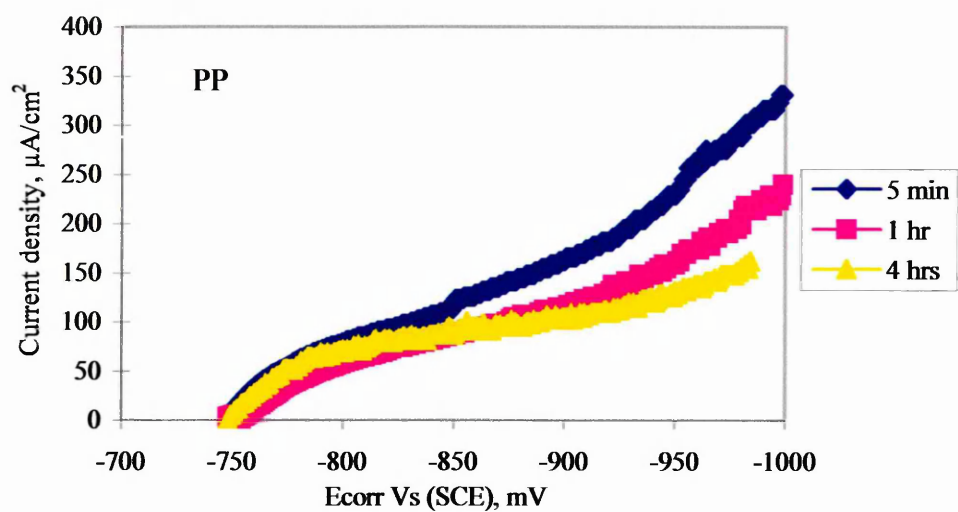


Figure 45 Cathodic polarisation curves showing, the effect CO_2 saturation of time on the protective film formation for different microstructures of St-1.

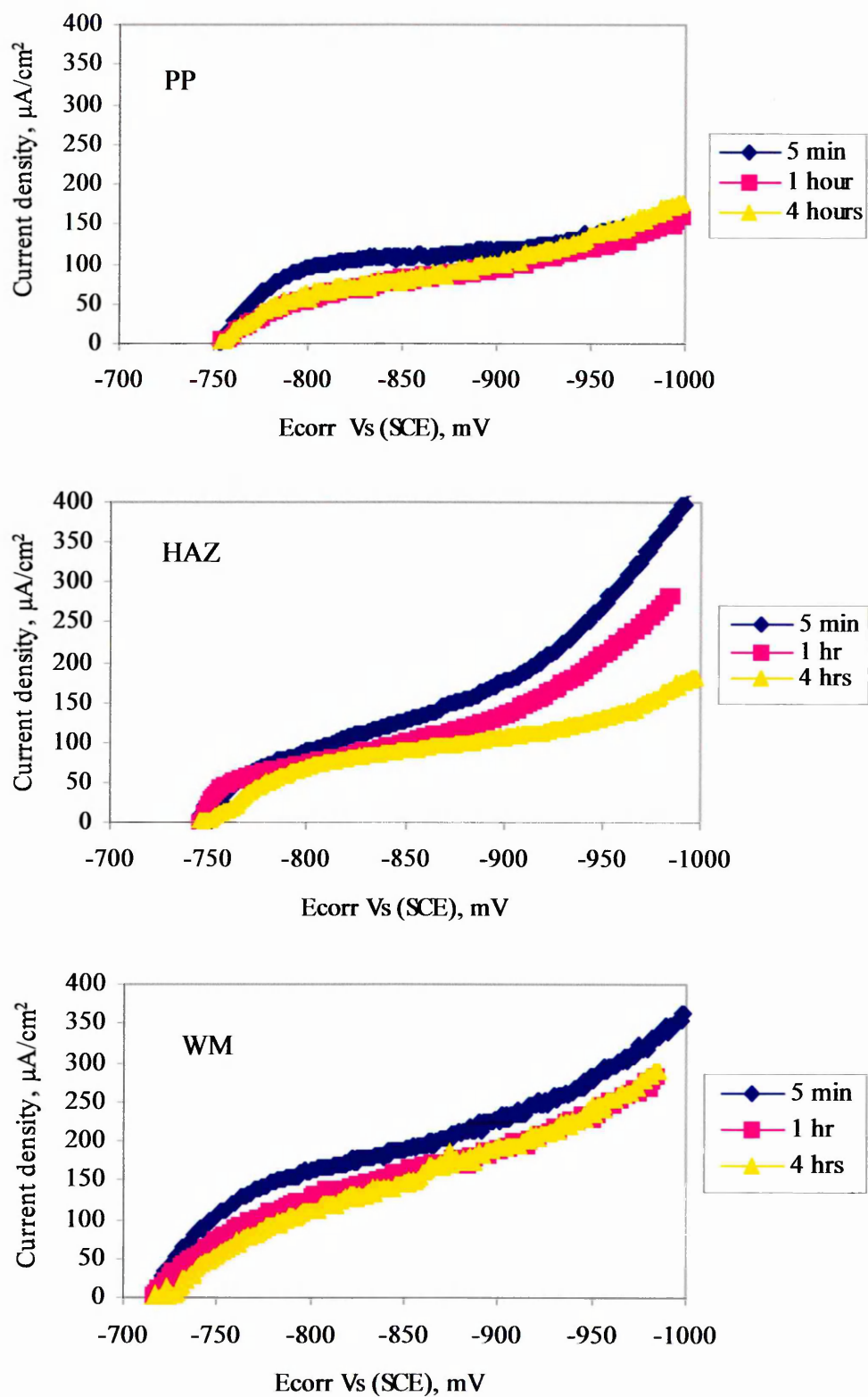


Figure 46 Cathodic polarisation curves showing, the effect CO_2 saturation of time on the film formation for different microstructures of St-2.

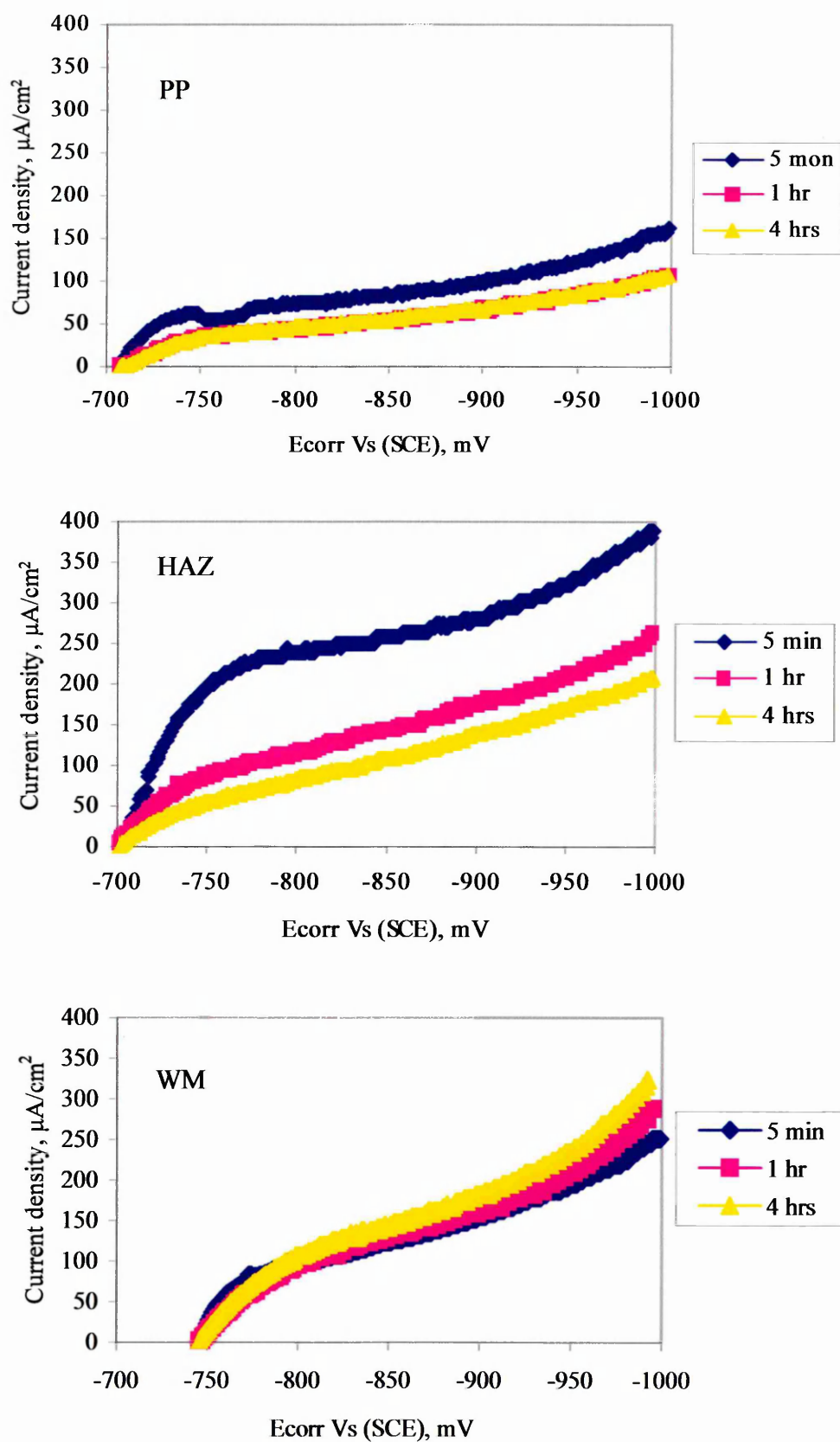


Figure 47 Cathodic polarisation curves showing, the effect CO₂ saturation of time on the film formation for different microstructures of St-3.

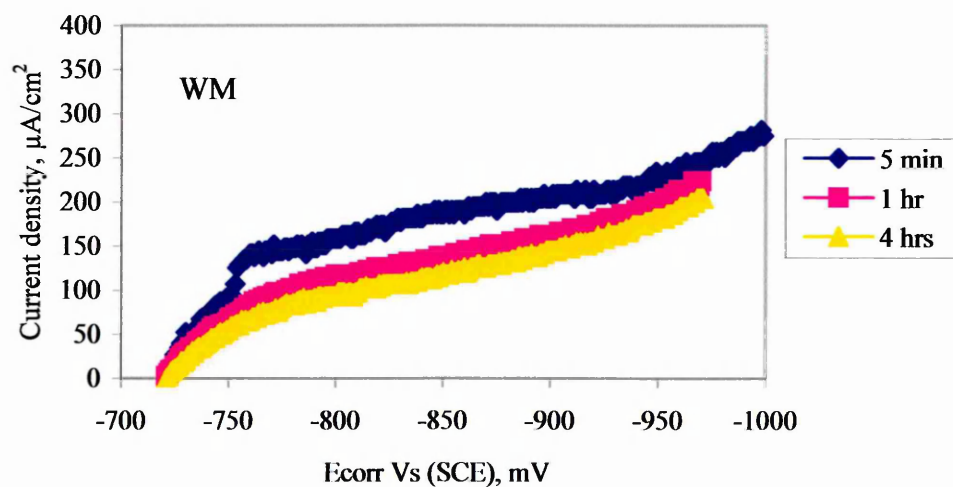
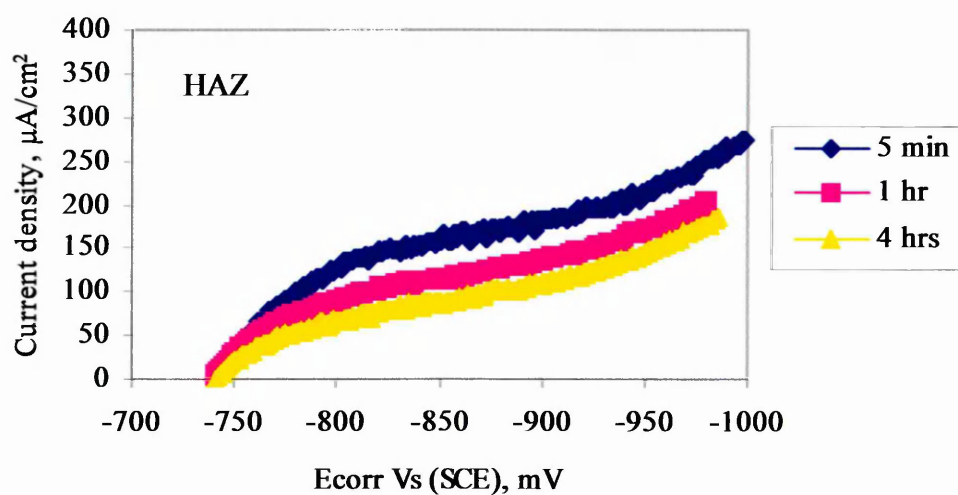
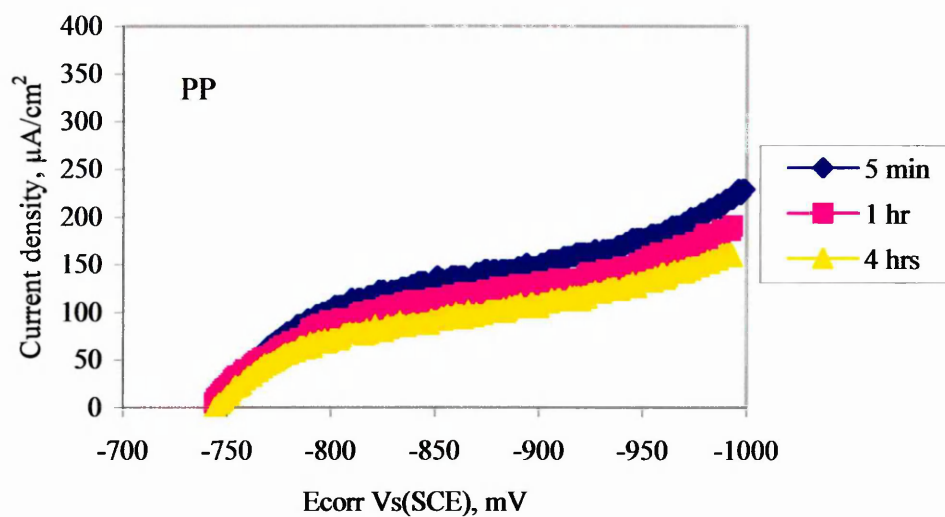


Figure 48 Cathodic polarisation curves showing, the effect CO_2 saturation of time on the film formation for different microstructures of St-4.

4.4 SVET measurements

All SVET measurements were carried out within aqueous 0.35% NaCl solution alone and buffered 0.35% NaCl solution with CO₂ saturation using a vibrating platinum microelectrode tip, mechanically scanned at a small fixed distance from the corroding surface. SVET map scans were recorded at room temperature over a period of 1, 2, 3 and 4 hours.

Due to the fact that SVET resolution and output signal is dependent upon the conductivity of the solution, low conductivity solution were used for this analysis.

It should be noted that resolution and output signal decrease with increasing conductivity [76].

4.4.1 Calibration of the SVET System

SVET calibrations were carried out as a primary activity to determine the electric field generated at a point current source, that is a point in space (PIS) gold electrode having a diameter of 200 μm immersed in the electrolyte solution. The voltage output from the PIS was determined for an injected current of 9.4 μA . The SVET instrument was that of an EG&G SVP100 system, coupled to a Radiometer potentiostat acting to provide a constant current source. The SVET parameters used were vibration amplitude (VA) 30 μm , probe scan speed, 500 $\mu\text{m}/\text{sec}$ and probe-sample distance approximately 100 μm . Before calibration, the PIS electrode was adjusted to give a constant probe-sample distance of 100 μm . This was achieved using a travelling microscope. The probe can be moved mechanically or manually over the PIS whilst a

current is flowing through it, in order to obtain the maximum output signal from the PIS by moving the probe in the X and Y directions. The same experimental conditions were used for both PIS and SVET tests. The calibration factors (CF) have been determined in two different environments, e.g., 0.35% NaCl solution alone and buffered 0.35% NaCl solution with CO₂ saturation using the equations given below;

$$CF = \frac{Current, \mu A}{Area(PIS), cm^2} \equiv V_{out}, mV \quad (19)$$

For chloride solution alone,

$$CF = 0.10625 mV \equiv 30 mA/cm^2 \quad (20)$$

$$\therefore 1 mV \equiv 282 mA/cm^2 \quad (21)$$

For chloride solution saturated with CO₂,

$$CF = 0.12897 mV \equiv 30 mA/cm^2 \quad (22)$$

$$\therefore 1 mV \equiv 233 mA/cm^2 \quad (23)$$

4.4.2 SVET tests within chloride solution

Figures 49-52 present the area map scans of steels 1-4 respectively within sodium chloride solution alone. The colours at the more positive end of the palette, i.e., red, represents relatively anodic potentials, whereas those at the negative end of the palette, i.e., blue, represents cathodic areas. The SVET tests were conducted on the welded sections for periods of time between one and four hours due to the aggressiveness of the electrolyte, which induced highly localised attack.

The localised activity for steel-1 seemed to be concentrated on the HAZ and WM during the first two hours and being uniform over the following 3-4 hours.

Localised activity for steel-2 moved towards to the PP and less than that in the HAZ and WM during 1-2 hours and being uniform for all microstructures after 3-4 hours.

Localised activity of the steel-3 concentrated on the PP whilst less activity observed in the weld zone during first two hours and thereafter reduced over the following 3-4 hours in the PP. Finally, the SVET maps showing the least localised activity observed for steel-4 during 1-2 hours and being uniformly distributed across the different weld areas over the following 3-4 hours.

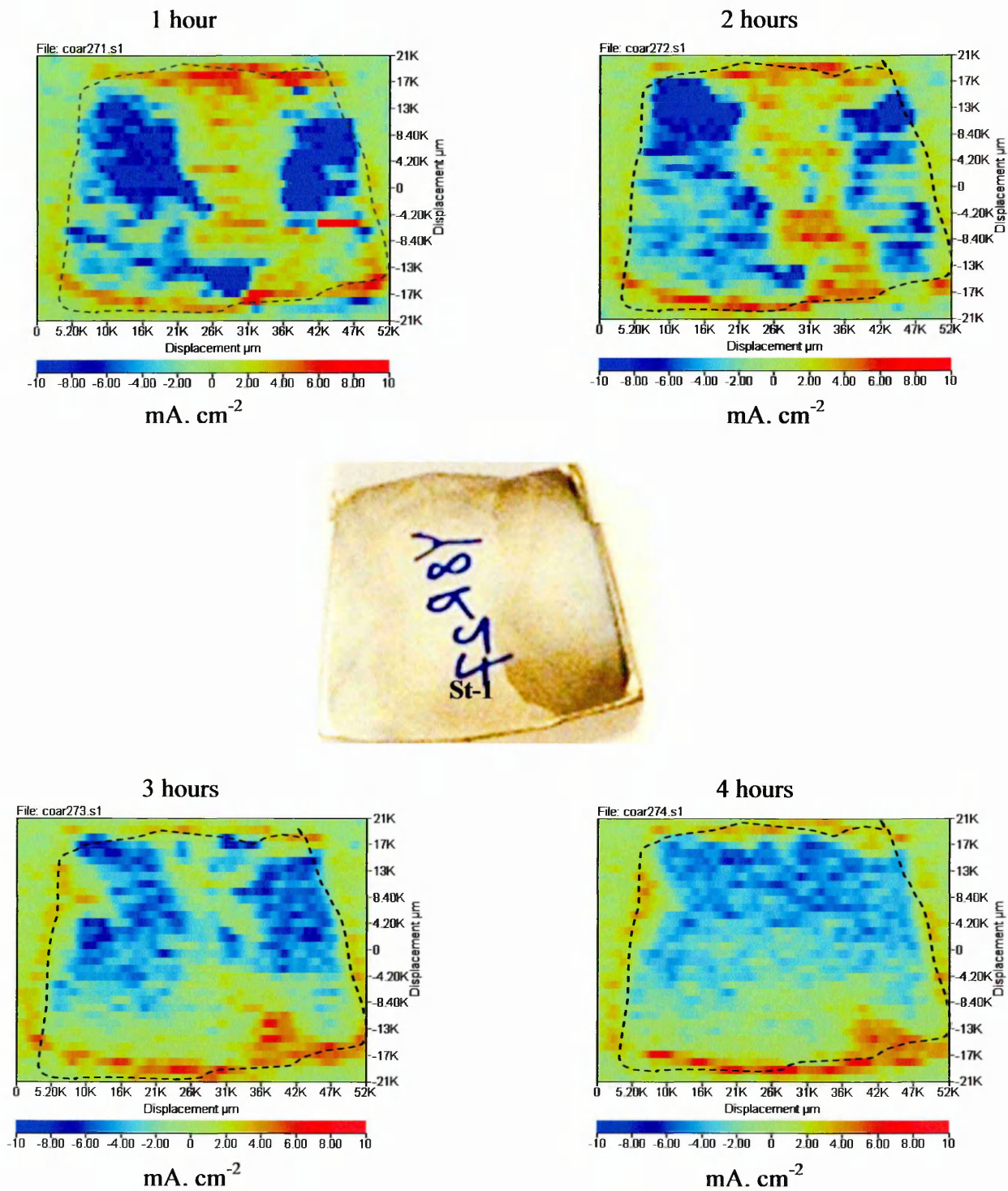


Figure 49 Showing the SVET area map scan on welded carbon steel pipeline designated of St-1 within aqueous chloride solution for different time scans.

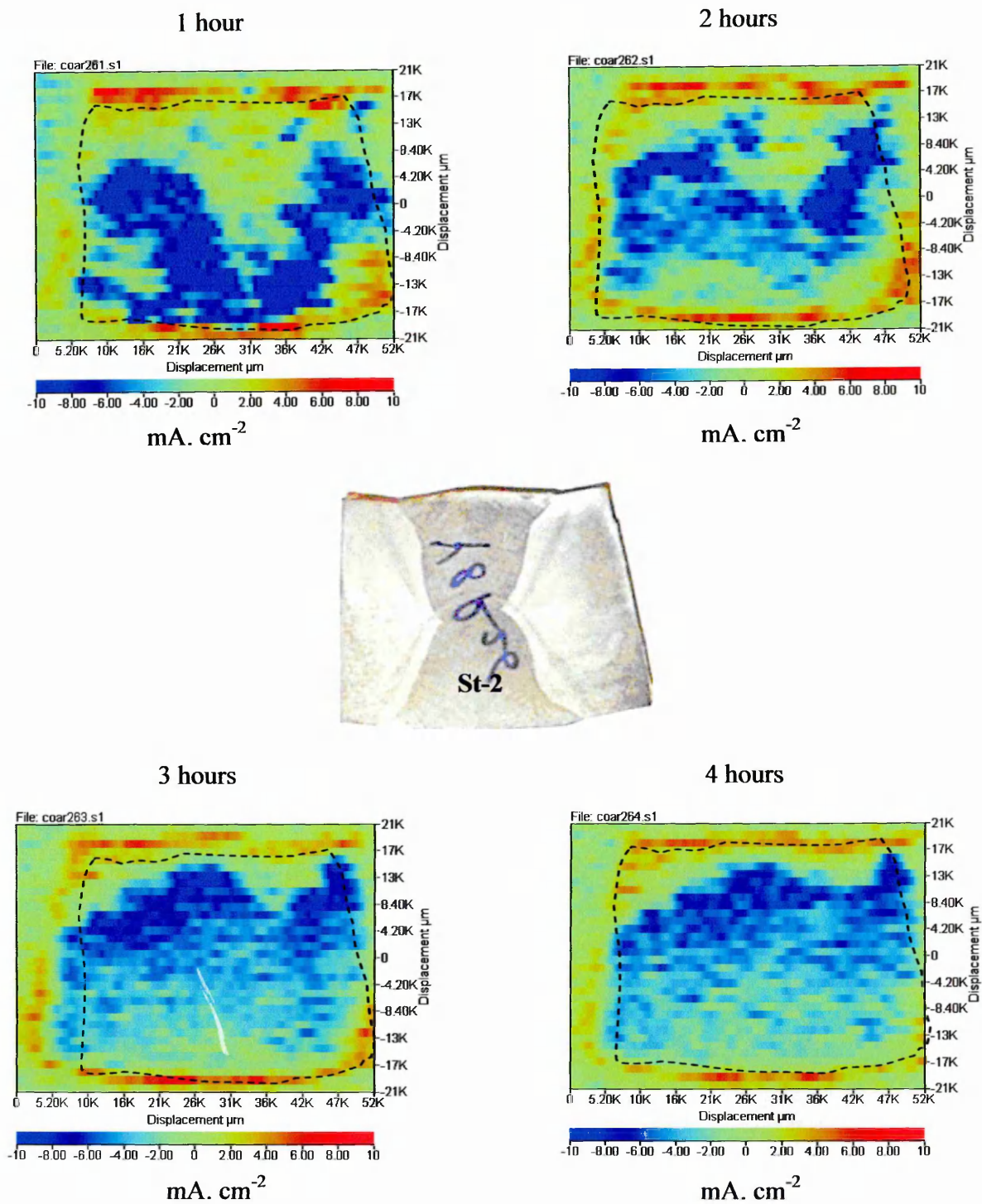


Figure 50 Showing the SVET area map scan on welded carbon steel pipeline designated of St-2 within aqueous chloride solution for different time scans.

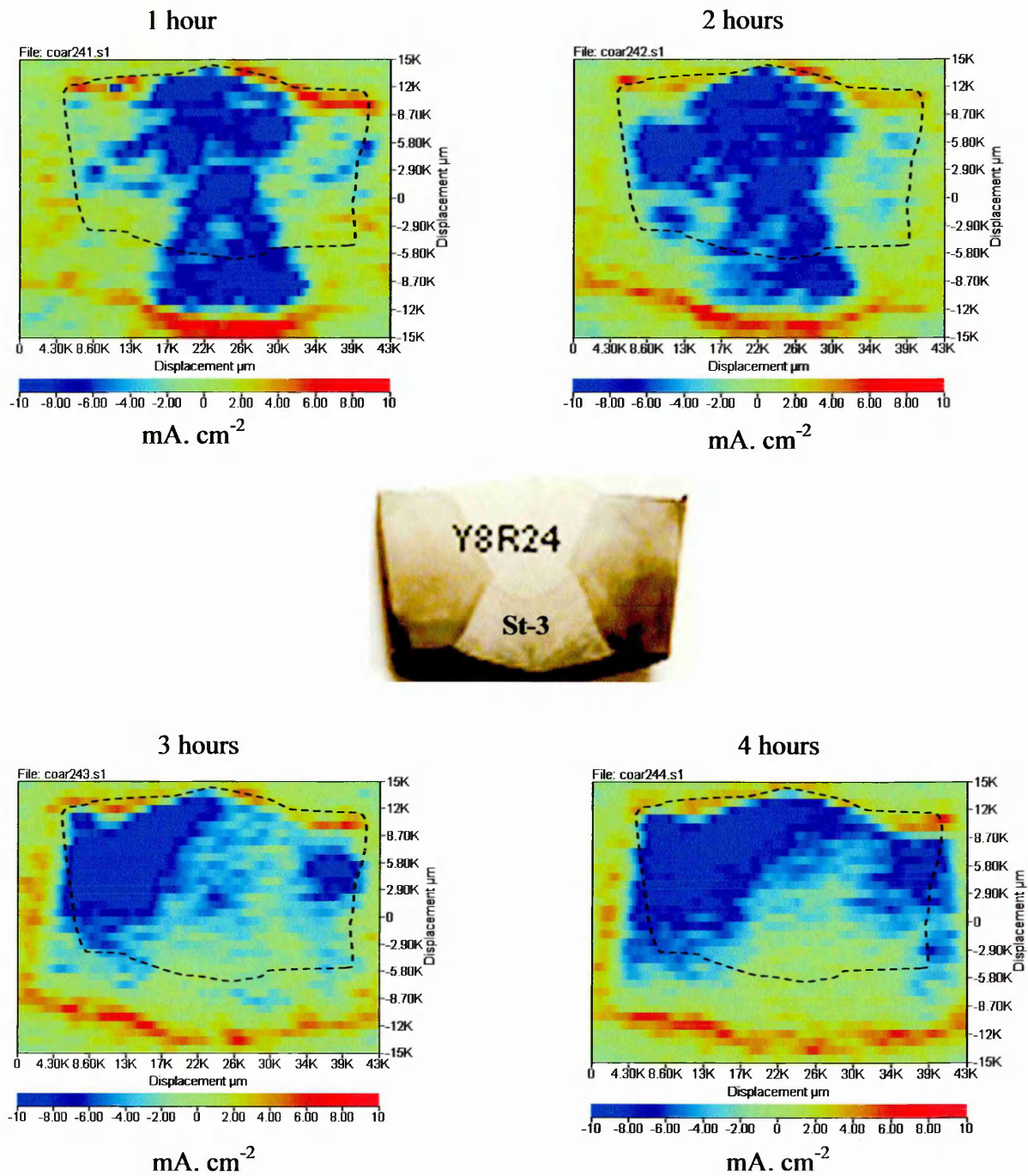


Figure 51 Showing the SVET area map scan on welded carbon steel pipeline designated of St-3 within aqueous chloride solution for different time scans.

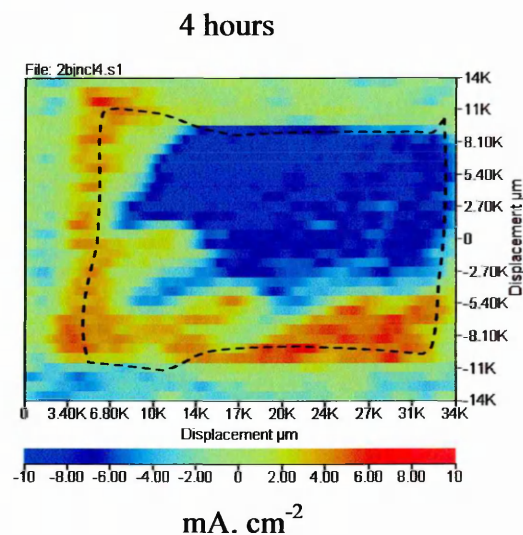
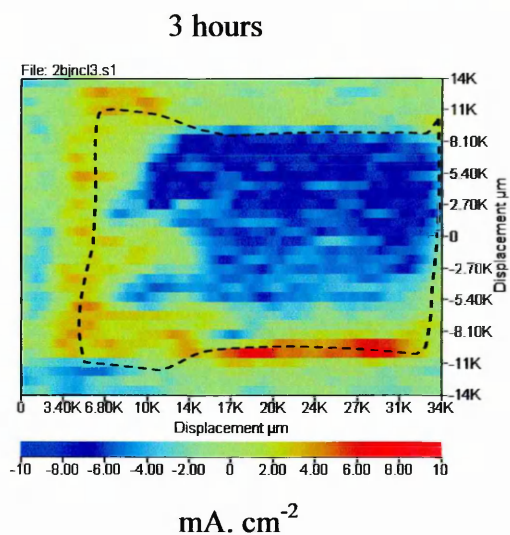
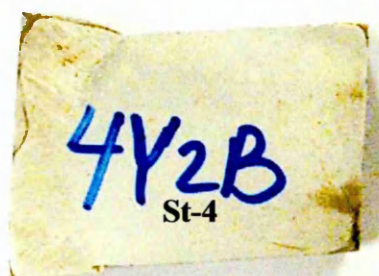
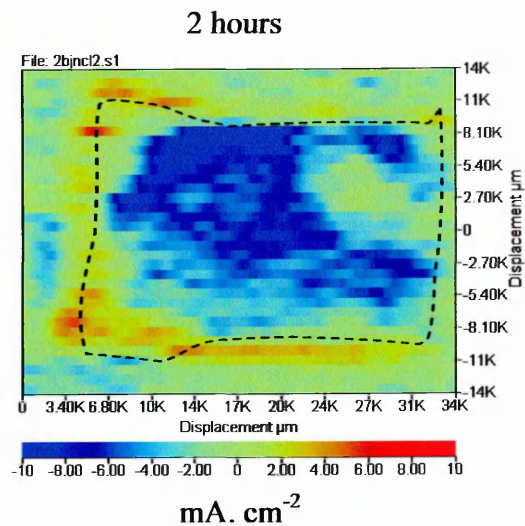
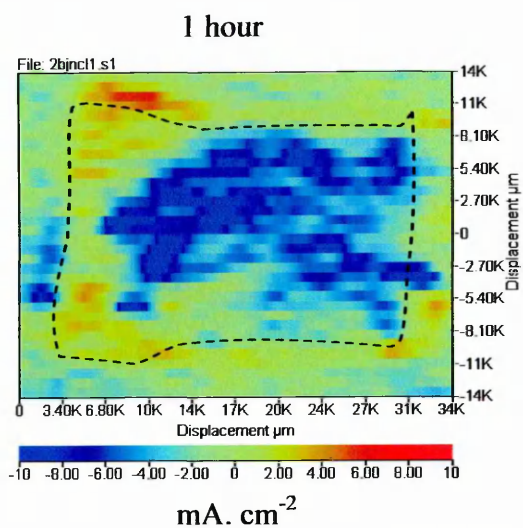


Figure 52 Showing the SVET area map scan on welded carbon steel pipeline designated of St-4 within aqueous chloride solution for different time scans.

4.4.3 SVET tests within chloride solution with CO₂ additions

Figures 53-56 represent the area map scans for the different microstructures of welded steels within buffered chloride solution saturated with CO₂. The localised attack could be seen in Figure 53, the area maps of the sites with localised activity produced of the St-1 on the HAZ and WM and to some extent at the PP and less than that on the PP during 1-2 hours and over the following 3-4 hours there is less activity on the PP and more corrosion attack at the HAZ and WM. Figure 54 present SVET map scans for St-2, where the higher localised activity is recorded on the HAZ and PP on first exposure to the solution and somewhat extent at the WM after 3-4 hours. Figure 55 shows area map scans for steel-3, where localised activity is being uniformly during 1-4 hours for all the steel microstructures. Figure 56 shows localised activity during 1-4 hours is being uniformly distributed on the different microstructures after 3-4 hours of the steel-4.

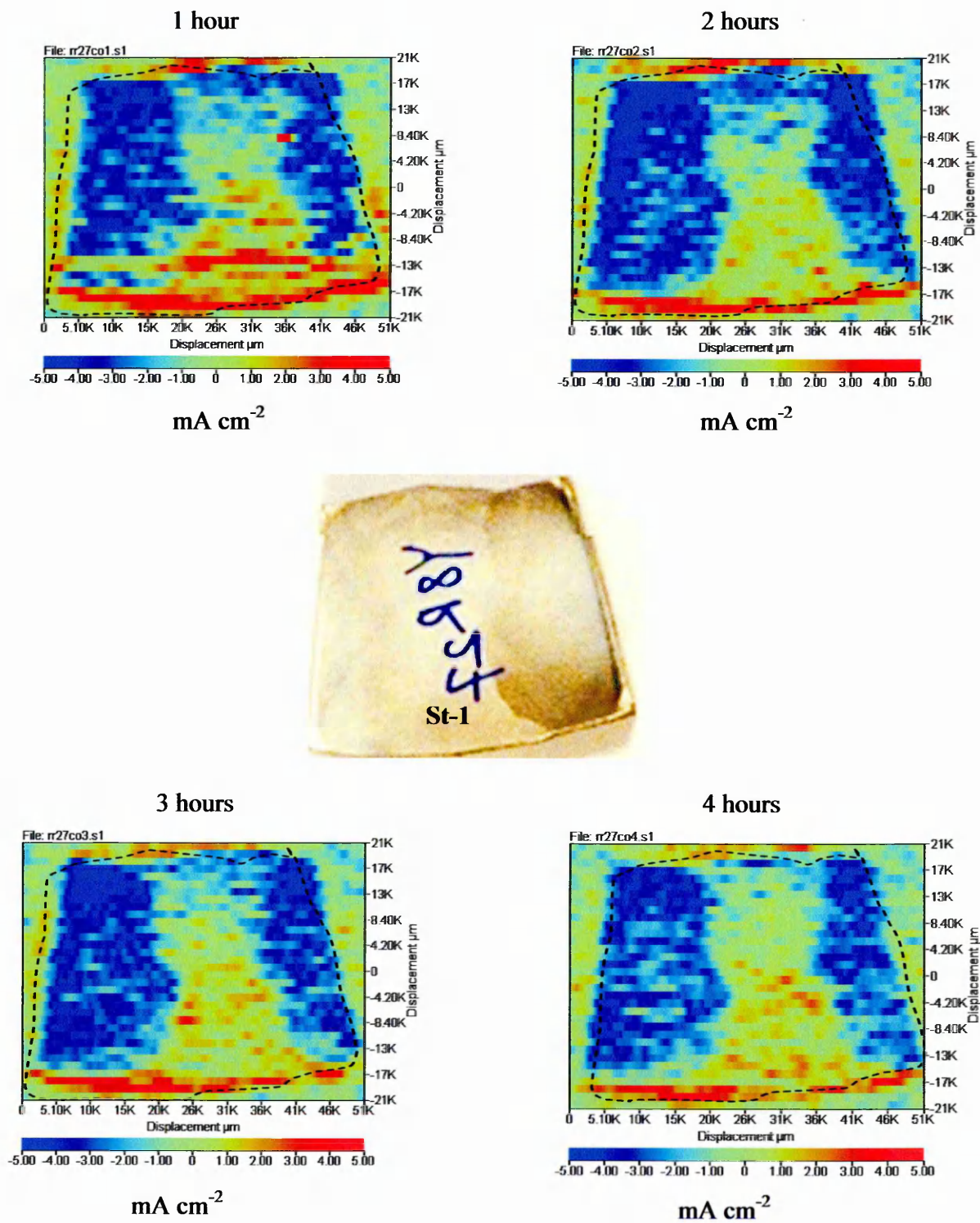


Figure 53 Showing the SVET area map scan on welded carbon steel pipeline designated of St-1 within buffered chloride solution with CO_2 saturation for different time scans.

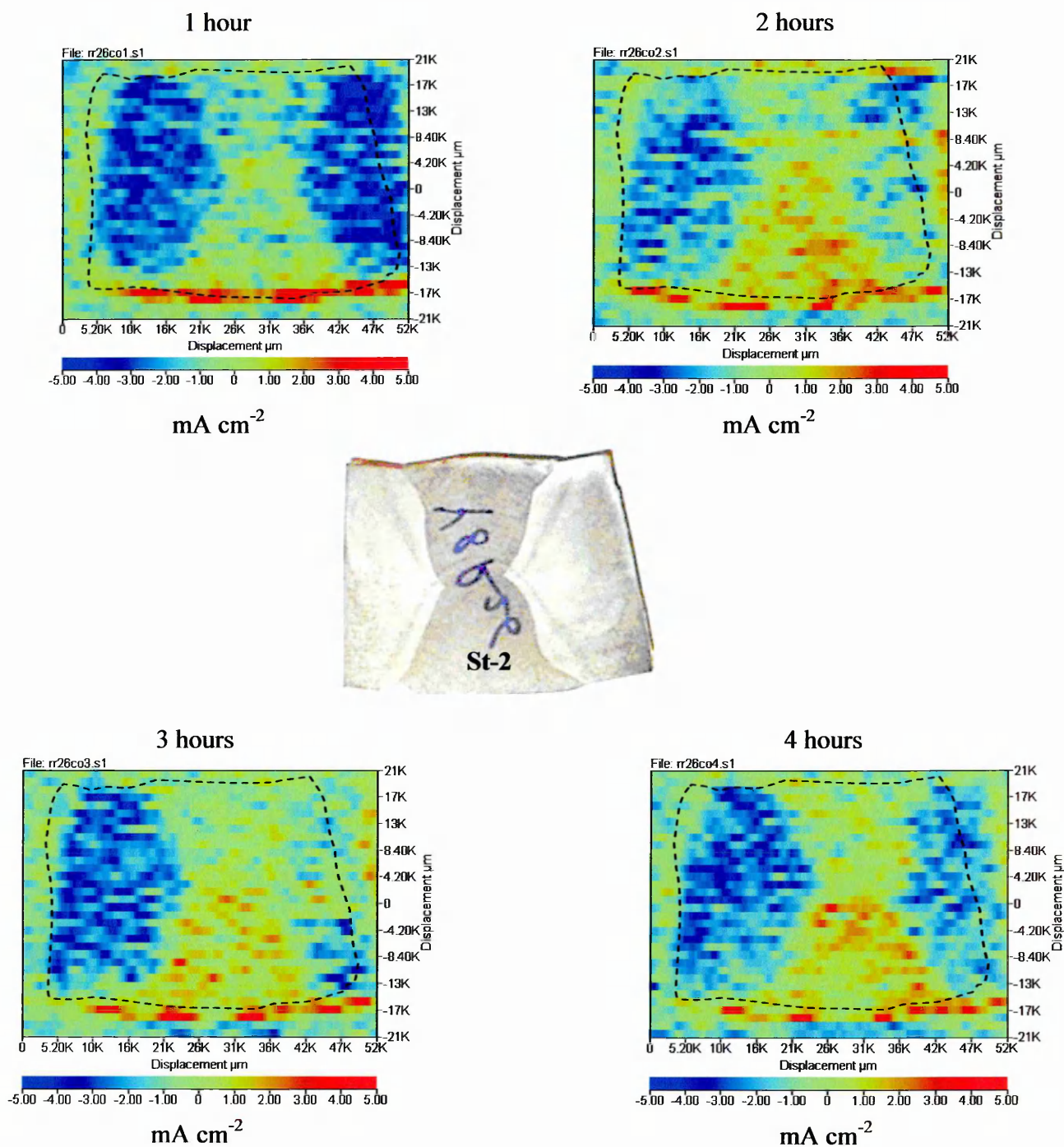


Figure 54 Showing the SVET area map scan on welded carbon steel pipeline designated of St-2 within buffered chloride solution with CO_2 saturation for different time scans.

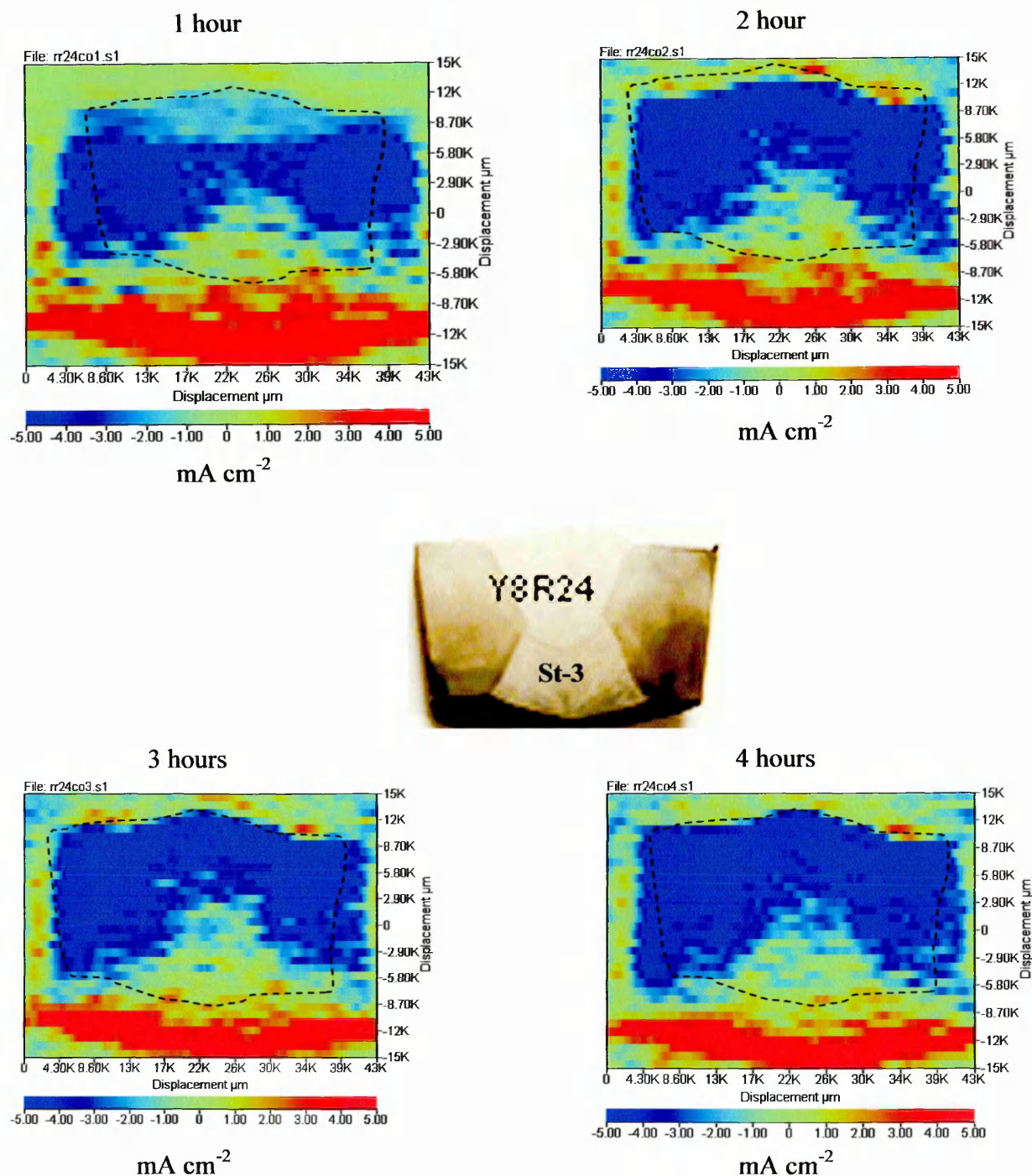


Figure 55 Showing the SVET area map scan on welded carbon steel pipeline designated of St-3 within buffered chloride solution saturated with CO₂ for different time scans.

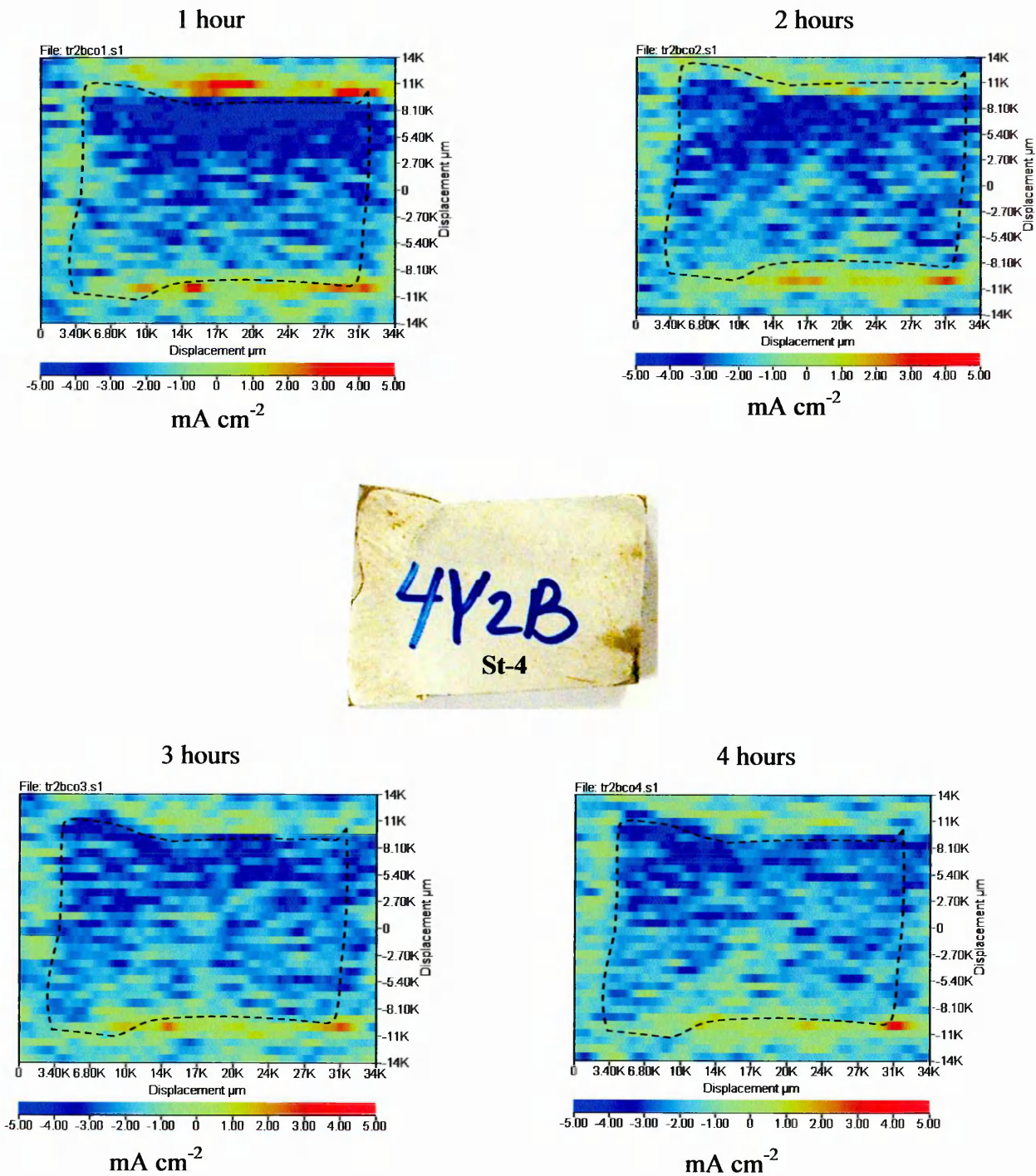


Figure 56 Showing the SVET area map scan on welded carbon steel pipeline designated of St-4 within buffered chloride solution saturated with CO_2 for different time scans.

5. Discussion

5.1 Introduction

The main objective of this research work was to evaluate the corrosion behaviour (rates) of welded carbon steel joints using both traditional and novel electrochemical scanning techniques.

Corrosion of carbon steel welds has been known to exist from the very first application of pipelines within aggressive aqueous environments.

For example, the oil and gas industries have considerable experience of operating materials in aggressive environments via materials selection or controlling the corrosion through modifying the corrosivity of the electrolyte.

The large tonnages of steel required for pipelines, for onshore or offshore installation makes the use of corrosion resistant alloys prohibitive. This means that traditionally the environment has to be controlled through either removal of the aggressive species or inhibition of the corrosion reaction by chemical treatments.

The carbon steel welded pipeline-sodium chloride solution alone system, with and without CO₂ additions, was chosen to conduct the experimental work due to its industrial importance in the oil and gas industry and the large amount of information available related to the localised corrosion and preferential or selective corrosion attack of this metal within different aggressive environments combination.

Emphasis was given to the use of conventional electrochemical DC steady state and novel scanning vibrating electrode techniques.

5.2 DC Electrochemical Tests

5.2.1 Introduction

The DC electrochemical tests conducted on the four different carbon steel welded pipelines were performed using linear polarisation resistance, cathodic polarisation and zero resistance ammetry in order to understand the corrosion behaviour of the individual and coupled microstructures which constituted the welded joints.

5.2.2 Open circuit potential (OCP) within 3.5% NaCl solution

Corrosion potentials for the different microstructures of the welded steels have been measured as a function of immersion time within 3.5% NaCl solution.

The corrosion potential of St-1 shifts in the active direction by some 100 mV (SCE) within the first 2 hours, see Figure 13 a. After 24 hours immersion the corrosion potential becomes stable for all microstructures, although the HAZ is slightly more noble (cathodic) than that of the PP and WM with the potential difference between the HAZ and WM after 72 hours immersion being 15 mV. The trend in corrosion potentials for the coupled microstructures was similar to that of the uncoupled microstructures, depicted in Figure 13 b. The WM/PP couple was found to be more noble than those of PP/HAZ and HAZ/WM with the potential difference for couples HAZ/WM and WM/PP being around 11 mV.

The variation of corrosion potentials for the uncoupled and coupled microstructures of St-2 are given in Figures 14 a and b respectively. The initial drop in E_{corr} values was

around 200 mV for both coupled and uncoupled samples. Again E_{corr} values after 24 hours immersion become steady state for both individual and coupled microstructures. In this case, the PP is found to be more noble than that of both the HAZ and WM microstructures where the potential difference between PP and WM after 72 hours immersion was recorded to be 15 mV.

The potential for the coupled samples of the HAZ/WM is more noble than that of the PP/HAZ and WM/PP. A final potential difference between HAZ/WM and PP/HAZ of 14 mV was recorded.

Figures 15 a and b show E_{corr} versus immersion time for individual and coupled microstructures of the St-3. As with St-1 and St-2 the corrosion potential drops around 100 mV within the first 6 hours, with the exception of the PP, which decreases by some 180 mV. After 72 hours all the microstructures showed similar E_{corr} values with a difference of only 5 mV. A similar trend was noted for the coupled microstructures with little difference between the individual couples. The maximum potential difference was found for the PP/HAZ and HAZ/WM at 7 mV.

The variation in E_{corr} potentials for the uncoupled and coupled microstructures of The St-4 are given in Figures 16 a and b respectively. The initial E_{corr} values shift in the active direction as in the case of the other steels. However, it was noted that the time to steady state values was greater, up to 25 hours compared to 2-8 hours for the other steels.

Furthermore, the differences in E_{corr} values after 72 hours were greater, namely, a difference of 26 mV between that of the PP and the HAZ. The coupled microstructures showed a similar trend with a greater time to stable E_{corr} values. The greatest difference in E_{corr} values was found for the WM/PP and PP/HAZ of 12 mV.

5.2.3 OCP within 3.5% NaCl solution with CO₂ saturation

Figures 17-20 (a and b) present open circuit potentials versus immersion time for uncoupled and coupled microstructures of steels 1-4 respectively, immersed within buffered 3.5% NaCl saturated with CO₂. All the microstructures of St-1 show steady state values (after around 48 hours immersion), see Figure 17 a. This trend also occurs for the coupled microstructures, depicted in Figure 17 b. One further observation from Figures 17 a and b is that there is little change in E_{corr} value over a 72 hour period and at the end of this period differences of only 10 mV are observed.

Figure 18 a shows open circuit potentials, as a function of immersion time, for different microstructures of St-2. Here, the open circuit potential of the WM is slightly more positive than those of the HAZ and the PP although the corrosion potential difference between WM and PP after 72 hours immersion is still only 9 mV. Interestingly, when coupled together the WM/PP is more noble than those of both the HAZ/WM and PP/HAZ couples. This suggests WM raises both the E_{corr} values of the PP and HAZ; see Figure 18 b.

Figure 19 a shows E_{corr} values for St-3. Here steady state conditions are observed for each microstructure after 3-4 hours with the WM showing the most positive corrosion potential value. The corrosion potential difference between PP and HAZ after 72 hours immersion was 14 mV. On coupling the different microstructures, Figure 19 b, the HAZ raises the E_{corr} values of both the PP and WM. The potential difference for WM/PP and PP/HAZ after 72 hours was 11 mV.

Changes in the open circuit potentials of the PP, HAZ and WM as a function of immersion time of the St-4, are shown in Figure 20 a. Like steel-2 the open circuit potential of the WM is more noble than those of the HAZ and PP.

On coupling the different microstructures the PP appears to have the greatest influence on the mixed potential values.

It can be seen from Figures 17-20 (a and b) that the trend in E_{corr} values for a CO_2 saturated environment is different to that of the chloride environment, namely the E_{corr} values become more noble on immersion within the solution.

5.3 Zero resistance ammetry (ZRA)

The galvanic current densities for different coupled microstructures of the welded steels 1-4 respectively are illustrated in Figures 21-28. In these experimental tests were carried out for immersion times of 48 hours within 3.5% NaCl solution alone and buffered 3.5% NaCl solution with CO_2 saturation.

5.3.1 ZRA tests within chloride solution

Figures 21-24 present the results of the coupling two different microstructures for different welded steels within 3.5% NaCl solution. The sign of the galvanic current density measured in these experiments will depend upon the electrical connections made to the samples. In this respect the main parameter to record is the modulus of the galvanic current. These values are shown in Table 9 for the chloride environment. The HAZ/WM values are negative for steels 1-3 and those of the coupled PP/HAZ and WM/PP are positive. This suggests that the galvanic currents flow from coupled PP/HAZ and WM/PP to the coupled HAZ/WM and hence the HAZ/WM is anodic to the PP/HAZ and the WM/PP. It is supposed the preferential corrosion of the HAZ/WM

is likely to occur if these welded steels are immersed in chloride environment. The coupled WM/PP for the St-4 was found to be anodic and those of the PP/HAZ and HAZ/WM are cathodic. It suggests that the current flows from the coupled PP/HAZ and HAZ/WM to the WM/PP. This suggests that the preferential corrosion of the WM/PP is likely to occur if this steel immersed in the chloride solution. This generally agrees with the SVET results shown in Figures 49-52.

5.3.2 ZRA tests within chloride solution with CO₂ saturation

Figures 26-28, present the results of the ZRA measurements for different coupled microstructures for steels 1-4. Again a measure of the galvanic activity was made from the modulus values of the ZRA measurement. These values are shown in Table 10. This Table shows that, the sign of the galvanic current density of the steels 1-4 for the coupled WM/PP is negative and those of the PP/HAZ and HAZ/WM are positive. This suggests that the galvanic currents flow from both PP/HAZ and HAZ/WM to the WM/PP and hence, the WM/PP is anodic to the PP/HAZ and HAZ/WM. It is expected that, preferential corrosion of WM/PP is likely to occur if these welded steels are immersed in a CO₂ containing environment. The preferential corrosion of the HAZ/PP identified in the ZRA tests correlates with that observed in the SVET tests, see Figures 53-56.

This result agrees with the results that have been reported by Endo et al [77]. They concluded that the galvanic current density is positive when the chemical composition differences of (Cu + Ni) and Mo are more than 0.5% and 0.1% respectively. Hence the addition of Cu and Ni or Mo is effective in preventing preferential corrosion of weld metals in CO₂ containing environments. In the current study, (Cu + Ni) % and

Mo% values are less than the values of (0.5% and 0.1%) see Table 1. This suggests that corrosion attack is likely to occur for either WM or HAZ of these steels.

ZRA data for chloride solution only shows major galvanic action (derived) from the HAZ/WM couples of all steels with the exception of St-4, where the WM is the most active or susceptible to corrosion attack. The major galvanic activity within buffered chloride solution with CO₂ saturation was found in the PP and WM. Any differences in ZRA response between the chloride solution alone and the buffered chloride solution with CO₂ environments will affect the ability of a carbonate film to form on the different microstructures.

5.4 Linear polarisation resistance measurements

Linear polarisation resistance (LPR or R_p) is a second measurement that has been made to assess the corrosion resistance of the different welded steel microstructures.

5.4.1 LPR within 3.5% NaCl solution

Figures 29 a and b present the LPR values for St-1 as a function of immersion time for individual and coupled microstructures. Here the highest LPR value is obtained for the PP, being $1995 \Omega \cdot \text{cm}^2$ whilst the lowest value of $832 \Omega \cdot \text{cm}^2$ is obtained for the HAZ. Using equation 16 it can be concluded that the HAZ was corroding at a rate 0.28 mm/yr and the PP is corroding at 0.12 mm/yr . All the LPR values and calculated corrosion rates are given in Table 15 for both the uncoupled and coupled samples. From this Table it can be seen that the highest corrosion rates are found for either the WM or HAZ depending upon the steel tested.

As shown in Figures 30 a and b, LPR values versus immersion time of the St-2 for uncoupled and coupled microstructures identify the highest uncoupled corrosion rate (0.28 mm/yr) in the WM, while the highest corrosion rate (0.23 mm/yr) was observed in the WM/PP couple.

Figures 31 a and b show the LPR values versus immersion time for St-3 for individual and coupled microstructures. Here the highest uncoupled corrosion rate (0.42 mm/yr) was found in the HAZ. The highest coupled corrosion rate (0.28 mm/yr) was observed for the PP/HAZ couple.

Figure 32 a and b show the LPR values versus immersion time for the uncoupled and coupled microstructures of St-4. The highest corrosion rate (0.30 mm/yr) is observed

in the WM, whilst a higher corrosion rate value of (0.35 mm/yr) was observed in the WM/PP couple.

Overall the LPR results show that the HAZ and PP are the least corrosion resistant. Where the individual weld metal is seen to show a low LPR value, the WM/PP couple also has a low LPR value, suggests a tendency of the PP to corrode when coupled to the WM. These is also reflected in the SVET results recorded for these steels, see Figures 49-52.

5.4.2 LPR within 3.5% NaCl solution with CO₂ saturation

In Figures 33 a and b it can be see that there is significant differences in corrosion rate between the different uncoupled and coupled microstructures of the St-1.

The highest corrosion rate was observed in the WM at approximately 1.0 mm/yr than the PP and HAZ microstructures, see Figure 33 a.

The corrosion rate for coupled microstructures of (b) is less than that of the uncoupled microstructures of (a) being recorded in the HAZ/WM at about (0.85 mm/yr).

As shown in Figures 34 a and b, the significant differences in corrosion rate between the different uncoupled and coupled microstructures of St-2 after 72 hours immersion shown the most severe corrosion in the WM microstructure (1.28 mm/yr) compared than those of the PP and HAZ microstructures, see Figure 34 a. The corrosion rate for coupled segments is less than for uncoupled segments and was observed of (0.82 mm/yr) in the HAZ/WM couple.

Figures 35 a and b show the significant differences in corrosion rate between the different individual coupled microstructures of the St-3. Again the highest corrosion rate was recorded for the WM microstructure (1.16 mm/yr) when compared to those of the PP and HAZ microstructures. The corrosion rate differences for coupled microstructures were only 0.68 mm/yr.

Figures 36 a and b present the differences in corrosion rate between the different uncoupled and coupled microstructures for St-4 after 72 hours immersion. As with the previous steels the highest corrosion rate was recorded in the WM microstructure (0.68 mm/yr). Whilst the corrosion rate differences of coupled segments was observed to be 0.58 mm/yr.

A clear comparison of the differences in corrosion behaviour and effects of coupling the microstructures together can be seen in Figures 37-44 for the two different environments. Analysis of the data shows that on average the highest corrosion rates are found in the WM, with the exception of St-3 within chloride solution. Whilst on average the highest coupled corrosion rates are found for the HAZ/WM for both environments. In both solutions the lowest corrosion rates on average are found for the PP.

Typical observations of the corrosion rate between different microstructures of the welded steels in different environments are reported in Tables 15 and 16. These results agree with the data reported by Gulbrandsen et al [72] where they concluded that preferential corrosion is most likely in the weld zone of steels tested.

In summary the WM is seen to produce the lowest LPR values i.e., highest corrosion rates. This correlates well with the SVET results as shown in Figures 53-56.

5.5 Cathodic polarisation tests

Cathodic polarisation curve measurements were conducted for each steel of the three different steel microstructures within buffered 0.35% NaCl solution saturated with CO₂ at room temperature and a solution pH of 6.2 ± 0.1 . Polarisation curves were recorded at a scan rate of 10 mV/min and over the potential range of around 300 mV, Figures 45-48. This method is appropriate for identifying the development of any protective films, namely, iron carbonate (FeCO₃) that may develop in the CO₂ containing environment.

The different microstructures, e.g., PP, HAZ and WM of the welded joints were immersed for times of 5 min, 1 hour and 4 hours, in the CO₂ saturated chloride solution at open circuit potential. Following each time interval a polarisation curve was obtained.

Differences in the cathodic current density were recorded at a given potential, notably -950 mV Vs (SCE). Table 17 summaries this data. From this Table and Figures 46-49 it can be seen that the greatest change (film development) occurs for the HAZ of St-3. However what is perhaps more important is that the highest cathodic currents are sustained (after 4 hours) on the WM, which will in turn sustain corrosion rates. This is confirmed in the data obtained from the ZRA tests, which show the highest galvanic currents for the WM couples.

Comparison between the LPR data and the cathodic polarisation results for different microstructures of steels within chloride solution saturated with CO₂ as follows;

LPR values of the WM for St-1 are greater than that of (St-2 = St-4) and less than that the St-3, whilst the cathodic current values for St-1 are less than that the St-3 and the (St-2=St-4).

The LPR values of the HAZ for St-3 are less than that the values of the St-4 and the (St-1=St-2), whilst the cathodic current values of the St-3 are the higher than that the St-4 and (St-1=St-2) values.

LPR data of the PP for St-4 are less than that of the St-3 and the (St-1=St-2), whereas the cathodic current values of the St-4 is the highest of the St-2 and the (St-1=St-3).

Generally, St-1 exhibits the lowest LPR values for the WM and cathodic currents are approximately equal for WM/HAZ/PP. In addition, St-2 shows the lowest LPR values whereas the highest cathodic current is found in the WM and the PP where the HAZ was registered the lowest current. LPR values are the lowest for St-3 in the WM/or HAZ regions whilst the highest cathodic current was registered in the HAZ and the lowest in the PP. The LPR values for St-4 are the lowest in the PP and WM whilst the highest cathodic currents for WM/HAZ/PP microstructures are similar.

St-3 shows similar cathodic current is small HAZ where the WM became active after one hour. In addition the highest cathodic current and the lowest LPR values approximately equal for high anodic activity (poor anode).

As a general statement it is observed that the HAZ shows to greatest changes in cathodic polarisation curves, i.e., the greatest film formation. To date no analysis has been carried out to determine the individual micro-compositions of each of the microstructures. This is considered an important next step as the development of the carbonate film reduces the corrosion rate of the steel.

5.6 Effect of microstructure

The resultant microstructures of the three different segments for the different steels are shown in Figures 9-12. The welding procedures used for these steels are unfortunately unknown and therefore it is difficult to predict which microstructures are expected.

The important phases have been addressed from the fit with all electrochemical data and were observed to be more anodic and susceptible to the preferential weld corrosion are martensite and bainite phases. These phases represent the WM and HAZ samples. However the microstructures of the PP for steels 1-4 consist mainly of fine-grained ferrite (light grains) and pearlite phase (dark grains). Steel-3 exhibited a slightly elongated pearlite phase. The microstructure of the HAZ was found to be a mixture of pearlite with upper bainite structure for the steels.

Finally the microstructures of the WM consist primarily of lower bainite and martensite structure for steels 1-3, whilst St-4 exhibits a microstructure of lower bainite and δ -phase precipitates on the grain boundaries of this steel. Such microstructures were also reported by Lancaster [21].

Majid et al [78] found the low value of corrosion rate of steel welds was due to the microstructural changes. Another factor that strongly affects corrosion behaviour is the residual stresses that develop in the WM and HAZ and although these have not been measured they may play some part in accelerating corrosion of the weld microstructure.

Uhlig [79] reported that the higher the residual surface stresses, the higher the corrosion rate in welded joints.

Bainitic and martensitic structures were found to be more anodic and susceptible to the preferential corrosion than ferritic-pearlitic microstructures within the CO₂ containing environment. This result is in agreement with the previous work conducted by Nesic and Lunde [14] and has also been reported by Ueda et al. [80]. They concluded that using steel with a ferrite-pearlite microstructure showed good corrosion resistance for localised corrosion compared with steel with bainite-martensite microstructures when tested within CO₂ containing environments.

5.7 SVET measurements

5.7.1 Introduction

SVET is a relatively new technique and offers the opportunity to obtain information concerning corrosion activity on a localised scale.

However, its utilisation to investigate the corrosion of welds has so far been limited. It has been applied to differentiate between relative anodic and cathodic sites of welded joints; for example, Sephton and Pistoruis [73] used a number of techniques, including the SVET to investigate the role of sulphur in the localised corrosion of welds in high manganese carbon steels. They suggested that hardened microstructures within the HAZ, such as bainite and martensite structures do not form galvanic couples with the surrounding microstructure but the information of networks of sulphides in the fusion line area is the most likely explanation for corrosion grooving parallel to the weld line in corrosive environments.

SVET has been used in this study to map across the PP/HAZ/WM interface for four different steels within chloride solution alone and buffered chloride solution with CO₂ saturation.

5.7.2 SVET tests within chloride solution

The SVET area map scans performed on samples of steels 1-4 are presented in Figures 49-52 for different time scans respectively.

It can be seen from St-1 that highly localised activity initiates within the HAZ and WM during 1-2 hours. After 3-4 hours the corrosion activity has extended to the PP and WM. Over time the activity becomes more general being focused on the HAZ and WM and less activity observed on the HAZ during first two hours.

Steel-2 initially exhibits less localised attack in the PP region and more-localised activity in the PP and less than that in the HAZ and WM regions. After 3-4 hours corrosion is more uniform with little differential between the different microstructures.

Steel-3 shows less activity being in the WM and HAZ during 1-4 hours.

Finally, steel-4 shows the least localised activity during of all the other steels, with corrosion being uniformly distributed across the different weld microstructures.

Therefore it can be concluded from the results obtained from the SVET technique in chloride solution for St-3 and St-4, the weld zones for these steels are more/less susceptible to preferential corrosion whilst most of the PP in steels 2-4 has acted as anode.

5.7.3 SVET test within chloride solution saturated with CO₂

The results of SVET scan for steels 1-4 within buffered chloride solution saturated with CO₂ environment are shown in Figures 53-56 respectively.

From SVET tests for steel-1 it can be seen the localised activity is initially concentrated at the WM and to some extent at the HAZ, whilst, most of the PP acted as a cathode during 1-2 hours. After 3-4 hours there is less activity on the PP and more uniform corrosion at the HAZ and WM.

St-2 shows less localised activity in the HAZ and WM on first exposure to the solution. After 2-4 hours this has somewhat increased on the WM microstructure.

Steel-3 exhibits the least activity has observed with more uniform corrosion activity for all microstructures of the steel.

Steel-4 shows more intense activity at all the microstructures after 1-4 hours with corrosion being observed on the different areas of the steel.

Therefore the results of the area map scans over the weldments show that although the activity somewhat varied from time to time, the most pronounced attack seemed to be associated with bainite/martensite microstructures with the exception of the highest activity concentrated in the ferrite/pearlite microstructures of the steel-3 within buffered chloride solution with CO₂ saturation.

6. Conclusions

Electrochemical measurements and metallographic studies were performed using welded carbon steel pipeline materials designated types Y8R27 (St-1), Y8R26 (St-2), Y8R24 (St-3) and 4Y2BJ (St-4). The preferential corrosion of the welded joints within chloride solution alone and buffered chloride solution with CO₂ saturation is the result of galvanic differences between the parent plate heat affected zone and weld metal. The most active region suffers accelerated attack, with a reduction of the corrosion over more noble surfaces. Corrosion tests were conducted within naturally aerated chloride solution alone and buffered chloride solution saturated with CO₂ at room temperature. The pH for both environments was measured and found to be 6.3 ± 0.3 and 6.2 ± 0.1 respectively.

Two aspects have been addressed experimentally, (i) DC steady state behaviour namely, open circuit potential, galvanic current density, linear polarisation resistance and cathodic polarisation response and; (ii) Corrosion activity distribution using a scanning vibrating electrode technique (SVET). Three different microstructures, namely, weld metal, heat affected zone and parent plate have been examined.

The following conclusions were drawn from this study;

1. The electrochemical test results showed that a clear difference existed in the corrosion behaviour between different microstructures of the welded steels.
2. The highest corrosion rate within chloride solution, based on LPR measurements, was found in the HAZ of St-3, although in general the WM microstructure of steels 1, 2 and 4 was found to give the highest average corrosion rate.

3. On testing in a carbon dioxide containing environment the weld zone for most of the steels gave the highest corrosion rates.
 4. ZRA tests showed that the highest corrosion rate in the chloride solution was observed in the HAZ/WM couples of steels 1-3, whilst steel-4 showed the highest rate of corrosion in the WM/PP couple. In buffered chloride solution with CO₂ saturation, the greatest corrosion rates were found in the WM/PP couples for all steels. In general the data obtained from ZRA tests, identified the highest galvanic currents in the WM couples.
 5. Cathodic polarisation tests within buffered chloride solution with CO₂ saturation showed that the greatest change of film development occurred on the HAZ microstructure for steels 2-3. However, the highest currents after four hours are sustained on the WM microstructure for most of the steels.
 6. SVET was found to be a sensitive and reliable technique that can be used for rapid and reliable evaluation of weldments. Results of the map scans over weldments show that, although the activity varied from time to time, the most pronounced attack seemed to be concentrated in the bainite and martensite microstructures and least activity for some steels occurred in the pearlite and ferrite microstructures.
- Results from the corrosion tests showed a clear significant difference in the corrosion behaviours between the weld zone and parent plate microstructures, i.e., some location for welded steel microstructures are more attacked than others.

7. Suggestions for further work

The list of possible further work in this field is numerous with several aspects broached in this thesis needing further exploration. The following aspects are considered to be of prime importance to investigate the corrosion behaviour associated for steel welds found in the oil and gas industries.

- 1) Study the effect of alloy additions on the weld metal in order to render the weld metal immune to localised attack, i.e., be cathodic to the parent plate and heat affected zone.
- 2) Conduct a microprobe analysis of each of the local microstructures and correlate this with the WM/HAZ/PP electrochemical measurements conducted in order to determine why specific microstructures are anode or cathode.
- 3) Initiate a study on the corrosion behaviour associated with weldments and the effect of microstructure for steels of known compositions. Different microstructures may be produced from the same composition by a series of heat treatments such as quenching and tempering, etc. In this way the effect of ferrite, pearlite, bainite and martensite structures may be systematically evaluated.
- 4) Welding processes and parameters could be undertaken, e.g., Submerged Arc Welding, Gas Metal Arc Welding and Shield Metal Arc Welding and the effect of the composition of the weld consumable should be investigated.
- 5) The influence of welding procedure, on the production of residual stresses and their influence on the corrosion behaviour of welded joint may be investigated.
- 6) Conduct scanning electron microscope (SEM) analysis to evaluate the corrosion products and the effect of heterogeneities, e.g., magnesium sulphide inclusions (MnS), on the initiation of corrosion.

References

1. J. E. Donham, ASM, Metals Handbook, 9th Edition, Vol. 13, 1987.
2. M.M. Osman and M.N. Shalaby, Mater. Chemist. And Physics, Vol. 77 No. 1, 2003, pp.261.
3. O.A. Tomas and P.R. Alan, Production Operations, Vol. 2, Oil and Gas Consultants International, Inc. Tulsa, 1985.
4. Corrosion Control in Petroleum Production, An Official NACE Publication, 1979.
5. A.J. McMahon Colloids and Surfaces, Vol. 59, 1991, pp. 187.
6. ASM Metals Handbook, 9th Edition, Vol. 11, 1986.
7. S. Higuchi, J. of Iron and Steel, Vol. 79, No. 8, 1993, pp. 961.
8. G.A. Cash, et al., Corrosion. Science. Vol. 33, No. 33, 1993, pp. 113.
9. R.T. Jones, "Carbon and Alloy Steels, in Process Industries Corrosion", NACE, 1986.
10. C.P. Larrabee and S. K. Coburn, First International Congress on Corrosion- Butterworths, 1962, pp.276.
11. C.P. Larrabee, Materials Protection, Vol. 1, No. 12, 1962, pp.95.
12. J.L. Crolet, EURROCORR`93 Congress, the Institute of Materials, London, Vol. 1, 1993, pp. 473.
13. A. Dugstad, Corrosion/92, paper No. 14, NACE, Houston, TX. 1992.
14. S. Nesic and L. Lunde, Corrosion-NACE, Vol. 50, No. 9, 1994, pp. 717.
15. S. Endo, et al., OMAE Vol. III-A, Mater. Eng. ASME, 1992 pp95.
16. K.G. Mishra and C.R. Das, Brit. Corros. J. Vol. 22, No. 3, 1987, pp195.

17. C.A. Loto and M.A. Matanmi, Brit. Corros. J. Vol. 24, No. 1, 1989, pp.36
18. A. Turnbull, Rev. Coatings Corrosion., 1982, Vol. 5, No 1/4, pp 43.
19. Metals Handbook, 9th Edition, Vol. 1, 1987.
20. ASM Handbook, Vol. 6, Welding Brazing and Soldering, 1993, pp.641.
21. J. F. Lancaster, Metallurgy of Welding 3rd edition, George Allen, 1980.
22. A.G. Ostroff, Introduction of Oilfield Water Technology; NACE, Houston, TX. USA. 1979, pp.17.
23. J.O'M. Bockris and A. K. Reddy, "Modern Electrochemistry", Vol. 2, 1970 Plenum Press, USA.
24. L.L Shrier, "CORROSION", 1976, Vol. 1, 2nd Edition, Newness-Butterworths, London, UK.
25. M. G. Fontana and N. D. Greene, Corrosion Engineering, 1978.
26. K.R. Trethewey, et al., Corrosion/96, paper No. 317, 1996.
27. S.J. Bates, et al, Mater. Sci. and Tech., Vol. 5, 1989, pp. 356.
28. I.L. Rosenfeld and I.S. Danilov, Corros. Sci., Vol. 7, 1967, pp.129.
29. E. Mattsson, Brit. Corros. J., Vol. 13, No. 1, 1978, pp. 5.
30. Y. M Kolotyrkin, Corrosion- NACE, Vol. 19, 1963, pp.261.
31. M. Pourbaix, J. of Electrochem. Society, Vol. 131, No. 8, 1984.
32. S. C. Dexter, Localised corrosion, Metals Handbook, Vol. 13, 1987, pp. 104.
33. H. R. Amler and A. J. Bain, J. Applied Chemistry, Vol. 5, 1955, pp.437.
34. R.C. Buchen, Corrosion-NACE, Vol. 6, 1950, pp.178.
35. H.L. Bilharz, Corrosion-NACE, Vol. 7, 1951, pp. 256.
36. C.K. Eilerts et al, Corrosion-NACE, 1948, Vol.4, No.7, pp.321.
37. A. Ikeda, et al., Advances in CO₂ Corrosion, NACE, Houston, TX, 1984, pp.39.

38. F.C. Riesenfeld and C.L. Blohm, Petroleum Refiner, Vol. 29, 1950, pp.141.
39. M. G. Fontana, Corrosion Engineering, 3rd Edition, 1986.
40. D.D. Macdonald, J. Electrochem. Soc., Vol. 139, 1992, pp3434.
41. J. L. Crolet, et al, Mem . Sci. Rev. Met., Vol.71, No. 12, 1974, pp.797.
42. A.J. Sedriks, Corrosion-NACE, Vol. 45, 1989, pp.510.
43. K. R. Trethewey and J. Chamberlain, Corrosion for Science and Engineering, 2nd Edition, 1995, pp. 162.
44. H. H. Uhlig and R. W. Revie Corrosion and Corrosion Control, 3rd Edition, Wiley, New York, 1985.
45. S.M. Sharland, Corrosion Science, Vol. 33, No. 2, 1992, pp.183.
46. M. K Watson and J. Postlethwaite, Corrosion Science, Vol. 32 1991, pp.1253.
47. S. Bernhardsson, et al., 8th International Congress on Metallic Corrosion, Mainz, Germany, 1981, pp. 193.
48. J. W. Oldfield and W. H. Sutton, Br. Corros. J., Vol. 13, No. 1, 1978, pp. 13.
49. E. Halmoy, Welding Technique 3rd Edition, NTH, 1993.
50. N. Rothwell and M.E. Turner, Metals and Materials, 1989, pp. 352.
51. M. Henthorne, Corrosion-NACE, Vol. 30, No. 2, 1974, pp. 39.
52. D.A. Jones, Principle and Prevention of Corrosion, 2nd Edition, Prentice Hall, Upper Saddle River, NJ, 1996.
53. K. F. Krysiak and Hercules, Metals Handbook, Vol. 13, 9th Edition, ASM, 1987 p.344.
54. S. Bagnall, Microstructural Science Vol. 13, Welding Failure Analysis and Metallography, ASM, 1986.
55. R.E. Reed-Hill, Physical Metallurgy, 2nd Edition, 1973, pp. 662.

56. G.M. Evans, *Welding Journal*, Vol. 62, 1983, pp. 313.
57. C. Kato, et al., *Corrosion Science* Vol. 18, 1978, pp. 61.
58. R. Raty, et al, *Acta Polytechnica*, 1971, pp. 78.
59. V.S. Voruganti, et al., *Corrosion-NACE*, Vol. 47, 1991, pp343.
60. G.A. Nelson, *Corrosion -NACE*, 1958, Vol. 14, No. 3, pp. 415.
61. J.N. Bradley and J.C. Rowlands, *Brit. Welding J.*, 1962, Vol. 9, No.8, pp 476.
62. J.L. Dawson, et al, *EUROCORR* 99 Part 26, 1999 pp. 155.
63. J.E. Simmons, *Corrosion-NACE*, Vol. 11, 1955, pp. 255.
64. R.V. Skold and T.E. Larson, *Corrosion- NACE*, Vol. 13, 1957, pp. 139.
65. E. Heitz and W. Schwenk, *Brit. Corros. J.*, Vol. 11, No. 2, 1976, pp. 74.
66. F. Mansfeld, *Corrosion-NACE*, Vol. 29, No 10, 1973, p. 397.
67. H. S. Isaacs and B. Vyas, *Electrochemical Corrosion Testing*, ASTM STP 727, 1981, pp. 3.
68. H.S. Isaacs and Y. Ishikawa, *Electrochem. Technique*, ed. R.Baboian, Houston, TX. NACE, 1986, pp. 17.
69. H.S. Isaacs, *Corrosion Science* Vol. 28, 1988, pp. 547.
70. M. J. Franklin et al, *Corrosion. Sci.*, Vol. 32, No. 9, 1991, pp. 945.
71. T. Shibata et al., *Corrosion Engineering*, Vol. 39, 1990, pp. 331.
72. E. Gulbrandsen et al., 15th Internat. Corrosion Congress, Spain, 2002
73. M. Sephton and P.C. Pistoruis, *Corrosion-NACE*, Vol. 56, 2000, pp. 1272.
74. V. C. Wagner and W. Traud, *Z. Electrochem.*, Vol. 44, 1938, pp. 391.
75. M. Stern and A. L. Geary, *J. Electrochem. Soc.*, Vol. 104, No. 1, 1957 pp. 56.
76. R. Akid and M. Garma, *Electrochimica Acta*, Vol. 49, 2004, pp. 2871.
77. S. Endo et al, 3rd Internat. Offshore and Polar Eng. Conf., Singapore, 1993 pp. 321.

78. T.M. Majid, et al., Corrosion-NACE, Vol. 46, No. 1, 1990, pp. 37.
79. H. H. Uhlig, Corrosion Handbook, New York, John Wiley and Sons, 1961 pp. 595.
80. M. Ueda and A. Ikeda., Corrosio/96, paper No. 13, NACE International., 1996.

Publications

- A. Abdurrahim, R. Akid and N. Farmilo, 44th Corrosion Science Symposium, Paper No. 88, September, 2003, Southampton, UK.